RECOVERY OF COAGULANTS FROM ACID MINE DRAINAGE

Brian Mwewa

A thesis submitted to the Faculty of Engineering and the Built Environment, University of Witwatersrand, Johannesburg in fulfillment of the requirements for the degree of Doctor of Philosophy

Johannesburg, 2020

Declaration

I, Brian Mwewa, declare that this thesis is my own unaided work. It is being submitted to the degree of Doctor of Philosophy to the University of the Witwatersrand, Johannesburg. It has not been submitted before for any other degree or examination in any other University.

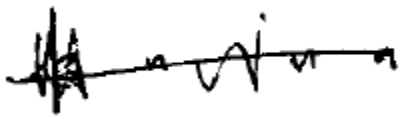

September, 2020

Abstract

The wastes generated from both operational and abandoned coal and metal mining operations are an environmental concern. These wastes, including acid mine drainage (AMD), are normally treated to abate the devastating effects they have on the environment before disposal. At the moment, the most widely applied methods for remediation of AMD is the high density sludge process (HDS) which involves chemical-neutralization. Although the HDS process is relatively cheap and easy to operate, it has several disadvantages. These include; the formation of gelatinous sludge which is difficult to filter, sludge handling problems due to the low solids concentration resulting in considerable water losses and a large land area is needed for sludge disposal. In light of the disadvantages of the HDS process, this study was conducted to develop process flowsheets to recover iron (Fe) and aluminium (Al) which were used to produce a poly-alumina-ferric sulphate (AMD-PAFS) coagulant for water treatment. The flowsheets were developed with the understanding that the recovery of Fe(III) and Al(III) would reduce the sludge volume by over 90%, more so act as a source of revenue to partly offset the treatment cost.

The first part of this experimental program focused on developing an understanding of the oxidation of ferrous iron, Fe(II) to ferric iron, Fe(III) using air in the pH range pH of 5.0-7.0. Synthetic AMD, prepared using ferrous sulphate and aluminium sulphate salts, was used for this part of the experimental program and contained only Fe(III) and Al(III). This was done to evaluate the effect of pH, the Al(III) cations and seeding on the Fe(II) oxidation rate. The results showed that the Fe(II) oxidation rate was dependent on pH. At pH of 5.0, the average oxidation rate was 2.16 mg/L/min. The oxidation rate increased to 7.73 mg/L/min with an increase in pH to 7.0. The studies revealed that the oxidation rate was first order with respect to Fe(II) in the pH range 5.0-7.0. The order of reaction with respect to OH^- was 1.35. In the oxidation-precipitation reaction, seeding, regardless of the seed concentration, was found to increase the rate of oxidation. For example, the oxidation reaction rate increased from 2.16 mg/L/min in unseeded experiment to 2.7 mg/L/min at pH 5 for seed concentration, Cs= 0.5. The study also demonstrated that Al(III) cations did not affect the Fe(II) oxidation rate.

The iron oxidation experimental program was followed by precipitation studies to recover both Fe(III) and Al(III) using sodium hydroxide. The co-precipitation of Fe(III) and Al(III) was carried out at the pH range of 5.0-7.0. Real AMD was used in these tests. In order to improve the precipitate particle size and subsequent settling and dewatering capabilities, seeded precipitation was employed with the single pass precipitate used as recycle sludge. Three different recycle sludge concentration levels (C_s = 0.5, 1.0 and 2.0) were studied. The results showed that at pH 5.0, a precipitation yields of 99.9 and 94.7% for Fe(III) and Al(III), respectively were obtained. An increase in the pH to 7.0 increased the recovery of Al(III) to 99.1%, while the recovery of Fe(III) remained the same. An attempt was made to relate the effect of seeding on the precipitate settling rates and it was established that the sludge settling rate and particle size improved with increase in seed concentration from Cs = 0.5 to Cs= 1.0. Above a C_s of 1.0, there was no significant improvement in the settling rate. The precipitate was used to produce a coagulant (AMD-PAFS^{p}) consisting of 89.5% and 10.0% Fe(III) and Al(III), respectively by dissolving the AMD precipitate in 5.0% (w/w) sulphuric acid.

A solvent extraction process was also evaluated to extract Fe(III) and Al(III) from AMD using Cyanex 272 in Shellsol D70. Cyanex 272 concentration of 0.16 M – 0.63 M was tested in the pH range 1.5-3.0. The Fe(III) and Al(III) stripping was carried out using 1.0, 2.0 and 3.0 M sulphuric acid. The number of stages required for both extraction and stripping processes of Fe(III) and Al(III) was also evaluated. The experimental results showed that quantitative removal of Al(III) >99.0% and Fe(III) >99.0% in a two-stage extraction stage using 0.47 M Cyanex 272 at pH 2.5 and 25°C is achievable. A single-stage stripping of both elements was achieved using 2 M sulphuric acid. The strip liquor contained 91.7% Fe(III) and 8.33% Al(III) and was subsequently used as a coagulant (AMD-PAFS^{sx}).

The treatment of the brewery wastewater using 10-150 mg/L AMD-derived coagulants shows that the AMD-derived coagulants were as effective as the poly ferric sulphate coagulant (PFS) in the brewery wastewater treatment. The turbidity removal was 91.9 and 87.8%, while the chemical oxygen demand (COD) removal was 56.0 and 64.0% for AMD-PAFS^{p} and PFS coagulants, respectively. The AMD-PAFS^{sx} showed slightly better

performance as compared to the AMD-PAFS^{p} coagulant. This was attributed to the possibility of co-extraction of manganese and magnesium, which in itself has been used as a coagulant. The developed process, especially the precipitation based process, which can easily be incorporated into existing AMD treatment plants, not only reduces the sludge disposal problems but also creates revenue from waste.

Addendum to report on conference and symposia presentations and journal paper

Journal publications

1. **Mwewa, B**., Stopić, S., Ndlovu, S., Simate, G.S., Xakalashe, B. and Friedrich, B., 2019. Synthesis of poly-alumino-ferric sulphate coagulant from acid mine drainage by precipitation. *Metals*, *9*(11), p.1166.

2. **Brian Mwewa**, Sehliselo Ndlovu, Geoffrey Simate, Elias Matinde, 2020. Extraction of Rare Earth Elements from Acid Mine Drainage: A Concise Review of Extraction Methods

Conferences and workshops attended

1. **Brian Mwewa**, Sehliselo Ndlovu, Geoffrey Simate, Young professional conference, South Africa 2018. Recovery of coagulant from acid mine drainage

2. **Brian Mwewa**, Sehliselo Ndlovu, Geoffrey Simate, Wits University acid mine drainage workshop, Wits University, 2018. Potential recovery of poly-alumino-ferric sulphate coagulant from acid mine drainage

3. **Brian Mwewa**, Sehliselo Ndlovu, Geoffrey Simate, Wits University acid mine drainage workshop, Wits University, 2018. Potential recovery of poly-alumino-ferric sulphate coagulant from acid mine drainage

4. **Brian Mwewa**, Srecko Stopic, Sehliselo Ndlovu, Geffrrey S. Simate, Buhle Xakalashe, Bernd Friedrich., 2019 Synthesis of poly-alumino ferric sulphate coagulant from acid mine drainage

Dedication

Dedicated to my wife Iris Ndina Lumano Mwewa and our son Chikwepe Chisungusho Mwewa for the love, encouragement and patience during the time of the study

‘’MORE GRACE’’

Acknowledgements

My appreciations go to;

- The Almighty God for giving me the strength to utilize the God given intelligence to do the research.
- Prof Sehliselo Ndlovu and Professor Geoffrey Simate for the tireless effort, dedication, inspiration and guidance rendered to me to successfully complete my research.
- DST/NRF SARChI: Hydrometallurgy and Sustainable Development for the financial support.
- Wits University School of chemical and metallurgical engineering for administrative and technical assistance.
- My wife Iris Ndina Lumano Mwewa, our son Chikwepe Chisungusho Mwewa, my Mother Ms. Theresa Nsemba Mwila Mwewa, My siblings and all my friends for the support and encouragements showered on me.

For "I can do all things through Christ who strengths me".

Table of Contents

Declaration ..... **i**

Abstract ..... **ii**

Addendum to report on conference and symposia presentations and journal paper ..... **v**

Dedication ..... **vi**

Acknowledgements ..... **vii**

Table of Contents ..... **viii**

List of figures ..... **xiv**

List of Tables ..... **xviii**

Nomenclature ..... **xxi**

List of abbreviations ..... **xxii**

Introduction **1**

1 General Introduction **1**

1.1 Sources of AMD 1

1.2 Chemistry of AMD formation 2

1.3 Environmental and ecological impact of acid mine drainage 8

1.4 Treatment of acid mine drainage 9

1.4.1 Source control 9

1.4.2 Remediation 10

1.5 Motivation 13

1.6 Objectives 14
1.7 Deliverables 15
1.8 Significance of the study 16
1.9 Research methodology 16
1.9.1 Literature review 16
1.9.2 Experimental design and laboratory testing 17
1.9.3 Data analysis 17
1.9.4 Conclusions and recommendations 18
1.10 Thesis layout 18
1.11 Summary 19
References 20
Literature review 27
2 Oxidation and precipitation 27
2.1 Chemistry of ferrous iron oxidation 27
2.1.1 The Hyber Weiss reaction sequence 27
2.1.2 Kinetics of ferrous iron oxidation 29
2.1.3 Summary 36
2.2 Precipitation 37
2.2.1 Theory of precipitation kinetics 37
2.2.2 Nucleation 41
2.2.3 Crystal Growth 43
2.2.4 Seeding during precipitation processes 46
2.2.5 Theory of co-precipitation mechanisms 48

2.2.6 Iron and aluminium hydrolysis and precipitation 50
2.2.7 Iron and aluminium recovery from AMD/hydrometallurgical solutions 59
2.2.8 Summary 63
References 64
3 Solvent extraction of iron and aluminium 72
3.1 Theory of solvent extraction 72
3.2 Extraction 74
3.3 Solvent extraction of Fe(III) and Al(III) from acidic sulphate solutions 78
3.4 Solvent extraction of other metals associated with AMD 83
3.5 Methods of extraction 83
3.5.1 Batch wise single stage extractions: 83
3.5.2 Multistage counter current continuous processes: 84
Chapter summary 85
References 86
4 Coagulation 90
4.1 Coagulation process 90
4.2 Coagulation with Al(III) and Fe(III) 91
4.3 Coagulation with polymers 91
4.4 Coagulation mechanisms 94
4.4.1 Adsorption and charge neutralization 95
4.4.2 Sweep coagulation 97
4.5 Effect of operating conditions on coagulation 99

4.5.1 Controllable parameters 99
4.5.2 Uncontrollable parameters 101
4.6 Chapter summary 103
References 104
Experimental work 107
5 Oxidation and precipitation experimental methods and results 107
5.1 Hypothesis and objectives 107
5.2 Materials 108
5.3 General experimental setup 108
5.4 Oxidation experimental procedure 109
5.5 Fe and Al co-precipitation experimental procedure 111
5.6 Settling tests 112
5.7 Analytical methods 112
5.8 Oxidation and precipitation experimental results 115
5.8.1 Fe(II) oxidation kinetics results and discussion 115
5.8.2 Effect of seeding on Fe(III) oxidation 118
5.8.3 Effect of Al(III) cations on Fe(II) oxidation rate 119
5.8.4 Fe-Al precipitation results 121
5.9 Conclusion 134
5.9.1 Fe(II) oxidation 134
5.9.2 Fe(III) and Al(III) precipitation 135
References 136
6 Solvent extraction experimental methods and results 140

6.1 Hypothesis and objectives 140
6.2 Materials used in the solvent extraction test works 141
6.3 General experimental setup 141
6.4 Extraction and stripping experimental procedure 143
6.5 Analytical methods 144
6.6 Experimental results and discussion 145
6.6.1 Effect of Cyanex 272 concentration 145
6.6.2 Effect of equilibrium pH on extraction 147
6.6.3 Separation factor of Fe(III) over Al(III) 150
6.6.4 Theoretical number of stages required for extraction 152
6.6.5 Effect of sulphuric acid concentration on Fe(III) and Al(III) stripping 154
6.7 Conclusion 156
References 157
7 Coagulation experimental methods 159
7.1 Hypothesis and objectives 159
7.2 Coagulation experimental methods 160
7.2.1 Procedure used to obtain coagulant from the AMD precipitate 160
7.2.2 Procedure used to obtain coagulant from solvent extraction 161
7.2.3 Materials 161
7.2.4 Coagulation test equipment 162
7.2.5 Test procedure 163
7.2.6 Water Quality Analyzes 164
7.3 Experimental results and discussion 166

7.3.1 Precipitate solubility and coagulant production 166
7.3.2 Characteristics of the brewery wastewater 169
7.3.3 Effect of the coagulant on turbidity and chemical oxygen demand 169
7.3.4 Effect of the Coagulants on Electric Conductivity 170
7.3.5 Effect of the Coagulant Dose on Total Dissolved Solids 172
7.3.6 Performance of precipitation derived against solvent extraction derived AMD-PAFS 173
7.4 Conclusion 175
8 Flowsheets and mass balances 176
8.1 Precipitation based flowsheet 176
8.2 Solvent extraction based flowsheet 178
8.3 Economic evaluation 180
9 Conclusions and recommendations 182
9.1 Fe(III) oxidation 182
9.2 Fe(III) and Al(III) precipitation 182
9.3 Fe(III) and Al(III) solvent extraction and stripping 183
9.4 Coagulation 183
9.5 Recommendations 183
References 184

List of figures

Figure 1.1: Abandoned mine and AMD generation 2

Figure 1.2: Hypothetical schemes for the oxidation of pyrite or metal sulphide by iron and Sulphur-oxidizing acidophilic bacteria producing sulphuric acid 4

Figure 1.3: The major effects of AMD on the environment 8

Figure 1.4: The conventional process for AMD neutralization 11

Figure 1.5: The High Density Sludge process for AMD neutralization 12

Figure 2.1: Oxidation rate of Fe as a function of pH 33

Figure 2.2: Precipitation kinetic processes 37

Figure 2.3: Crystallization free energy vs nuclei size 42

Figure 2.4: pH profile for ferrous hydroxide, $Fe(OH)_3$ at 25°C 53

Figure 2.5: Concentration of Fe(III) remaining in solution after hydrolysis as a function of pH 56

Figure 2.6: Equilibrium Concentration of Metal Hydroxides 59

Figure 2.7: Stability regions of various compounds in the Fe-S-O system 60

Figure 3.1: Example of complexation of Al(III) by chelation 75

Figure 3.2: Typical Cyanex 272 extraction curves at different pH values 79

Figure 3.3: Schematic representation of the proposed extraction species of Fe(III) with primary amine and TBP (Jiayong et al., 1992) 82

Figure 4.1: Schematic diagram of conventional coagulation / flocculation / sedimentation process 93

Figure 4.2: Concentration of soluble Fe and Al species in equilibrium with amorphous hydroxides. (Fe_T and Al_T represent total soluble species) 97

Figure 5.1: Fe(II) oxidation and precipitation experimental setup 109

Figure 5.2: Change in ferrous Fe(II) concentration with time..... 117

Figure 5.3: Log species – pH diagram of soluble ferrous hydroxide species..... 117

Figure 5.4: Change of reaction rate constant with pH during Fe(II) oxidation..... 118

Figure 5.5: Effect of seeding on Fe oxidation (Fe(II) = 1000 mg/L, pH = 5)..... 119

Figure 5.6: Effect of Al(III) on the oxidation of Fe(II)..... 120

Figure 5.7: Titration curve of AMD with 4 M NaOH 121

Figure 5.8: Effect of pH on Fe(III) and Al(III) recovery through precipitation of the AMD 25°C 124

Figure 5.9: Solubility of the major heavy metals as a function of pH during Fe(III) and Al(III) precipitation at 25°C 125

Figure 5.10: SEM micrographs of the precipitates formed at pH 5; 25°C; A = C_S 0; B = Cs 0.5; C = Cs 1.0..... 128

Figure 5.11: X-ray powder diffraction pattern of the precipitate formed in the recycled solids experimental system at pH 5, 25°C and different seed concentration..... 129

Figure 5.12: BET surface area and PSD of precipitate at pH 5 131

Figure 5.13: Figure showing raw and settled precipitate (C_s = 2.0) after 120 min of settling..... 132

Figure 5.14: Settling rate of precipitate at different seed loading fraction..... 133

Figure 6.1: Organic/aqueous dispersion experimental setup with conical flasks 142

Figure 6.2: Separating funnels for phase separation 142

Figure 6.3: Effect of Cyanex 272 concentration on Fe(III) and Al(III) extraction. Experimental conditions: [Cyanex 272] = 0.06–0.63 M, [Al(III)] = 396 mg/L, [Fe(III)] = 4290 mg/L, O/A = 1:1, pH = 1.5, Temperature = 25 °C 146

Figure 6.4: Effect of Cyanex 272 concentration on Fe(III) and Al(III) extraction. Experimental conditions: [Cyanex 272] = 0.06–0.63 M, [Al(III)] = 396 mg/L, [Fe(III)] = 4290 mg/L, O/A = 1:1, pH = 2.5, Temperature = 25 ± 2°C, Equilibrium time = 45 min.147

Figure 6.5: Effect of equilibrium pH on Fe(III) extraction by 0.47 M Cyanex 272. Experimental conditions: [Cyanex 272] = 0.47 M, [Al(III)] = 396 mg/L, [Fe(III)] = 4290 mg/L, O/A = 1:1, pH = 1.5–3.0, Temperature = 25 ± 2°C, Equilibration time = 45 min.148

Figure 6.6: Effect of equilibrium pH on Al extraction by 0.47 M Cyanex 272. Experimental conditions: [Cyanex 272] = 0.47 M, [Al(III)] = 396 mg/L, [Fe(III)] = 4290 mg/L, O/A = 1:1, pH = 1.5–3.0, Temperature = 25 ± 2°C, Equilibration time = 45 min.149

Figure 6.7: McCabe-Thiele diagram for the extraction Fe(III) by 0.47 M Cyanex 272. Experimental conditions: [Cyanex 272] = 0.47 M, [Al(III)] = 396 mg/L, [Fe(III)] = 4290 mg/L, O/A = 1:1, pH = 2, Temperature = 25 ± 2°C, Equilibration time = 45 min. 153

Figure 6.8: McCabe-Thiele diagram for the extraction Al(III) by 0.47 M Cyanex 272. Experimental conditions: [Cyanex 272] = 0.47 M, [Al(III)] = 396 mg/L, [Fe(III)] = 4290 mg/L, O/A = 1:1, pH = 2, Temperature = 25 ± 2°C, Equilibration time = 45 min. 153

Figure 6.9: Effect of Sulphuric acid on Fe(IIII) and Al(III) stripping at 2:1O/A ratio 155

Figure 7.1: Experimental setup for precipitate dissolution to produce a coagulant 160

Figure 7.2: Jar tester for coagulation tests 163

Figure 7.3: Solubility of ferrihydrite precipitate dissolved in sulphuric acid of varying strengths (w/w) 166

Figure 7.4: AMD-PAFS^{p} coagulant 168

Figure 7.5: Performance evaluation of poly-alumino-ferric sulphate (Initial pH 7.0, temperature = 24.6 °C) during the treatment of brewery wastewater 171

Figure 7.6: Performance evaluation of poly ferric sulphate coagulant (Initial pH 7.0, temperature = 24.6 °C) during the treatment of brewery wastewater 171

Figure 7.7: Total dissolved solids as a function of coagulant dose during treatment of brewery wastewater 172

Figure 7.8: Performance of precipitation derived against solvent extraction derived AMD-PAFS coagulant 173

Figure 7.9: Total dissolved solids as a function of coagulant dose during treatment of brewery wastewater 174

Figure 8.1: Coagulant recovery flowsheet through oxidation-precipitation-dissolution 176

Figure 8.2: Coagulant recovery flowsheet through oxidation-solvent extraction..... 178

List of Tables

Table 1.1: Equivalent acidities 5

Table 1.2: Typical composition of acid mine drainage streams from different sources ... 7

Table 2.1: Values of standard electrode potential (E°), Gibbs free energy (G°) and equilibrium constant (K) for the one electron steps in the reduction of $O_{2(aq)}$ 28

Table 2.2 : Fe(II) oxidation expressions in acidic sulphate solutions 31

Table 2.3: The effect of ionic strength on Fe(II) oxidation rate constants 34

Table 2.4: Crystallographic data for ferrihydrite and goethite 47

Table 2.5: Hydrolysis of Fe(II) 51

Table 2.6: Hydrolysis of Fe(III) 54

Table 2.7: Solubility of the different iron oxyhydroxide mineral phases 55

Table 2.8: Hydrolysis of Al^{3+} 57

Table 2.9: Summary of solubility products of aluminium hydroxide 58

Table 5.1: Reagent grade chemicals used in oxidation and precipitation experiments 108

Table 5.2: Summary of Fe(II) oxidation test conditions 111

Table 5.3: Factors and values selected for co-precipitation of Fe and Al 112

Table 5.4: Summary of the chemical composition of raw AMD and effluents after precipitation 123

Table 5.5: The effect of seeding on precipitation at pH 7 126

Table 5.6: Effect of seeding on the particle settling rates..... 132

Table 6.1: Reagent grade chemicals in the extraction and stripping test work 141

Table 6.2: Extraction and stripping experimental conditions..... 144

Table 6.3: Some reported optimal equilibrium pH for Fe(III) and Al(III) extraction by different authors. 150

Table 6.4: Distribution coefficient and separation factor for Fe(III) and Al(III) at various Cyanex 272 concentrations and pH levels 151

Table 6.5: Chemical composition of raw AMD and loaded organic (loaded using 0.47 M Cyanex 272 at pH 2.5 and O/A ratio 1:1). 152

Table 6.6: Chemical composition of loaded organic and strip solution (stripped using 2M sulphuric acid and 2:1 O/A ratio). 154

Table 7.1: Experimental conditions..... 161

Table 7.2: Materials used in coagulation tests 162

Table 7.3: Coagulation experimental conditions 164

Table 7.4: Chemical composition of AMD-PAFS^{p} coagulant produced by precipitation at pH 5.0 and dissolution in 5.0% w/w sulphuric acid, AMD-PAFS^{sx} by SX using 0.47 M Cyanex 272 and stripping using 2 M sulphuric acid and conventional poly ferric sulphate coagulant..... 167

Table 7.5: Characteristics of the brewery wastewater that was treated with the AMD-PAFS and PFS coagulants..... 169

Table 8.1: Precipitation based flowsheet mass balance for coagulant recovery 177

Table 8.2: Solvent extraction based flowsheet mass balance for coagulant recovery 179

Table 8.3: Cost of chemicals..... 180

Table 8.4: Chemical needed to produce AMD-PAFS^{p} 181

Table 8.5: Chemical needed to produce AMD-PAFS^{sx} 181

Nomenclature

Symbol	Unit	Meaning
D	m^2s^{-1}	Diffusivity
Gr	$m^{-1}s$	Growth rate
ΔG	$Jmol^{-1}$	Gibbs free energy change
ΔG_r	$Jmol^{-1}$	Gibbs free energy of reaction
ΔG_{vol}	$Jmol^{-1}$	Gibbs free energy – generation of embryo volume
ΔG_{surf}	$Jmol^{-1}$	Gibbs free energy - generation of embryo surface
ΔG_{max}	$Jmol^{-1}$	Maximum activation Gibbs free energy barrier
J	m^3s^{-1}	Molar flux volume
K		Equilibrium constant
k_B	JK^{-1}	Boltzman constant
K_g	$m^4mol^{-1}s^{-1}$	Growth rate constant
K	s^{-1}	Rate constant
K_{sp}	$molL^{-1}$	Solubility product
M	kg	Mass
M	$molL^{-1}$	Molarity
N	mol	Number of moles
P	Pa	Pressure
pH		Negative log of H^+ activity
P_{O2}	Pa	Oxygen partial pressure
r_c	μm	Embryo critical size
R	$Jmol^{-1}K^{-1}$	Ideal gas constant
S		Saturation ratio
T	˚C or K	Temperature
T	min, h, s	Time
V	m^3	Volume
%		Percentage

List of abbreviations

AMD – Acid mine drainage

BET- (Brunauer-Emmett-Teller)

Cyanex 272 - bis(2,4,4-trimethylpentyl) phosphinic acid

D - Distribution coefficient (extraction)

D2EHPA - di-2ethylhexylphosphoric acid

H2DEH[MDP - PP′-di(2-ethylhexyl) methanediphosphonic acid

H2MEHP - mono 2-ethyl hexyl phosphoric acid

HEHEHP - 2-ethylhexyl-phosphonic acid (HEHEHP)

HCl - Hydrochloric acid

MIBK - Methyl isobutyl ketone

PSD – Particle size distribution

SX - Solvent extraction

TBP - Tributylphospate

TBT – Tributylphosphate

TDS – Total dissolved solids

TOPO - Trioctyle phosphine

XRD – X-ray diffraction

Introduction

1 General Introduction

This chapter serves as the general introduction to the work done in the study where Acid mine drainage (AMD) is introduced followed by its chemistry and the environmental repercussions associated with AMD generation. The chapter also discusses the objectives of the study.

1.1 Sources of AMD

The AMD is one of the largest environmental threats facing the world today. It is rated second only to global warming and stratospheric ozone depletion in terms of the ecological effects (Manders et al., 2009). The AMD emanates from the active or abandoned surface or underground mines and highway construction. During mining operations, a significant amount of mineral deposit containing pyrite, which is deprived of oxygen when it is still beneath the earth's surface, is exposed. The ores are crushed to liberate the desirable minerals like copper (Cu), gold (Au), zinc (Zn), nickel (Ni) or coal, prior to extraction. The waste product (tailings) containing the pyrite becomes exposed to surface conditions i.e., oxygen and water and results in the generation of AMD (Cotter-Howells et al., 2000). In the case of abandoned open-pit or underground mines, water may enter the mines through several ways including via mine faults, galleries and adits from the surface as rainwater or from groundwater. If this water is not pumped out in a timely manner, AMD will be formed due to the reaction of water and oxygen with the exposed sulphide minerals. Highway constructions also contribute to AMD generation due to the presence of sulphides in the disturbed land. **Figure 1.1** shows AMD coming from an abandoned mine.

Figure 1.1: Abandoned mine and AMD generation (Michaud, 2015**)**

1.2 Chemistry of AMD formation

The AMD is caused by the weathering of metal sulphide minerals, predominantly pyrite (FeS_2) when exposed to air and water. The weathering of these minerals produces acidic waters (pH>3) which solubilize other heavy and toxic metals. It is one of the major environmental impacts of coal and metal mining processes. This is because mineral resources such as coal and other metal ores are often rich in sulphide minerals. When exposed to water and air, either during mining operations or once the mine has been abandoned or because of natural weathering, the sulphide bearing minerals are oxidized and generate sulphuric acid. The oxidation of the mineral sulphides is a complex function of water, oxygen and the presence of extremely acidophilic microorganisms (Simate and Ndlovu, 2014). The formation of AMD from pyrite can be represented by a series of reactions and side reactions (Schippers and Sand, 1999). However, the pyrite oxidation process may be represented according to **Equation 1.1**.

$$2FeS_{2(s)} + 7O_{2(g)} + 2H_2O_{(l)} \rightarrow 2Fe^{2+}_{(aq)} + 4H^{+}_{(qa)} + 4SO^{2-}_{4(aq)} \quad 1.1$$

The reaction represented in **Equation 1.1** produces acid, soluble ferrous iron cations, Fe(II), sulphate anions (SO_4^{2-}) and the aqueous hydrogen cations (H^+). The Fe(II) produced is further oxidized by oxygen to ferric ions, Fe (III), according to **Equation 1.2**, with the reaction catalyzed by the presence of acidophilic microorganisms.

$$4Fe^{2+}_{(aq)} + 4H^{+}_{(aq)} + O_{2(g)} \rightarrow 4Fe^{3+}_{(aq)} + 2H_2O_{(l)} \quad 1.2$$

The Fe(III) produced can either undergo hydrolysis or acts as an oxidant to further oxidize the pyrite according to **Equation 1.3** and **1.4**, respectively.

$$Fe^{3+}_{(aq)} + 3H_2O_{(l)} \rightarrow Fe(OH)_{3(s)} + 3H^{+}_{(aq)} \quad 1.3$$

The reaction, according to **Equation 1.4**, leads to the production of more hydrogen ions. The reaction sequence continues until all the exposed pyrite is oxidized (Tuszyński et al., 1994).

$$FeS_{2(s)} + 14Fe^{3+}_{(aq)} + 8H_2O_{(l)} \rightarrow 15Fe^{2+}_{(aq)} + 2SO^{2-}_{4(aq)} + 16H^{+}_{(aq)} \quad 1.4$$

The net reaction results in the generation of 4 moles of hydrogen ions per mole of pyrite oxidized and can be represented by **Equation 1.5** below**.** Figure 1.2 is a hypothetical scheme for the oxidation of pyrite or metal sulphide by Fe and Sulphur-oxidizing acidophilic bacteria producing sulphuric acid. The detailed explanation of the pyrite oxidation scheme is provided by Schippers and Sand (1999).

$$4FeS_{2(s)} + 15O_{2(g)} + 14H_2O_{(l)} \rightarrow 4Fe(OH)_{3(s)} + 8SO^{2-}_{4(aq)} + 16H^{+}_{(aq)} \quad 1.5$$

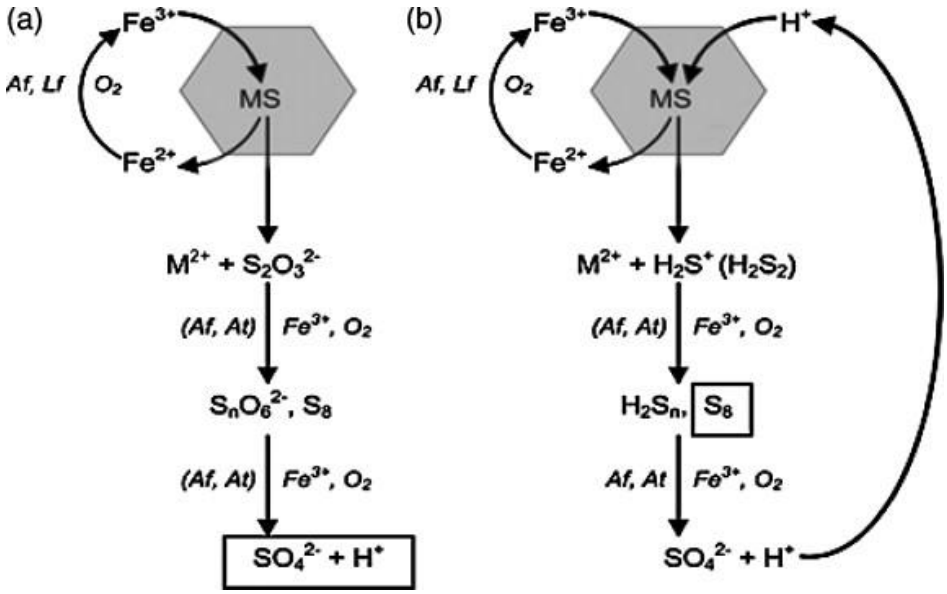

Figure 1.2: Hypothetical schemes for the oxidation of pyrite or metal sulphide by iron and Sulphur-oxidizing acidophilic bacteria producing sulphuric acid (Schippers and Sand, 1999)

The net acidity of a solution sample can be measured directly by titration with a standard base solution. Net acidity is often reported as mg/L calcium carbonate equivalent. Acidity in AMD can be as high as 10,000 mg/L calcium carbonate equivalent (Stauffer and Lovell, 1968). However, the total acidity of AMD is the sum of the hydrogen ion (H^+) content and the potential acid that can be produced by the hydrolysis of the mineral cations present. For coal mine drainage, the acidic components are primarily accounted for by free protons and dissolved Fe(II), Fe(III), Al(III), and Mn(II). The base component is primarily accounted for by the bicarbonate. A standard way to calculate the acidity for coal mine drainage is (Hedin, 2006);

$$\text{Acid}^{cal}=50\left(\left(2\times\frac{Fe^{2+}}{56}\right)+\left(3\times\frac{Fe^{3+}}{56}\right)+\left(3\times\left(\frac{Al}{27}\right)\right)+\left(2\times\frac{Mn}{55}\right)+1000\times10^{-pH}\right)-\text{alkalinity} \qquad 1.6$$

The acidity and alkalinity are measured as mg/L $CaCO_3$ and metal ions in mg/L. On the other hand, Zawadzki, (1968) presented equivalent acidities corresponding to the main

cationic constituencies of AMD based on stoichiometric calculations as shown in **Table 1.1**.

There are several other minerals that are found in association with the pyrite such as sphalerite, millerite, galena, chalcopyrite, k-fieldspar, etc. The acid formed during the weathering of pyrite results in the dissolution of these minerals, thus releasing the associated metal and metalloid species (Stumm and Morgan, 2012; Jacobs et al., 2014) such that the concentration of heavy metals in AMD can be in excess of 3000 mg/L (Govind et al., 1997). **Equations 1.7** to **1.11** represents the dissolution of these minerals (Costello, 2003; Younger et al., 2005). In addition to the elements already stated, there are still other elements found AMD, especially coal AMD which include calcium and magnesium due to the dissolution of limestone ($CaCO_3$), dolomite ($CaMg(CO_3)_2$) and magnesite ($MgCO_3$). These elements are significant in mine water because they form highly insoluble hydroxides at pH levels of most coal mine drainage treatment. **Table 1.2** shows the t**y**pical composition of acid mine drainage from different sources.

Table 1.1: Equivalent acidities

Cation (1 mg/L)	Acidity in mg/L H_2SO_4	Acidity in mg/L $CaCO_3$
H^+	49	50
Fe^{2+}	1.77	1.80
Fe^{3+}	2.65	2.70
Al^{3+}	5.44	5.55
Mn^{2+}	1.78	1.82

Chalcopyrite: $$CuFeS_{2(s)}+4O_{2(aq)} \rightarrow Cu^{2+}{}_{(aq)}+Fe^{2+}_{(aq)}+SO^{2-}_{4(aq)} \quad (1.7)$$

Galena: $$PbS_{(s)}+2O_{2(aq)} \rightarrow Pb^{2+}{}_{(aq)}+SO^{2-}_{4(aq)} \quad (1.8)$$

Sphalerite: $ZnS_{(s)} + 2O_{2(aq)} \rightarrow Zn^{2+}_{(aq)} + SO^{2-}_{4(aq)}$ 1.9

Millerite: $NiS_{(s)} + 2O_{2(aq)} \rightarrow Ni^{2+}_{(aq)} + SO^{2-}_{4(aq)}$ 1.10

K-fieldspar $KAlSi_3O_{8(aq)} + 4H^{+}_{(aq)} + 4H_2O_{(l)} \rightarrow Al^{3+}_{(aq)} + 3Si(OH)^{0}_{4(aq)} + 4K^{+}_{(aq)}$ 1.11

Table 1.2: Typical composition of acid mine drainage streams from different sources

AMD source	Vaal Barrage, SA[1]	SA gold mine[2]	Upper free port seam, West Virginia USA[3]	Santa Catarina, Brazil[4]	Berkeley pit mine, Montana USA[5]	Mattabi mines ltd, Ontario Canada[6]	SA discharge standard[7]
pH	2.3	1.65	2.6	2	2.2	2.2	6-9
Fe	5999		172.5	3360	514	2360	
Al	911.3	249	88.6	1260	293	160	10
Ca	649	300	205	11.8	-	112	200
Mg	2023	359	54.1	8.4	-	517	200
Mn	43.3	113	2.3	161.5	223	160	10
Zn	59.6	10.1	3.1	82.9	630	1630	10
Ni	-	5.75	1.16		2.14	2.1	
Cu	-	1.8	0.07	0.27	223	19	
Pb	-	0.349	-	0.08	-	3.8	
As	-	-	-	0.02	0.15	-	
SO_4^{2-}	17804	6305	-	9120	2400	7528	300

[1]Steffen, 1989; [2]Feng et al., 2000; [3]Wei et al., 2005; [4]Menezes et al., 2010; [5]Tabak et al., 2003; [6]Rao et al., 1992

[7]National Gazette, 2013

1.3 Environmental and ecological impact of acid mine drainage

As discussed in the previous section, pyrite weathering introduces acid and heavy metals into the environment. At low heavy metal concentration, there is an autonomous ability by the environment to absorb the effects of AMD through a combination of dilution, biological action and neutralization. However, this ability is drastically reduced at a high heavy metal concentration (Evangelou, 1998). The dissolved heavy metals pose a serious threat not only to human health, but animal and ecological systems. The AMD has the potential to devastate streams, rivers and aquatic life (Fripp et al., 2000; Garland, 2011; Ndlovu et al., 2013; Singh et al., 2011; Monachese et al., 2012). This is largely because the heavy metals are non-biodegradable and tend to accumulate in living organisms thereby causing various diseases and disorders (Moreno et al., 2001). These effects of AMD on the environment are summarized in **Figure 1.3**.

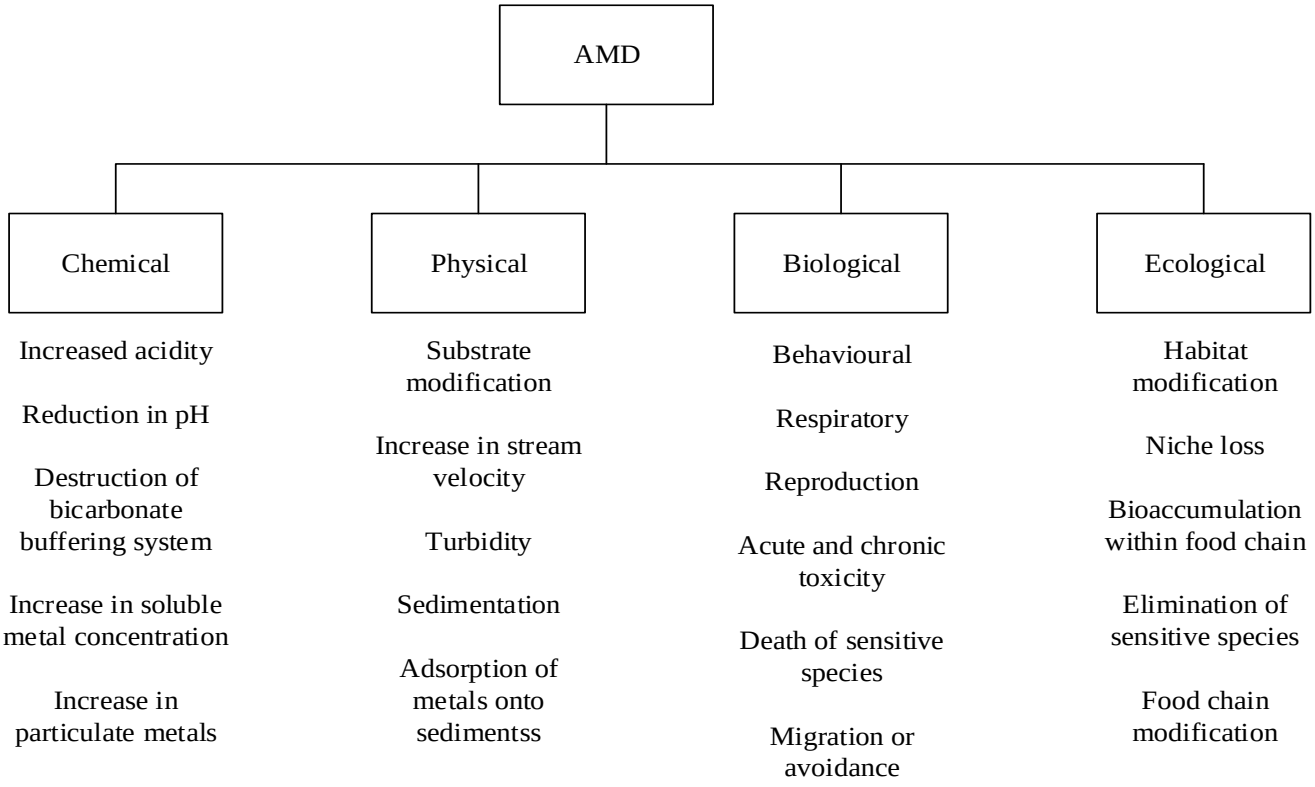

Figure 1.3: The major effects of AMD on the environment (Gray, 1997)

1.4 Treatment of acid mine drainage

The dangers that AMD poses means it must be treated to abate the devastating effects it has on the environment. Currently, there are two categories of AMD treatment technologies, i.e., prevention (or source control) and remediation techniques.

1.4.1 Source control

As already alluded to, AMD discharges occurs when sulphide bearing minerals are exposed to oxygen and water. It simply means that if the pyrite is starved of oxygen and water, the generation of AMD could be avoided. Flooding and sealing the mine could be considered a source control option (Fernández-Rubio et al., 1987). Flooding and sealing of the mine could result in the rapid depletion of dissolved oxygen by microbial activity and oxidizing reactions and thus stabilizing the system. However, the scarcity of knowledge of the underground working at historic mine sites remains a challenge (Florence, 2015). Source control is not limited to the underground workings and discharges from the mine adits. For example, surface waters can be diverted in order to help reduce the amount of water entering the mine (Skousen et al., 2000). Mine tailings and waste rock piles are also a major source of diffuse pollution. Exposure of these types of wastes to the atmosphere and weathering causes the metals in the waste tips to leach into nearby water courses and percolate through the sediments below. This is, therefore, a potential risk of contaminating the ground water. These wastes can be kept out of contact with water and limit the diffusion of oxygen by capping such areas with soil or organic layer thereby reducing the possibility of weathering (Johnson and Hallberg, 2005). Furthermore, capping of the waste tips can help prevent the spread of the contaminated fines material that is easily transported by wind to the surrounding areas (Herbert, 1999). Although source control of AMD has been researched and explored, the prevention of AMD from forming is difficulty. As such, the only way to control pollution coming from AMD sources is often to use treatment technologies that clean the acidic water prior to discharge into the receiving water body.

1.4.2 Remediation

The practical difficulties in constraining AMD formation at the source makes remediation the widely used treatment technique to reduce the impact of this pollutant (Johnson and Hallberg, 2005). The type of treatment option used depends on many factors such as inflow water chemistry, flow rate, discharge consent, topography, land availability, the cost, operations management, waste disposal and security. At the moment, the most widely applied methods for remediation of AMD is an active treatment process involving chemical neutralization reagents (Coulton et al., 2003; Johnson and Hallberg, 2005).

There are three different neutralization processes employed, including the conventional neutralization, the recycle sludge and the high density sludge processes (HDS) (Streeter et al., 1971; Günther et al., 2003). The conventional process, shown in **Figure 1.4**, is a very simple process which involves contacting the AMD with lime while ensuring good mixing, aerating the mixture and subsequent removal of the precipitate by solid/liquid separation. The disadvantage of this process has largely been the longer settling times because of the formation of finer precipitate particles which lead to gel formation. In addition, the sludge produced is voluminous, contains 2-5% solids, which create disposal challenges (Coulton et al., 2003; Streeter et al., 1971). These challenges, associated with the conventional process, led to the development of the recycle sludge process and later the HDS process (Streeter et al., 1971; Coulton et al., 2003; Günther et al., 2003). The two processes are similar in many respects and differ only in the fact that the recycle sludge process involves the addition of the recycle sludge to the fresh AMD prior to lime addition, while the HDS process involves contacting the recycle sludge with lime prior to contacting it with AMD. **Figure 1.5** shows the HDS process flow diagram. In the recycle sludge and HDS processes, the addition of the recycled sludge to the neutralization tanks forces precipitation to occur on the surface of the existing recycled sludge. This results in the elimination of gel formation, which is typical of a single pass system and improves the dewaterability of the sludge as well as the solids concentration which is typically around 15-30%. The recycle sludge and HDS processes offer the following advantages over the conventional process;

- The density of the sludge is 5-10 times higher than that of the conventional process
- The improved dewaterability and settling rates means that a saving is made on the equipment and running costs

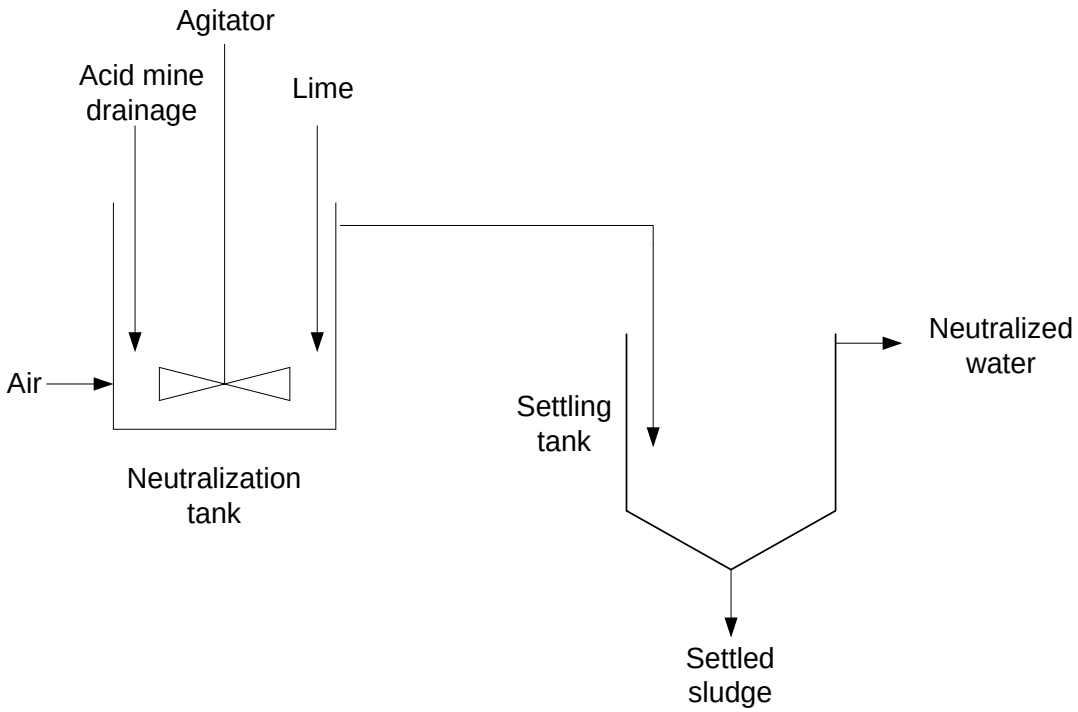

Figure 1.4: The conventional process for AMD neutralization

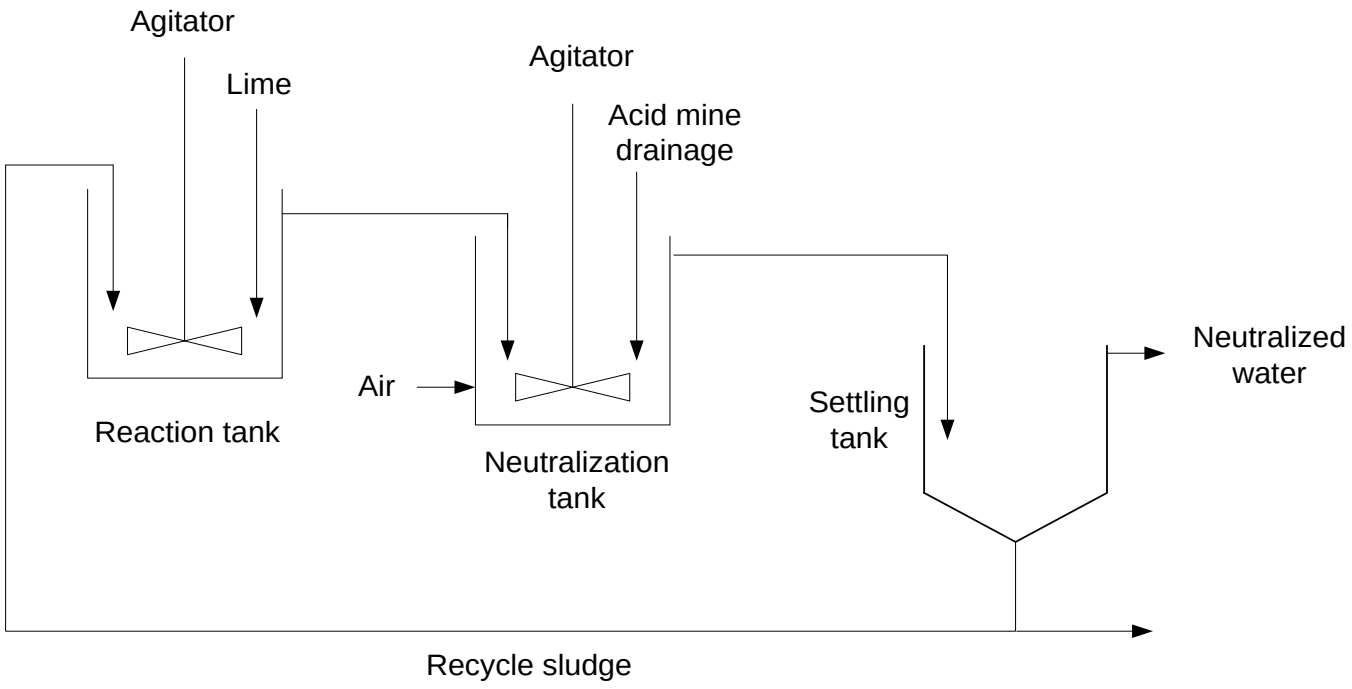

Figure 1.5: The High Density Sludge process for AMD neutralization

Although the recycle sludge and HDS processes offers some advantages, many challenges still exist including (Hove, 2008);

- Although there is an improvement in the solids concentration compared to the conventional process, significant quantities of water which could be recovered, is lost;
- The large volume of sludge produced needs a land area for disposal;
- The process produces metastable phases whose long-term stability has not been established. As such, post precipitation stabilization before final solids disposal is required.
- The high cost of treatment because no revenue is realized
- The metals that could have been recovered from the AMD are lost.

In addition to the stated challenges, the environmental legislations being implemented today are increasingly stringent. This means that there is need for a well-managed disposal site for the sludge. Mostly, the polymer linings in combination with soil and clay layers are used to make the sludge disposal ponds to avoid contamination of the soil and the surrounding environment (Lahtinen, 2006). The cost of the sludge disposal ponds adds to the overall cost of AMD treatment.

The challenges discussed as well as the environmental legislation have led to investigations of either improving the recycle sludge and HDS processes to produce a stable sludge (Hove et al., 2009; John, 2016) or resource recovery techniques that would produce a waste-free and stable residue (Černá, 1995; Mansur, 2011).

1.5 Motivation

As discussed in **Section 1.4,** the chemical neutralization of AMD produces a sludge which typically contains about 2-5% and 15-30% solids, for the conventional and recycle sludge/ HDS processes, respectively. The sludge contains a high concentration of the heavy metals including Fe, Al, Mg, Mn Zn and other metals, predominantly as hydroxides (Menezes et al., 2010). The voluminous sludge is difficult to dispose because of the scarcity of land as well as the possibility of the metals to re-dissolve. However, the metals in the AMD can be recovered with the objective of obtaining valuable products while meeting the effluent discharge limits. This is one of the potential ways to extend the use of natural resources. Additionally, the benefits such as mitigation of liabilities and the generation of revenue to subsidize AMD treatment cost may be realized (Simate and Ndlovu, 2014). This paradigm shift has led to several studies being conducted to investigate the recovery of valuable products from AMD. This including iron oxide pigments for production of paint (Hedin, 2003; Macingova and Luptakova, 2014; Ryan et al., 2017); ferric oxide nanoparticles (Wei and Viadero, 2007); inorganic pigments (Marcello et al., 2008); metals like Fe, Al, Zn, and Cu (Michalková et al., 2013; Park et al., 2015; Sahinkaya et al., 2009; Wei et al., 2005); acid and water (Buzzi et al., 2013; Martí-Calatayud et al., 2014; Masindi, 2017; Nleya, 2016); the use of AMD neutralization sludge in brick and cement production, and as an artificial soil

additive (Dudeney et al., 2004; Evenson and Nairn, 2000; Silsbee, 2006). Simate and Ndlovu (2014) also cites several other projects that have been undertaken to recover valuable material from AMD including; CSIRABC (alkali–barium–calcium) process, SAVMIN process, SPARRO process, GYP-CIX process, THIOPAQ process and The Rhodes BioSURE process. There is also a huge potential to recover alternative coagulants from AMD for water and wastewater treatment. The high concentration of Fe(III) and Al(III) in AMD, as high as 5000 mg/L for Fe and 500 mg/L for Al(III), has led to studies that have focused on developing an understanding of its potential reuse as a coagulant in wastewater treatment (Lopes, 2011; Rao et al., 1993, 1992; Salama et al., 2015). Most of these studies have focused on recovering of Fe-based coagulants.

This study sought to develop a method of recovering a coagulant containing both Fe(III) and Al(III) from AMD with a view of partly offsetting the treatment cost of the AMD remediation process. The research aimed at alleviating the problems of the handling and disposal of coal and gold mining AMD neutralization sludge through the recovery of Fe(III) and Al(III), which are two of the major constituents of AMD. The removal of Fe(III) and Al(III) would subsequently reduce the volume of the sludge by 90%. Therefore, the research was undertaken with the understanding that the economic viability of the AMD treatment processes is a complex issue which must be examined with the view of the recovery of resources while considering the condition of the final sludge and its disposal concerns.

1.6 Objectives

The mining-metal industry is aware of the opportunities to recover valuable resources from AMD. This combines the generation of revenue with environmental sustainability. This study, therefore, explored sustainable recovery of Fe(III) and Al(III) based coagulants from an AMD solution. To achieve this, the following specific objectives were pursued;

- Characterization of AMD solutions;
- Study the kinetics of ferrous sulphate oxidation reactions;

- Develop and test the flowsheets for the recovery of poly-alumino-ferric sulphate (AMD-PAFS) coagulant by;
    i. Seeded precipitation (recycle sludge process)
    ii. Solvent extraction (SX)
- Test the AMD-derived coagulants for application in water treatment processes
- Compare the efficiency of the AMD-derived coagulants to the commercially available reagents
- Perform an economic analysis for the developed flow sheets

1.7 Deliverables

The following were the deliverables of the study:

i. A literature review of the Fe(III) and Al(III) precipitation chemistry backed by a thermodynamic study of the most important species and stability regions, at room temperature as a function of pH and Eh
ii. A literature review of SX of Fe(III) and Al(III)
iii. Kinetics of Fe(II) oxidation
iv. Kinetics of the precipitation and SX of Fe(III) and Al(III) from AMD
v. Characterization of precipitate and SX liquor
vi. The study of the precipitate dissolution in sulphuric acid to produce a coagulant
vii. Developed and tested process flow sheets for coagulant recovery

1.8 Significance of the study

Although resources recovery from AMD has been studied extensively in the last decade, a practical and economic benefit of the recovery of two of the most predominant species (Fe and Al(III)) has not been widely explored. This work, therefore, presents an opportunity to expand on the current knowledge to include;

1. The economic benefits of employing the HDS principle in the recovery of Fe(III) and Al(III) to produce a precipitate that has;
    i. good filtration characteristics
    ii. improved purity
    iii. the potential to be used to produce a coagulant
2. The economical evaluation of SX to recover Fe(III) and Al(III) to produce a marketable coagulant

The results of this study are expected to expand the potential use of AMD as a resource and conjure up further research into possible industrial application.

1.9 Research methodology

The research methodology for this study involved the following tasks;

1.9.1 Literature review

The literature review was conducted to discuss the characterization of AMD, from different mines, the oxidation of Fe(II) to Fe(III), the precipitation and SX of Fe and Al(III) as well as the associated metals found in AMD and the review of the coagulation process.

1.9.2 Experimental design and laboratory testing

Based on the information from literature, an experimental design program which included material selection was formulated. The design, which included experimental testing at various conditions, involved;

1. Fe(II) oxidation using air at various test conditions
2. The oxidation and precipitation of Fe(III) and Al(III) using sodium hydroxide
3. Dissolution of Fe/Al precipitate in various concentration of sulphuric acid to obtain a coagulant
4. The SX of Fe(III) and Al(III) using Cyanex 272 in Shellsol D70
5. Stripping of Fe(III) and Al(III) using various concentrations of sulphuric acid to obtain a coagulant
6. Testing the AMD-derived coagulants against the conventional poly ferric sulphate coagulant.

1.9.3 Data analysis

In line with the experimental design, a series of laboratory tests under various conditions were carried out to test each quality determinant chosen. The output data from these laboratory tests were used to determine the efficiency of air oxidation of Fe(II), co-precipitation of Fe(III) and Al(III), extraction and stripping of Fe(III) and Al(III) and the effectiveness of AMD-derived coagulants in wastewater treatment, brewery wastewater used in this study.

1.9.4 Conclusions and recommendations

When the data analysis and review was completed, the experimental results were used to draw conclusions and recommendations. The conclusions include significant findings of the production of Fe(III) and Al(III) containing coagulants from AMD using oxidation-precipitation - dissolution or oxidation – extraction - stripping processes. The recommendations highlight some of the shortcomings of the process flowsheets develop and the need to improve on the work that has been done.

1.10 Thesis layout

Chapter 1 gives a general overview of AMD and the widely used AMD treatment technologies. The problem statement to the present research is then discussed followed by the objectives and the research methodology used to meet the set objectives.

Chapter 2, **Chapter 3** and **Chapter 4** are the literature review chapters. In the literature review of each chapter, a theoretical background is firstly evaluated before discussing the related applied research. A literature survey covering the oxidation of Fe(II) by molecular oxygen (from air) as well as the precipitation of Fe(III) and Al(III) at atmospheric conditions is presented in **Chapter 2**. Concepts related to different precipitation mechanisms and their effect on Fe and Al(III) removal efficiencies, properties such as particle surface area, particle sizes, particle settling rates and solid-liquid separation are reviewed. **Chapter 3** discusses the SX principles, the applied research of Fe(III) and A(III) extraction and stripping using different extractants and stripping agents. The chapter also discusses the extraction and stripping of the other heavy metals found in AMD. **Chapter 4** presents the theoretical background of coagulation followed by the discussion of the conventional coagulants that are used in water and wastewater treatment.

Presented in **Chapter 5**, **Chapter 6** and **Chapter 7** is the experimental work conducted in this study. In each chapter, the experimental materials and methodologies are discussed followed by the presentation of the results obtained.

Chapter 5 is divided into three main parts: (i) experimental materials and methodologies, (ii) Fe(II) oxidation experimental results and (iii) Fe(III) and Al(III) precipitation and precipitate characterization results. In **Chapter 6**, the SX experimental materials and methodologies as well as the experimental results are presented. **Chapter 7** discusses the production of the coagulants from Fe(III) and Al(III) precipitate and SX strip liquor. The chapter further compares the performance of the AMD-derived coagulants against conventional poly ferric sulphate (PFS) coagulant. Presented in **Chapter 8** are the suggested flowsheets and mass balances.

The main conclusions are presented in **chapter 8.3** together with the recommendations for future work. Immediately after the conclusions and recommendations follows the Appendices.

1.11 Summary

Chapter 1 gives the background and problem statement of the study and spells out the objectives. The significance of the study, which is to expand on the current knowledge base, is also spelled out. The chapter is concluded with the brief discussion of the research methodology and the dissertation layout.

References

Buzzi, D.C., Viegas, L.S., Rodrigues, M.A.S., Bernardes, A.M., Tenório, J.A.S., 2013. Water recovery from acid mine drainage by electrodialysis. Minerals Engineering 40, 82–89. https://doi.org/10.1016/j.mineng.2012.08.005

Černá, M., 1995. Use of solvent extraction for the removal of heavy metals from liquid wastes. Environmental monitoring and assessment 34, 151–162.

Costello, C., 2003. Acid mine drainage: innovative treatment technologies. Washington DC: US Environmental Protection Agency Office of Solid Waste and Emergency Response.

Cotter-Howells, J., Campbell, L., Valsami-Jones, E., Batchelder, M., 2000. Environmental mineralogy: microbial interactions, anthropogenic influences, contaminated land and waste management. Mineralogical Society.

Coulton, R., Bullen, C., Hallett, C., 2003. The design and optimisation of active mine water treatment plants. Land Contamination and Reclamation 11, 273–280.

David Michaud, 2015. Acid rock drainage. 911 Metallurgist. URL https://www.911metallurgist.com/blog/acid-mine-rock-drainage-amd-ard (accessed 3.11.20).

Dudeney, A., Neville, K., Tarasova, I., Heath, A., Smith, S., 2004. Utilisation of Ochreous sludge as a soil amendment. Presented at the Proceedings of the symposium: mine water, pp. 19–23.

Evangelou, V., 1998. Pyrite chemistry: the key for abatement of acid mine drainage, in: Acidic Mining Lakes. Springer, pp. 197–222.

Evenson, C., Nairn, R., 2000. Enhancing phosphorus sorption capacity with treatment wetland iron oxyhydroxides. Proceedings, 17th National Meeting of the American Society for Surface Mining and Reclamation. Tampa, Florida.

Feng, D., Aldrich, C., Tan, H., 2000. Treatment of acid mine water by use of heavy metal precipitation and ion exchange. Minerals Engineering 13, 623–642. https://doi.org/10.1016/S0892-6875(00)00045-5

Fernández-Rubio, R., Fernández-Lorca, S., Arlegui, J.E., 1987. Preventive techniques for controlling acid water in underground mines by flooding. International journal of mine water 6, 39–52.

Florence, K., 2015. Mechanisms of the removal of metals from acid and neutral mine water under varying redox systems.

Fripp, J., Ziemkiewicz, P.F., Charkavorki, H., 2000. Acid mine drainage treatment. DTIC Document.

Garland, R., 2011. Acid mine drainage-can it affect human health?

Govind, R., Kumar, U., Puligadda, R., Antia, J., Tabak, H., 1997. Biorecovery of metals from acid mine drainage, in: Emerging Technologies in Hazardous Waste Management 7. Springer, pp. 91–101.

Gray, N., 1997. Environmental impact and remediation of acid mine drainage: a management problem. Environmental Geology 30, 62–71.

Günther, P., Maree, J.P., Strobos, G., Mtimikulu, J.S., 2003. Neutralisation of acid leachate in a coal processing plant with calcium carbonate, in: Mine Water and the Environment: 8th International Congress on Mine Water & the Environment, Proceedings, Johannesburg, South Africa. pp. 367–382.

Hedin, R.S., 2006. The use of measured and calculated acidity values to improve the quality of mine drainage datasets. Mine Water and the Environment 25, 146–152.

Hedin, R.S., 2003. Recovery of marketable iron oxide from mine drainage in the USA. Land Contamination and Reclamation 11, 93–98.

Herbert, R., 1999. Sulfide oxidation in mine waste deposits–A review with emphasis on dysoxic weathering, MiMi 1999: 1, ISSN 1403-9478.

Hove, M., 2008. The kinetics and mechanisms of the oxidation and precipitation of iron : the high density sludge (HDS) process.

Hove, M., Van Hille, R.P., Lewis, A.E., 2009. The effect of different types of seeds on the oxidation and precipitation of iron. Hydrometallurgy 97, 180–184. https://doi.org/10.1016/j.hydromet.2009.03.001

Jacobs, J.A., Lehr, J.H., Testa, S.M., 2014. Acid mine drainage, rock drainage, and acid sulfate soils: causes, assessment, prediction, prevention, and remediation. John Wiley & Sons.

John, M., 2016. Low temperature synthesis of nano crystalline zero-valent phases and (doped) medal oxides as AxB3-xO4 (ferrite), ABO2 (delafossite), A2O and AO: a new process to treat industrial wastewaters? Ludwig-Maximilians-Universität München.

Johnson, D.B., Hallberg, K.B., 2005. Acid mine drainage remediation options: a review. Science of The Total Environment 338, 3–14. https://doi.org/10.1016/j.scitotenv.2004.09.002

Lahtinen, M., 2006. Hematite versus jarosite precipitation in zinc production. Presented at the Iron Control Technologies, Proceedings of the third international symposium on iron control in hydrometallurgy, Montreal, CANADA, 2006.

Lopes, F.A., 2011. Acid mine drainage as source of iron for the treatment of sewage by coagulation and Fenton’s reaction. Mine Water 4.

Macingova, E., Luptakova, A., 2014. Recovery of iron from acid mine drainage in the form of oxides. Inżynieria Mineralna 15.

Manders, P., Godfrey, L., Hobbs, P., 2009. Briefing note: Acid mine drainage in South Africa. CSIR, Pretoria, South Africa.

Mansur, M.B., 2011. Solvent extraction for metal and water recovery from industrial wastes and effluents. Rem: Revista Escola de Minas 64, 51–55.

Marcello, R.R., Galato, S., Peterson, M., Riella, H.G., Bernardin, A.M., 2008. Inorganic pigments made from the recycling of coal mine drainage treatment sludge. Journal of Environmental Management 88, 1280–1284. https://doi.org/10.1016/j.jenvman.2007.07.005

Martí-Calatayud, M.C., Buzzi, D.C., García-Gabaldón, M., Ortega, E., Bernardes, A.M., Tenório, J.A.S., Pérez-Herranz, V., 2014. Sulfuric acid recovery from acid mine drainage by means of electrodialysis. Desalination, Special Issue: Desalination Using Membrane Technology 343, 120–127. https://doi.org/10.1016/j.desal.2013.11.031

Masindi, V., 2017. Recovery of drinking water and valuable minerals from acid mine drainage using an integration of magnesite, lime, soda ash, CO (sub) 2 and reverse osmosis treatment processes.

Menezes, J.C.S.S., Silva, R.A., Arce, I.S., Schneider, I.A.H., 2010. Production of a poly-alumino-iron sulphate coagulant by chemical precipitation of a coal mining acid drainage. Minerals Engineering 23, 249–251. https://doi.org/10.1016/j.mineng.2009.11.008

Michalková, E., Schwarz, M., Pulišová, P., Máša, B., Sudovský, P., 2013. Metals Recovery from Acid Mine Drainage and Possibilities for their Utilization. Polish Journal of Environmental Studies 22.

Monachese, M., Burton, J.P., Reid, G., 2012. Bioremediation and Tolerance of Humans to Heavy Metals through Microbial Processes: a Potential Role for Probiotics? Applied and Environmental Microbiology 78, 6397–6404. https://doi.org/10.1128/AEM.01665-12

Moreno, N., Querol, X., Ayora, C., Pereira, C.F., Janssen-Jurkovicová, M., 2001. Utilization of zeolites synthesized from coal fly ash for the purification of acid mine waters. Environmental science & technology 35, 3526–3534.

National Gazette, 2013. National Gazette No. 36820, 06 September 2013, Vol. 579 [WWW Document]. URL https://www.greengazette.co.za/documents/national-gazette-36820-of-06-september-2013-vol-579_20130906-GGN-36820.pdf (accessed 9.20.19).

Ndlovu, S., Simate, G.S., Seepe, L., Shemi, A., Sibanda, V., Van Dyk, L.D., 2013. The removal of Co2+, V3+ and Cr3+ from waste effluents using cassava waste. South African Journal of Chemical Engineering 18, 51–69.

Nleya, Y., 2016. Removal of toxic metals and recovery of acid from acid mine drainage using acid retardation and adsorption processes (Thesis). Johannesburg, South Africa.

Park, S.-M., Yoo, J.-C., Ji, S.-W., Yang, J.-S., Baek, K., 2015. Selective recovery of dissolved Fe, Al, Cu, and Zn in acid mine drainage based on modeling to predict precipitation pH. Environmental Science and Pollution Research 22, 3013–3022.

Rao, S.R., Gehr, R., Riendeau, M., Lu, D., Finch, J.A., 1992. Acid mine drainage as a coagulant. Minerals Engineering 5, 1011–1020. https://doi.org/10.1016/0892-6875(92)90128-V

Rao, S.R., Leroux, M., Finch, J.A., 1993. Metals removal from acid mine drainage-chemical methods. (No. v4-1341– 03). , Noranda Technology Centre.

Ryan, M.J., Kney, A.D., Carley, T.L., 2017. A study of selective precipitation techniques used to recover refined iron oxide pigments for the production of paint from a synthetic acid mine drainage solution. Applied Geochemistry 79, 27–35. https://doi.org/10.1016/j.apgeochem.2017.01.019

Sahinkaya, E., Gungor, M., Bayrakdar, A., Yucesoy, Z., Uyanik, S., 2009. Separate recovery of copper and zinc from acid mine drainage using biogenic sulfide. Journal of Hazardous Materials 171, 901–906.

Salama, E.-S., Kim, J.R., Ji, M.-K., Cho, D.-W., Abou-Shanab, R.A.I., Kabra, A.N., Jeon, B.-H., 2015. Application of acid mine drainage for coagulation/flocculation of microalgal biomass. Bioresour. Technol. 186, 232–237. https://doi.org/10.1016/j.biortech.2015.03.078

Schippers, A., Sand, W., 1999. Bacterial leaching of metal sulfides proceeds by two indirect mechanisms via thiosulfate or via polysulfides and sulfur. Appl. Environ. Microbiol. 65, 319–321.

Silsbee, Michael, 2006. The Use of Sludge Generated by the Neutralization of Acid Mine Drainage in the Cement Industry (No. EPD06021). United States Environmental Protection Agency.

Simate, G.S., Ndlovu, S., 2014. Acid mine drainage: Challenges and opportunities. Journal of Environmental Chemical Engineering 2, 1785–1803. https://doi.org/10.1016/j.jece.2014.07.021

Singh, R., Gautam, N., Mishra, A., Gupta, R., 2011. Heavy metals and living systems: an overview. Indian journal of pharmacology 43, 246.

Skousen, J.G., Sexstone, A., Ziemkiewicz, P.F., 2000. Acid mine drainage control and treatment. Reclamation of drastically disturbed lands 41, 131–168.

Stauffer, T.E., Lovell, H.L., 1968. The oxygenation of iron (ji) - relationship to coal mine drainage treatment 167.

Steffen, R.& K., 1989. Research on the contribution of mine dumps to the mineral pollution load in the Vaal Barrage (No. WRC report No 136/1/89). Pretoria, South Africa.

Streeter, R.C., Young, R., Glenn, R.A., 1971. Studies on densification of coal mine drainage sludge.

Stumm, W., Morgan, J.J., 2012. Aquatic chemistry: chemical equilibria and rates in natural waters. John Wiley & Sons.

Tabak, H.H., Scharp, R., Burckle, J., Kawahara, F.K., Govind, R., 2003. Advances in biotreatment of acid mine drainage and biorecovery of metals: 1. Metal precipitation for recovery and recycle 14.

Tuszyński, J.A., Nip, M.L.A., Sept, D., 1994. Nonlinear Modelling of Chemical Kinetics for the Acid Mine Drainage Problem and Related Physical Topics. University of Alberta, Department of Physics.

Wei, X., Viadero, R.C., 2007. Synthesis of magnetite nanoparticles with ferric iron recovered from acid mine drainage: Implications for environmental engineering. Colloids and Surfaces A: Physicochemical and Engineering Aspects 294, 280–286. https://doi.org/10.1016/j.colsurfa.2006.07.060

Wei, X., Viadero, R.C., Buzby, K.M., 2005. Recovery of Iron and Aluminum from Acid Mine Drainage by Selective Precipitation. Environmental Engineering Science 22, 745–755. https://doi.org/10.1089/ees.2005.22.745

Younger, P.L., Coulton, R.H., Froggatt, E.C., 2005. The contribution of science to risk-based decision-making: lessons from the development of full-scale treatment measures for acidic mine waters at Wheal Jane, UK. Science of the Total Environment 338, 137–154.

Zawadzki, E.A., 1968. Status of acid mine drainage technology. Federal water polution control act Amendments 228–248.

Literature review

2 Oxidation and precipitation

This chapter discusses the literature of the kinetics Fe(II) oxidation and Fe(III) and Al(III) co-precipitation in the pH conditions relevant to this study.

2.1 Chemistry of ferrous iron oxidation

The Fe(II) oxidation has been a subject of numerous investigations in the past. The oxidation of ferrous sulphate by air is widely used in hydrometallurgical processes during leaching, solution purification by precipitation and wastewater treatment (Minegishi et al., 1983). The Fe is a transient species with a redox couple that continuously cycles between Fe(II) and Fe(III). This means that the rate of Fe(II) oxidation is critical in determining how much Fe is in the reduced state at any time. Fe(II) oxidation has been studied in a wide range of experimental conditions and in various aqueous media (Barry et al., 1994; Chmielewski and Charewicz, 1984; George, 1954; Huffman and Davidson, 1956, 1956; Kobe and Dickey, 1945; Mathews and Robins, 1972; Millero, 1985; Morgan and Lahav, 2007; Rönnholm et al., 1999; Ruiz et al., 2016; Singer and Stumm, 1970; Stauffer and Lovell, 1968, 1968; Verbaan and Crundwell, 1986). However, this section only reviews the abiotic Fe(II) oxidation in acidic sulphate solutions at pH ranges applicable in this study.

2.1.1 The Hyber Weiss reaction sequence

The Fe(II) oxidation is achieved using diatomic oxygen as an oxidant, either in air or as pure oxygen. The oxidation of Fe(II) by molecular oxygen involves the dissolution of oxygen into solution followed by the oxidation reaction. The dissolution of oxygen and the general stoichiometry reaction for the oxidation of Fe(II) by aqueous oxygen are represented in **Equations 2.1 and 2.2**, respectively.

$$O_{2(g)} \longrightarrow O_{2(aq)} \qquad 2.1$$

$$4Fe^{2+}_{(aq)} + O_{2(aq)} + 4H^{+}_{(aq)} \rightarrow 4Fe^{3+}_{(aq)} + 2H_2O_{(l)} \qquad 2.2$$

The reduction of each mole of oxygen consumes four moles of electrons and proceeds through a number of reaction steps. Haber and Weiss (1934) proposed the following reaction sequence:

$$\begin{aligned} &O_2 + e^- \leftrightarrow O_2^* \text{.....[a]} \\ &O_2^* + e^- \leftrightarrow H_2O_2 \text{.....[.b]} \\ &H_2O_2 + e^- \leftrightarrow HO^* + H_2O \text{.....[c]} \\ &HO^* + H^+ + e^- \leftrightarrow H_2O \text{.....[.d]} \end{aligned} \qquad 2.3$$

This is known as the Haber Weiss chain reaction. Haber and Weiss (1934) showed that the rate-determining step is reaction [a], which is the reduction of $O_{2(aq)}$ by the Fe(II). This was also confirmed by Wehrli (1990) who calculated the reduction potentials of the 4 steps (see **Table 2.1**) which showed that reaction step [a] was more endergonic.

Table 2.1: Values of standard electrode potential, Gibbs free energy and equilibrium constant for the one electron steps in the reduction of $O_{2(aq)}$ (Barnes, 2008).

Reaction step	**Oxygen species formed**	**E^o Volts**	**ΔG^o kJ mol-1**	**Log K**
$O_2 + e^- \leftrightarrow O_2^*$.....[.a]	Superoxide radical	-0.16	15.5	-2.7
$O_2^* + e^- \leftrightarrow H_2O_2$.....[.b]	Hydrogen Peroxide	1.72	-165.9	29.1
$H_2O_2 + e^- \leftrightarrow HO^* + H_2O$....[c]	Hydroxyl radical/Water	0.99	-95.3	16.7
$HO^* + H^+ + e^- \leftrightarrow H_2O$.....[d]	Water	2.53	-244.9	42.9

2.1.2 Kinetics of ferrous iron oxidation

2.1.2.1 Empirical models

Fe(II) oxidation by diatomic oxygen proceeds along two parallel pathways. It proceeds first through homogeneous oxidation in the solution, followed by heterogeneous oxidation in association with the mineral surface. Homogeneous oxidation is influenced by the solution chemistry i.e., Ionic strength, pH and Eh and is highly dependent on pH (Millero, 1985; Morgan and Lahav, 2007; Stumm and Lee, 1961; Sung and Morgan, 1980; Tamura et al., 1976a). Both homogeneous and heterogeneous oxidation are preceded by the dissolution or transfer of diatomic oxygen from the liquid phase into the aqueous phase as discussed in the previous section.

McBain (2002) was the first to study the oxidation of Fe in acidic solution at pH below 3. It was established that the oxidation reaction proceeds very slowly and usually shows no dependence on pH. The rate equation was obtained as follows;

$$\frac{d[Fe(II)]}{dt} = k[Fe(II)]^2 (O_2) \qquad 2.4$$

The validity of **Equation 2.4** has been confirmed for different media including sulphuric acid (Lamb and Elder, 1931), nitric acid (Pound, 1939) and perchloric acid (George, 1954).

The Fe(II) oxidation reaction is known to proceed more rapidly in slightly acidic (pH~4) to neutral pH conditions than in strongly acidic solutions. Stumm and Lee (1961) conducted quantitative study of Fe(II) oxidation kinetics. The Fe(II) oxidation at pH higher than 5 gave the following rate equation:

$$\frac{d[Fe(II)]}{dt} = k[Fe(II)][OH^-]^2 p(O_2) \qquad 2.5$$

Where k is the rate constant (M^{-2} atm^{-1} sec^{-1}), [Fe(II)] is the concentration of Fe(II) (M), [OH^-] is the concentration of the hydroxyl ions (M) and pO_2 is the oxygen partial pressure (atm). The rate law has been demonstrated to be first order with respect to [Fe(II)] and pO_2 and second order with respect to [OH^{-1}]

Since the study by Stumm and Lee (1961), a large number of studies on the kinetics and mechanism of Fe(II) oxidation have been undertaken under different conditions (Davison and Seed, 1983; Millero, 1985; Sung and Morgan, 1980; Tamura et al., 1976a, 1976 b). In the study by Millero (1985), the following rate equation was proposed for the oxidation of Fe:

$$\frac{d\ln[Fe(II)]}{dt} = \frac{k_1\beta_1\alpha_{Fe}}{H^+} + \frac{k_2\beta_2\alpha_{Fe}}{H^+} \qquad 2.6$$

Where [ ], k and p are as defined before, α_{Fe} is the fraction of the free Fe(II), β_1 and β_2 are the hydrolysis constants of Fe species $Fe(OH)^+$ and $Fe(OH)^0$, respectively.

Other relevant Fe(II) oxidation expressions by oxygen in the sulphate aqueous solutions are summarized in **Table 2.2**. As presented in this table, most of the researchers proposed a kinetic model for the rate of Fe(II) oxidation being second order with respect to Fe(II) concentration and first order with respect to oxygen partial pressure. Mathews and Robins (1972) and Verbaan and Crundwell (1986) used dissolved oxygen instead of oxygen partial pressure in their rate equations. Considering that these studies were generally conducted in the well-stirred reactors where the effect of mass transfer could be negligible, dissolved oxygen [$O_{2(aq)}$] should be equal to the saturation concentration. Under these conditions, the dissolved oxygen concentration is proportional to the partial pressure of oxygen in the gas phase. However, it must be noted that due to the large dependence of the oxygen solubility on the temperature, solution composition and the hydrodynamics of the system, the use of pO_2 instead of [$O_{2(aq)}$] in the kinetic equation could produce a significant difference in the value of the experimental activation energy.

Table 2.2 : Fe(II) oxidation expressions in acidic sulphate solutions

Rate law	E_a (kJ/mol)	[a]Other effects	Reference
$k[FeII]^2[O_2]$, $K \propto [H^+]^{-0.23}$	74 (25-40°C)	$[CuII]^y$ (2.5k), I	1
$k_{1[}FeII]pO_2 + k2[FeII]^2pO_2 + k_3[FeII][Cu]$	56_{k1}, 68_{k2} (140-180°C)	-	2
$k[FeII]^2[H^+]^{-0.35}[O_2]$	94 (20-50°C)	-	3
$k[FeII]^{1.84}[H^+]^{-0.25}[O_2]$, $k \propto [CuII]^{0.28}$	74 (20-80°C)	$[SO_4]^0$	4
$k[FeII]^2[O_2]$, $\propto [FeII]_{<3\text{-}8\ g/L}$	57 (40-135°C)	$[H_2SO_4]_{-x}$;$[CuII]^y$5	
$k[FeII]^{1.84}[H^+]^{-0.36}[O_2]$	69 (25-85°C)	-	6
$k_1[FeII]^2[O_2]/(1 + k_2[FeII])$	34 (60-130°C)	-	7
$k_1[FeII][OH^-]^2pO_2$			

[a]Not quantified in rate expressions;[1]George(1954); [2]Huffman and Davidson(1956); [3]keenen (1969); [4]Mathews and Robins(1972); [5]Chmielewski and Charewicz(1984); [6]Verbaan and Crundwell(1986); [7]Rönnholm et al.(1999)

2.1.2.2 Effect of process conditions on iron oxidation rate

The effects of the solution chemistry i.e., ionic strength, salinity, various anions, the effect of particle surface and temperature on the oxygenation of Fe(II) in aqueous solutions have also been reported (Millero, 1985; Sung and Morgan, 1980; Tamura et al., 1976a, 1976b). The oxidation rate has been found to be highly dependent on temperature. For example Stumm and Lee (1961) reported a ten-fold increase in the Fe(II) oxidation rate for a 15°C temperature increase. The temperature dependence on the oxidation rate is due to the variation in the water dissociation constant with temperature and the associated variation in the hydroxyl ions activity. Stumm and Lee

(1961) and Sung and Morgan (1980) used **Equation 2.5** to calculate the activation energy values of 96 kJ mol^{-1} and 105 kJ mol^{-1}respectively while Millero (1985) found 125 kJ mol^{-1} using **Equation 2.6**. These activation energy values signify the temperature dependency of the activation rate.

The pH-dependent of the Fe(II) oxidation was reported by Morgan and Lahav (2007). It was found that Fe(II) oxidation rate versus pH shows a central region where the rate is strongly pH dependent flanked by regions on either side where the rate is principally not affected by pH. It was observed that below pH 4 the rate of oxidation is very low and is fundamentally independent of pH. As the pH increases above 4, the oxidation rate is significantly affected by pH up to near neutral pH conditions (**Figure 2.1**). Stumm and Lee (1961) studied the effect of pH on the Fe(II) oxidation rate in the pH range 6-8 and reports that a unit changes in pH results in a 100-fold increase in the oxidation rate. Above the pH of 8, Morgan and Lahav (2007) concluded that the oxidation rate is independent of pH. This is in agreement with the work done by Hustwit et al. (1992) who proposed a rate law (**Equation 2.7**) for the treatment of AMD at near neutral conditions that is independent of pH. The change in the oxidation rate with pH can be interpreted to be because of the change in the Fe speciation which leads to the different kinetic rates associated with the different Fe species.

$$\frac{d[Fe(II)]}{dt} = 7k_{O_2}[o_2]_{sat} \qquad 2.7$$

Where k_{O_2} is the rate constant (min^{-1}), $[O_2]_{sat}$ is the saturation concentration of oxygen.

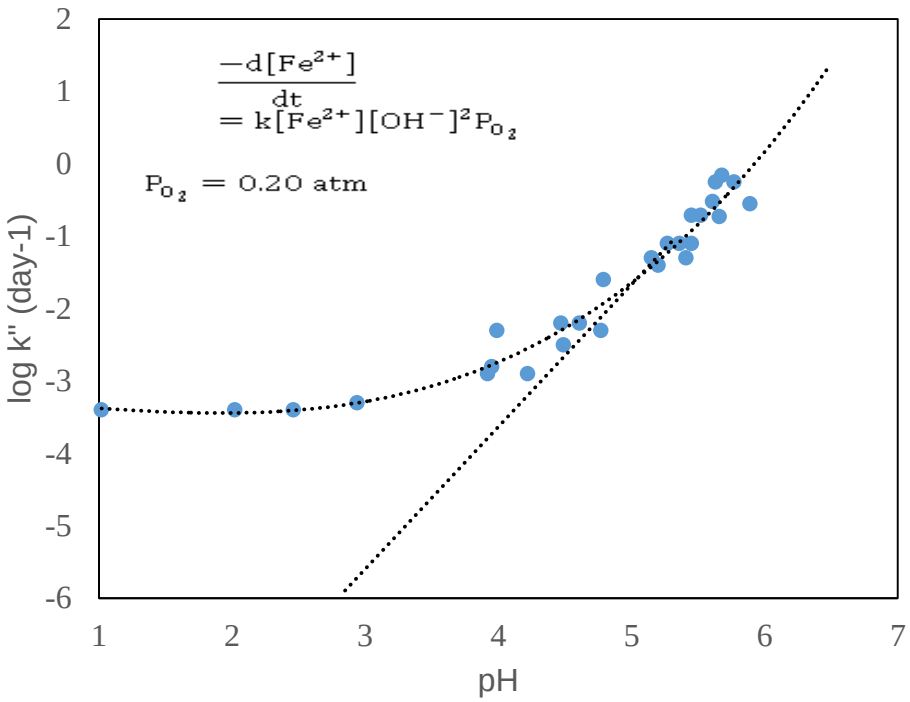

Figure 2.1: Oxidation rate of Fe as a function of pH (Redrawn from Morgan and Lahav, 2007)

Fe(II) oxidation rate has also been known to be affected by the ionic strength. Sung and Morgan (1980) reported a decrease in the rate constant with increases ionic strength. This is shown in **Table 2.3**. In the presence of ligands, the Fe-ligand integrations are expected to affect the oxidation rate. Tamura et al. (1976a) studied the effect of different types of anions including, ClO_4^-, SO_4^{2-}, NO_3^-, Cl^-, I^- and Br^- on the oxidation rate. It was established that the rate constant, and hence the oxidation rate, decrease in the order ClO_4^-, NO_3^-, Cl^-, Br^-, I^-, SO_4^{2-}. The effect of various cations on the Fe(II) oxidation rate has been investigated by various researchers (Chmielewski and Charewicz, 1984; Mathews and Robins, 1972). The catalytic effect of Cu(II) was confirmed by Mathews and Robins (1972) where they reported an increase in Fe(II) oxidation rate with the presence of cupric sulphate, while the various salts such as $HgCl_2$, $ZnSO_4$, $CoSO_4$, $NaSO_4$ and MnO_4 were found to have negligible effect.

Table 2.3: The effect of ionic strength on Fe(II) oxidation rate constants (Sung and Morgan (1980)

Ionic strength (M)	**K (M^{-2} sec^{-1})**
0.009	5.29×10^{14}
0.012	4.10×10^{14}
0.020	3.80×10^{14}
0.040	2.90×10^{14}
0.060	2.38×10^{14}
0.110	1.59×10^{14}

Another important finding to this work was the study that by Tamura et al. (1976b) who established that the presence of ferric hydroxide solids accelerated the Fe(II) oxidation rate. They proposed a rate equation for heterogeneous oxidation at constant pH and dissolved oxygen concentration:

$$\frac{d[Fe(II)]}{dt} = \left(k_1 + k_2[Fe(III)]\right)[Fe(II)] \qquad 2.8$$

Where k_1 and k_2 are the homogeneous and heterogeneous rate constants with units, min^{-1}. k_2 is a function of Fe(III) particle surface area (k_s), dissolved oxygen concentration, the adsorption constant of the Fe(II) on ferric hydroxide (K) and the pH and is given by:

$$k_2 = \frac{k_s[O_2]K}{\left[H^+\right]} \qquad 2.9$$

It was found that at lower pH, the oxide surface forms very slowly and as such the adsorption of Fe(II) takes place slowly. The catalytic effect is only significant at near

neutral pH. This is supported by the study by Sung and Morgan (1980) who found that lepidocrocite had the same catalytic effect as amorphous ferric hydroxide. In the same study, Sung and Morgan (1980) fitted their experimental data for autocatalytic oxidation of Fe by the reaction product (HFO) to the rate expression proposed by Tamura et al. (1976b). A reasonable agreement was found between the model and the experimental data for heterogeneous oxidation.

2.1.3 Summary

This section reviewed the literature concerning the oxidation of Fe(II) by dissolved oxygen in aqueous solution, with interest in acidic waters. The chapter can be summarized as follows:

- The Fe removal in hydrometallurgical solutions and waste water is mostly achieved by the precipitation of Fe(III). Oxidation of Fe(II) by molecular oxygen at atmospheric pressure involves the transfer of oxygen from gas to liquid phase and the chemical oxidation of Fe(II) by dissolved oxygen.

- The rate of homogeneous oxidation of Fe(II) is highly pH dependent. The oxidation rate is largely independent of pH below 4. As the pH increases above 4, the oxidation rate is significantly affected up to near neutral pH conditions. Between pH 5 and 8, the oxidation rate is inversely dependent on the square of the activity of the hydronium ion.

- The presence of cations such as copper catalyzes Fe(II) oxidation. It has been suggested that cupric copper gains an electron from Fe(II) to produce Fe(III) and Cu(II). However, the major cations found in AMD such as Mg(II) and Mn(II) have not been known to affect the oxidation rate. The other cation found in substantial quantity in AMD is Al(III) whose effect on the Fe(II) oxidation rate has not been established. It was thus the objective of this study to determine the effect of Al(III) ions on the oxidation rate of Fe(II).

- Ferric oxyhydroxide solids are also known to accelerate the Fe(II) oxidation rate with the catalysis effect only significant at near neutral pH.

2.2 Precipitation

2.2.1 Theory of precipitation kinetics

Precipitation is defined as the rapid formation of a sparingly soluble crystallite – or sometimes amorphous – solid phase from a liquid solution (Myerson, 2002). The precipitation process generally involves the simultaneous and rapid occurrence of nucleation and growth including the so-called secondary nucleation such as Ostwald ripening and agglomeration. **Figure 2.2** is the representation of the possible precipitation channels.

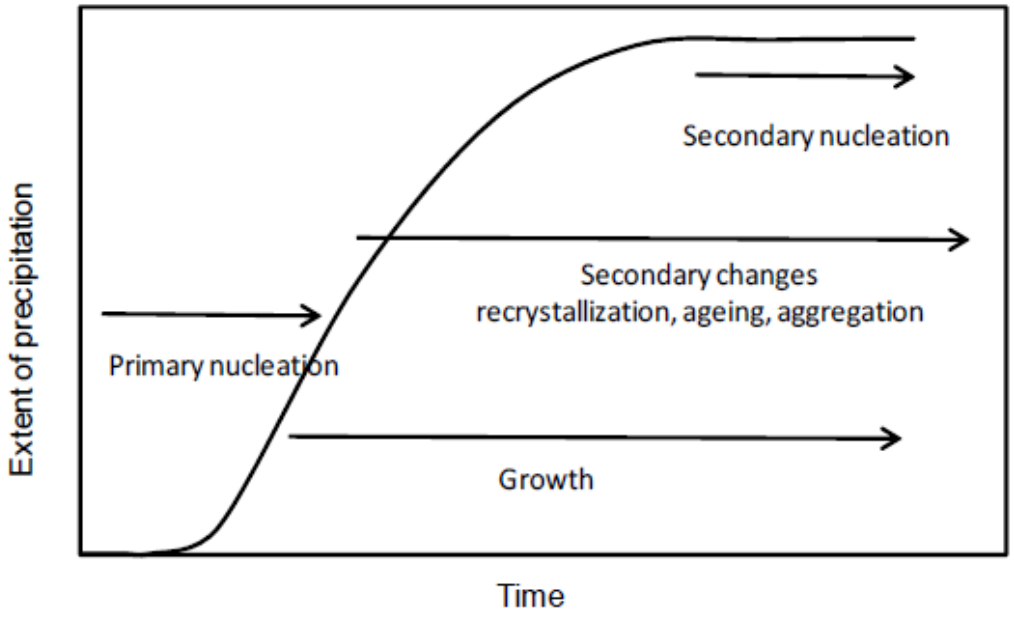

Figure 2.2: Precipitation kinetic processes (After Söhnel et al., 1992)

Thermodynamic driving force is necessary for precipitation to take place. This driving force is the difference between the actual and equilibrium chemical potentials of the solute in solution. At a constant temperature and pressure, this is represented mathematically by;

$$\Delta\mu = \mu - \mu^{*} \qquad 2.10$$

Where μ and μ* are the actual and equilibrium chemical potentials respectively and Δμ is the net thermodynamic driving force. Spontaneous precipitation only occurs when the net chemical potential, Δμ, is greater than zero. The chemical potential of a system can also be expressed by;

$$\mu = \mu_{o} + RT\ln\alpha \qquad 2.11$$

Where μ_o is the standard chemical potential of the crystallizing product ($Jmol^{-1}$) and α is the activity in solution ($mol\ m^{-3}$), *R* is the universal gas constant, (8.314 $J\ mol^{-1}\ K^{-1}$) and *T* is the absolute temperature, (K). The net chemical potential, Δμ, is generally referred to as supersaturation. From **Equation 2.11**, supersaturation can be expressed as;

$$\mu - \mu^{*} = RT\ln\left(\frac{\alpha}{\alpha^{*}}\right) \qquad 2.12$$

Where α^{*} is the solute equilibrium activity, $\left(\frac{\alpha}{\alpha^{*}}\right)$ is the supersaturation ratio, S. Thus, the chemical potential becomes;

$$\Delta\mu = RT\ln S \qquad 2.13$$

When a precipitation reaction is represented by **Equation 2.14**;

$$aA + bB \longleftrightarrow aAbB \qquad 2.14$$

Where *a* and *b* are the reaction coefficients, the supersaturation ratio, *S*, is given by;

$$S = \frac{\alpha_A^a \times \alpha_B^b}{\alpha_{A_{eq}}^a \times \alpha_{B_{eq}}^b} = \frac{\alpha_A^a \times \alpha_B^b}{K_s} \qquad 2.15$$

Although it is not possible to directly measure the species' activities, the activity coefficients can be used to convert the analytical concentrations into species activities using **Equation 2.16**:

$$\alpha_i = \gamma_i m_i \qquad 2.16$$

Where α_i is the activity of a species, m_i is the molality of the species, and γi is the activity coefficient. The activity coefficient, γ_i can be calculated using various models among which is the Debye-Hückel theory of electrolytes expressed as:

$$\ln \gamma = -AZ_i^2 \frac{I^{\frac{1}{2}}}{1 + BaI^{\frac{1}{2}}} \qquad 2.17$$

Where Z_i is the charge number of the ion, A and B are constants determined by the absolute temperature and dielectric constant of the system, and *a* is an adjustable parameter introduced in the Debye-Hückel expression as the distance of the closest approach between the center of the adjustable ions and the corresponding radius of the hydrated ion (typically in the range of 3 to 9 Å) (Batley, 1989). The ionic strength is itself is given by the **equation 2.18**:

$$I = \frac{1}{2} \sum m_i Z_i^2 \qquad 2.18$$

Where I, m and z_i have been defined.

While the Debye-Hückel expression is a solid foundation in classical thermodynamics and electrostatics, it does not account for all the interactions among solutes. In order to extend the applicability of the Debye-Hückel formula to higher ionic strength systems, a variety of empirical and semi-empirical expressions have been proposed. These include the WATEQ Debye-Hückel expression - **Equation 2.19**) and Davies equation - **Equation 2.20** (Truesdell and Jones, 1973)

$$\ln\gamma = -AZ_i^2 \frac{I^{\frac{1}{2}}}{1 + BaI^{\frac{1}{2}}} + \dot{B}I \qquad 2.19$$

$$\ln\gamma = -AZ_i^2 \left(\frac{I^{\frac{1}{2}}}{1 + I^{\frac{1}{2}}} - bI \right) \qquad 2.20$$

Where $\dot{B}$ and b are empirical parameters (b is typically in the range 0.2 to 0.3) The Davies equation provides reasonable estimates of activity coefficients up to an ionic strength of about 0.7 M. The other model that has been used to accurately estimate the activity coefficients at higher ionic strength is the Pitzer model (Pitzer and Mayorga, 1973). At higher ionic strengths both long-range electrostatic and short-range forces affect the complexations of ions in aqueous solutions. This specific ion-interaction model accounts for both of these sets of forces through the use of a virial coefficient expansion of the Debye-Hückel equation. This is expressed as:

$$\ln\gamma = \ln\gamma_{DH} + \sum_J B_{ij}X_J + \sum_j \left(\sum_k C_{ijk}X_jX_k \right) + ... \qquad 2.21$$

Where the first term is the Debye-Hückel activity coefficient, X_j is the molar concentration of the species j. The second viral coefficient B_{ij} accounts for specific interactions among pairs of ions, the third viral coefficients C_{ijk} accounts for specific interactions among the three ions and so on.

2.2.2 Nucleation

Nucleation is the progressive buildup of supersaturation in a solid-free solution and results in the formation of a new solid phase. Nucleation proceeds by two mechanisms i.e., primary and secondary nucleation. Primary nucleation occurs in the absence of a crystalline material. This is also termed as homogeneous nucleation. If the new solid-phase formation is induced by the presence of a foreign solid phase, the process is said to be secondary nucleation, also known as heterogeneous nucleation. During precipitation, unless the concentration of both or one of the reagents is very low, nucleation proceeds at a very high rate.

2.2.2.1 Homogeneous nucleation

Homogeneous nucleation will proceed when molecules in a saturated solution come together to form embryos of 10 to 1000 molecules per embryo. Until they attain the critical size, (r_c) the embryos keep on forming and disappearing. Beyond the critical size, the embryos stabilize. The free energy association for the formation of the embryo is shown in **Equation 2.22**.

$$\Delta G_{(r)} = \Delta G_{vol} - \Delta G_{surf} \qquad 2.22$$

Where, $\Delta G_{(r)}$ is the free energy required to form the embryo, ΔG_{vol} is the free energy associated with the generation of the embryo volume, ΔG_{surf} is the free energy associated with the generation of the embryo surface. A graphical representation of $\Delta G_{(r)}$ is shown in **Figure 2.3**.

The rate of homogeneous nucleation, as shown in **Equation 2.23**, can take the form of Arrhenius equation (Demopoulos et al., 1997);

$$J=\left(\frac{2D}{d^5}\right)\exp\left(\frac{\Delta G_{max}}{K_B T}\right) \qquad 2.23$$

Where,

J is the number of nuclei per unit volume (m^3) per unit time (s)

D is the diffusivity of solute (m^2/s)

d is the molecular diameter of the solute species (m)

k_B is the Boltzman constant; 1.38 x 10-23 $J.K^{-1}$

ΔG_{max} is the maximum activation Gibbs free energy barrier (J)

T is the temperature (K)

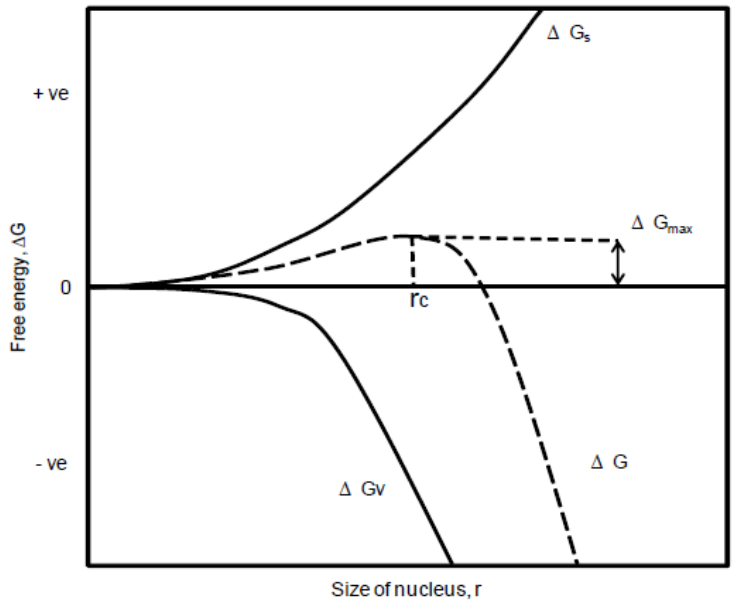

Figure 2.3: Crystallization free energy vs nuclei size (Demopoulos, 2009)

2.2.2.2 Heterogeneous Nucleation

The nuclei formed from homogeneous nucleation are a rare event. In most cases, the crystal formation is catalyzed by the presence of particulate contaminants of foreign materials. Even liquids from which physical impurities have been removed may contain from 10^{13} to 10^{23} of particulate contaminants per cubic meter (Söhnel et al., 1992). The decrease in the Gibbs free energy of formation of the nuclei has been used to explain the catalytic effect of the foreign particles on nucleation. Therefore, when foreign particles are present in solution, nucleation would take place at supersaturation ratios lower than those required for homogeneous nucleation. The formation of a solid phase in a supersaturated solution, in the presence of the very solid phase being synthesized, is called surface nucleation or secondary nucleation. It is also sometimes referred to as seeding. Seeding can be divided into two categories:

- Apparent secondary nucleation – a solid phase, like that desired to nucleate is introduced into the system as seed.

- True secondary nucleation – the nuclei is formed due to crystal and solution interactions; this is typical of a system that later engages in Ostwald ripening growth.

Ostwald (1886) further proposed that during phase transformation, it is not the thermodynamically stable phase that will preferentially be formed, but rather the phase that is nearest to the original phase in terms of stability. With time, the metastable phase transforms to the stable phase which is purer due to the cycle of crystallization, dissolution and recrystallization.

2.2.3 Crystal Growth

Immediately after the nuclei are formed in a supersaturated solution, they begin to grow into crystals. The crystal growth is controlled by mass transfer rather than heat transfer. Two types of growth sites have been described to accommodate atoms or growth units: the step site, where two nearest bonds are made between the growth unit and the

crystal, and the kink site, where three nearest bonds are made between the growth units and crystal. The steps that lead to growth can be summarized as follows (Dirksen and Ring, 1991):

- Interfacial transport of solute from the bulk solution to the crystal surface
- Adsorption of the solute on the surface of the particle
- Diffusion of solute onto a step or kink site
- Surface reaction or integration of the solute into the crystal lattice
- Heat of crystallization liberation and transfer away from the crystals

At molecular level, growth units diffuse towards the surface of the crystals and attach themselves. One of the important parameters during molecular level growth is the crystal-solution interface. The way the crystals interact with the solution determines the binding energy. Microscopic level growth involves growth that results from hundreds of molecular layers that have reduced diffusive flux. The trapping of impurities inside the crystal structure can be attributed to microscopic level growth. Macroscopic growth is attributed to the binding together of microscopic particles. The concentration gradient at macroscopic level will influence the surface concentration profile which results in instabilities at surface level. These instabilities can result in the formation of dendrite (Söhnel et al., 1992).

The growth rate of a particle is mathematically defined as shown in **Equation 2.24**.

$$G_{(r)} = K_g C_{eq} \left(S - 1\right) \qquad 2.24$$

Where,

Gr is the crystal growth rate (m s^{-1})

K_g is the growth constant (m^4 mol^{-1} s^{-1})

C_{eq} is the solubility of the solute (mol m^{-3})

S is the saturation ratio

If several mechanisms take place in parallel, the faster mechanism controls the overall rate. However, if the process is taking place in series (bulk diffusion and surface reaction or integration), the slower mechanism controls the growth rate (Dirksen and Ring, 1991).

At low supersaturation, the dominant nucleation mechanism is heterogenous and therefore the number of crystals formed is dependent on the availability of heteronuclei in the solution. At high supersaturation, crystals grow so fast such that the heat of crystallization cannot be transferred quickly enough away from the crystals to the surrounding solution. The depleted solution surrounds the crystal face because diffusion cannot provide the solute at the demanded rate. This causes elongation and crystal surface extensions as the crystal attempts to aid the transfer of crystallization heat (Demopoulos, 2009; Söhnel et al., 1992).

It is clear from the theoretical point of view that supersaturation has a significant influence on the precipitate quality. As discussed, higher supersaturation tends to produce poor quality crystals that inevitably gives rise to challenges during solid-liquid separation. Low supersaturation has the following advantages:

- Immobile and large polymeric species are avoided.
- Homogeneous nucleation and therefore amorphous crystal production is avoided.
- Surface integration proceeds undisturbed because of reduced external transfers (Dirksen and Ring, 1991)

A number of measures can be taken to control supersaturation: pH control, temperature control, dilution of solute, metal complexation and seeding. However, pH control, temperature control and seeding are the most suitable supersaturation control

parameters during the Fe precipitation in order to ensure that the process is as simple as possible (Claassen, 2006; Demopoulos, 2009; Dirksen and Ring, 1991)

2.2.4 Seeding during precipitation processes

Precipitation processes are characterized by fast kinetics due to low solubility. The primary particles are formed by primary nucleation at high supersaturation levels. The resulting particles are usually very small, in the order of 1 µm (Heffels and Kind, 1999). The growth of bigger size crystals can be achieved by reducing the supersaturation, either by dilution or introduction of seed crystals (Hove et al., 2007). The surface area of the seed material should be large enough to consume the supersaturation. This leads to the suppression of homogeneous nucleation. It is pertinent that the seed crystals are compatible with the substrate for the process to succeed. The lattice misfit is the criteria used to predict whether a given substrate is suitable for the overgrowth of another crystal lattice and is defined by **Equation 2.25** (Turnbull and Vonnegut, 1952). It was found that the lattice misfit of 10-20% between the substrate and the overgrowth is considered adequate for coherent layer deposition.

$$\delta = \frac{\Delta\alpha}{\alpha} \qquad 2.25$$

Where α is the lattice parameter of the stress-free crystal, Δα is the difference in the lattice parameter between the substrate and the overgrowth crystal.

Considering the generalized reaction mechanism for Fe(III) precipitation, ferrihydrite is known to be the precursor for the more crystalline ferric oxyhydroxide minerals e.g. goethite and hematite and is given by **Equation 2.26** (Grundl and Delwiche, 1993):

$$Fe^{2+} \rightarrow Fe^{3+} \rightarrow Fe(OH)_n^{3-n} \rightarrow \underset{(\text{usually ferrihydrite})}{\text{Amorphous crystallites}} \rightarrow \underset{(\text{usually goethite})}{\text{crystalline phase}} \qquad 2.26$$

It can be concluded that ferrihydrite can be used as seeding materials for Fe precipitation. The lattice misfit parameters of substrate overgrowth on the seed material are shown in **Table 2.4**. Ferrihydrite (recycle sludge) can be used as possible seeding material during Fe precipitation with a lattice misfit of 1% while ferrihydrite cannot coherently grow on goethite as the lattice misfit is about 96%.

Table 2.4: Crystallographic data for ferrihydrite and goethite (Hove et al., 2007)

Mineral	**Lattice parameter (α)**	**Lattice misfit (δ)**
Ferrihydrite	0.508	1.0%
Goethite	0.9956	96.0%
Hematite	0.503	1.0%
Lepidocrocite	1.252	146.5%
Schwermannite	1.066	109.8%
Maghemite	0.834	64.2%
Magnetite	0.839	65.2%
Feroxyhite	0.293	42.3%
Akanganeite	1.060	108.7%

Another important consideration during seeded precipitation is the mass of the seeding material added. According to Kubota and Onosawa (2009) homogeneous nucleation can be suppressed and the crystals can be grown safely if the following condition is satisfied.

$$C_s \geq C_s^* \qquad 2.27$$

Where C_s the seed loading ratio and is defined by Equation 2.28 and C_s^* is the critical value.

$$C_s = \frac{W_s}{W_{th}} \qquad 2.28$$

Where C_s is the mass ratio of the added seed material W_s (kg) to the theoretical crystal yield W_{th} (kg) calculated from **Equation 2.29** or can be determined experimentally.

$$W_{th} = w\left(C_i - C_f\right) \qquad 2.29$$

Where C_i is the initial solution concentration (kg-hydrate/ kg-free water), C_f is the final concentration (kg-hydrate/ kg-free water) and w is the mass of free-solvent water. For most systems, however, a seed concentration of $C_s = 1$ will be enough to cause the deposition of the precipitate on the seed material.

2.2.5 Theory of co-precipitation mechanisms

Co-precipitation, in the context of this research, can be defined as the existence of two or more phases in the intended precipitate. It is therefore critical to understand the mechanisms that promote co-precipitation. There are three mechanisms by which co-precipitation can occur (Kolthoff, 2002);

- Inclusion
- Occlusion and
- Surface adsorption

2.2.5.1 Inclusion

Inclusion is a mechanism of co-precipitation where chemical species, similar to precipitating ions, substitute into the chemical lattice via chemical adsorption. In

inclusion co-precipitation, the logarithmic distribution of ions applies according to **Equation** 2.31.

$$\log\left(\frac{C_i}{C_f}\right) = \lambda \log\frac{C_{pi}}{C_{pf}} \qquad 2.30$$

Where,

C_i is the initial concentration of the value metal in solution

C_f is the final concentration of the value metal in solution

C_{Pi} is the initial concentration of the primary ion, to be precipitated, in solution

C_{Pf} is the final concentration of the primary ion, to be precipitated, in solution

λ is the logarithmic distribution coefficient

Lambda, λ, decreases with increase in temperature therefore, inclusion co-precipitation is pronounced at lower temperatures. Homogeneous nucleation is also pronounced at lower temperatures.

2.2.5.2 Occlusion

Occlusion is the mechanism of co-precipitation that occurs when the unintended ions are mechanically trapped, either as solids or liquids, in the crystal layers of the parent precipitate. Therefore, it follows that these unintended ions cannot be washed off the precipitate to free them.

It has been suggested that occlusion is the main mechanism of co-precipitation in many freshly prepared oxides and hydroxides. This is because of high supersaturation that leads to higher nucleation rates and lower growth rates thereby trapping unintended ions between ‘rushed’ crystal layers (Claassen, 2006; Söhnel et al., 1992).

2.2.5.3 Surface adsorption

Surface adsorption is the mechanism of co-precipitation that occurs because of precipitate impurities being introduced through the surfaces of the precipitate itself. This mechanism occurs only when the precipitate surface ions are not completely coordinated and therefore able to attract oppositely charged ions that are still in solution.

When surface adsorption is the main mechanism of co-precipitation, higher co-precipitation is experienced when larger crystals are precipitated and when there is prolonged contact with solution (Demopoulos, 2009).

2.2.6 Iron and aluminium hydrolysis and precipitation

The nature and composition of the precipitate formed is determined by the equilibrium and kinetic relationship of the precipitate reaction. As already mentioned in **Section 2.2,** temperature, pH and seeding are the most important parameters which determine the nature of the precipitate. To explain the formation of the compound precipitated by hydrolysis of Fe(II), Fe(III) or Al(III), it is critical that the solution chemistry is completely explained. This involves a qualitative and quantitative identification of all species during the pre-nucleation, nucleation and particle growth stages. The speciation of the cations, Fe(II), Fe(III) and Al(III) are very important to understand their removal from process solutions including wastewater. This section discusses the various aspects pertaining to Fe and Al(III) hydrolysis. Hydrolysis is the interaction of hydrated metal ions with acids or bases in a ligand exchange reaction (Snoeyink and Jenkins, 1980)

2.2.6.1 Hydrolysis of Fe(II) and Fe(III)

In aqueous solution, the degree of Fe(II) hydrolysis is a function of pH. Thus, an increase in pH results in the loss of protons from water of hydration in a stepwise order. The monomer complex tend to form polymers of Fe-OH-Fe bonds followed by Fe-O-Fe bonds (Stumm and Morgan, 2012). Fe(II) complexes with the hydroxyl ligand to form

different complexes at specific conditions. The possible Fe(II) complexes and their corresponding equilibrium constants are shown in **Table 2.5**.

Table 2.5: Hydrolysis of Fe(II) (Flynn Jr, 1984)

Species	Reaction	Equilibrium constant
Fe^{2+}-free		
$FeOH^{+}$	$Fe^{2+}+H_2O \rightleftharpoons FeOH^{+}+H^{+}$	log K_1 = -4.5
$Fe(OH)_2^0$	$Fe^{2+}+2H_2O \rightleftharpoons Fe(OH)_2^0+2H^{+}$	log K_2 = -7.4
$Fe(OH)_3^-$	$2Fe^{2+}+2H_2O \rightleftharpoons Fe(OH)_3^-+3H^{+}$	log K_3 = -11.0
$Fe(OH)_4^{2-}$	$2Fe^{2+}+4H_2O \rightleftharpoons Fe(OH)_4^{2-}+4H^{+}$	log K_4 = -14.4

As described by equations in **Table 2.5**, the formation of complexes between metal ions in solution and a ligand requires displacement of one or more coordinated water molecules from the initial aquo complex. Therefore, the hydrolysis of metal ions can be visualized as a stepwise replacement of coordinated molecules of water of hydration by hydroxyl ions or as a series of consecutive proton transfer reactions. These reactions proceed by the transfer of a proton to a solvent water molecule where a coordinated H_2O is converted to a hydroxyl ion. Therefore, the hydrated metal ions formed by the reactions are acids and in view with the Bronsted acid base theory. Since the hydrolysis reaction is dependent on the acid-base reactions, the solution pH strongly influences the rate and distribution of the various hydrolysis species.

The total dissolved Fe(II) concentration can be calculated from the sum of the respective complexes according to **Equation 2.31**.

$$\left[Fe_T^{2+}\right]=\left[Fe^{2+}\right]+\left[Fe(OH)^{+}\right]+\left[Fe(OH)_2^0\right]+\left[Fe_2(OH)_3^-\right]+\left[FeSO_4^{2-}\right] \qquad 2.31$$

However, the solubility product of ferrous hydroxide is expressed as:

$$\left[Fe^{2+}\right]\left[OH^{-}\right]^{2}:K_s=7.94^{-16} \qquad \text{(Jackson, 1986)} \qquad 2.32$$

Combining **Equations 2.31** and **2.32**, the total concentration of the dissolved Fe(II) at a given time can be calculated at a given pH according to **Equations 2.33** to **2.37**.

$$\log\left[Fe^{2+}\right]=\log K_s-2\log K_w-2pH \qquad 2.33$$

$$\log\left[Fe(OH)^{+}\right]=\log K_s-\log K_1-pH \qquad 2.34$$

$$\log\left[Fe(OH)_2^{0}\right]=\log K_s-\log K_2-pH \qquad 2.35$$

$$\log\left[Fe_2(OH)_3^{-}\right]=\log K_s+\log K_3+\log K_w+pH \qquad 2.36$$

$$\log\left[Fe(OH)_2^{4-}\right]=\log K_s-\log K_4+2\log K_w+2pH \qquad 2.37$$

Although total metal ion remaining in the solution can be calculated from chemical equilibria, complexation is an undesirable phenomenon during metal removal from solution because it tends to reduce the amount of metal precipitated in the solid form. **Figure 2.4** shows the removal of Fe(II) from solution as a function of pH. It is evident from the figures that ferrous hydroxide is formed at high pH.

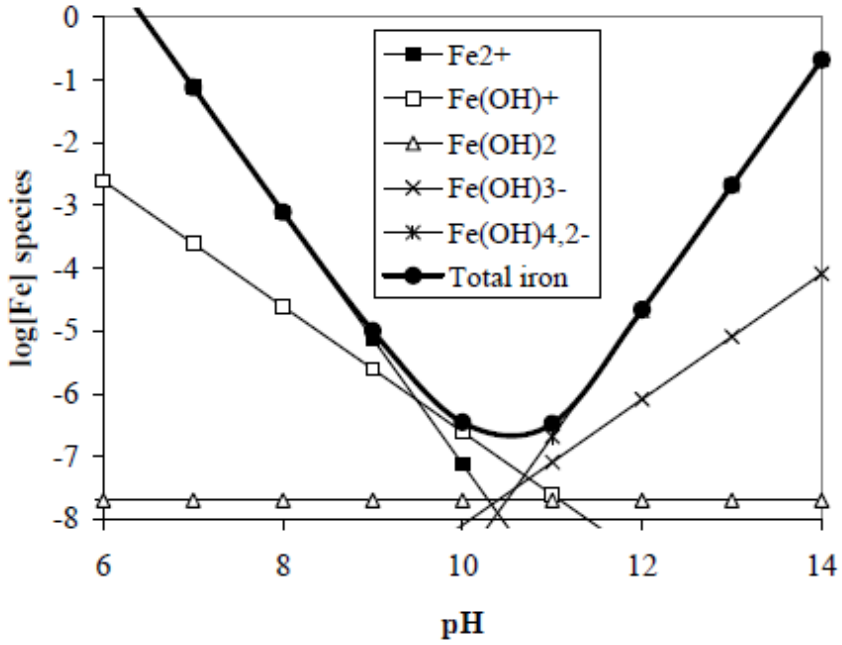

Figure 2.4: pH profile for ferrous hydroxide, $Fe(OH)_3$ at 25°C (Hove, 2008)

Fe(III) is easily hydrolyzed in aqueous solutions in the absence of competing ligands and most trivalent metal ions are already coordinated with OH^- within the pH range of natural waters. Therefore, an understanding of the mechanisms of Fe(III) hydrolysis and the formation of solid species of ferric hydroxide has been viewed as important in the field of Fe precipitation as well as destabilization and coagulation of particulates in water (discussed in **Chapter 4**). Fe(III) hydrolysis and subsequent polymerization and precipitation is the major formation pathway of the Fe oxides (Flynn Jr, 1984). The hydrolysis of Fe(III) proceeds by the deprotonation of hexa-aqua ferric complexes leading to the formation of monomeric complexes at varying pH conditions (Blesa and Matijević, 1989). The complexes formed modify metal species in solution, generally reducing the free metal ion concentration so that the effects and properties which depend on free metal ion concentration are altered (Snoeyink and Jenkins, 1980). Knowledge of the pathway at the molecular scale has important implications for understanding the environmental mineralogy and chemistry of Fe oxides. The phase diversity and the Fe oxide precipitated is dictated by the formation pathways. At any given pH conditions, the low molecular species determine the speciation of Fe(III). The

relevant hydrolysis reactions of Fe(III) that may be present during Fe(III) hydrolysis are summarized in **Table 2.6** (Blesa and Matijević, 1989). In the case of Fe(III) dissolved in water, there are six water molecules that coordinated with Fe^{3+} ion, leading to the more refined chemical symbolism $Fe(H_2O)_6^{3+}$ instead of Fe^{3+} for the hydrated ferric ion. The table also shows various precipitation reactions that occur, and which may affect Fe(III) availability in AMD. These reactions occur in solutions that are relatively concentrated as compared to natural waters. Thus, it is pertinent to evaluate the complexation and precipitation reactions of Fe(III) and its speciation in acidic conditions.

Table 2.6: Hydrolysis of Fe(III) (Flynn Jr, 1984)

Species	Reaction	Equilibrium constant (K)
Fe^{3+}-free		
$FeOH^{2+}$	$Fe^{3+}+H_2O \rightleftharpoons FeOH^{2+}+H^+$	log K_1 = -2.19
$Fe(OH)_2^+$	$Fe^{3+}+2H_2O \rightleftharpoons Fe(OH)_2^+ +2H^+$	log K_2 = -5.8
$Fe(OH)_4^-$	$Fe^{3+}+4H_2O \rightleftharpoons Fe(OH)_4^- +4H^+$	log K_3 = -21.6
$Fe_2(OH)_2^{4+}$	$2Fe^{3+}+2H_2O \rightleftharpoons Fe_2(OH)_2^{4+} +2H^+$	log K_4 = -2.9
$Fe_2(OH)_4^{5+}$	$3Fe^{3+}+4H_2O \rightleftharpoons Fe_3(OH)_4^{5+} +4H^+$	log K_5 = -6.3
$Fe(OH)_{3(s)}$	$Fe(OH)_{3(s)} = Fe^{3+}+3OH^-$	log K6 = -38.7

Just like with Fe(II), the total Fe(III) concentration of the system can then be calculated by combining the complex formation with the solubility product of each of the ferric oxide/hydroxide/sulphate complex according to **Equation 2.38**.

$$\left[Fe_T^{3+}\right]=\left[Fe^{3+}\right]+\left[FeOH^{2+}\right]+\left[Fe(OH)_2^{+}\right]+Fe(OH)_4^{-}+\left[Fe_2(OH)_2^{4+}\right]+Fe_2(OH)_4^{5+} \quad 2.38$$

The hypothetical ferric hydroxide, $Fe(OH)_3$ dissociates according to **Equation 2.39** to give the solubility of iron oxide as indicated by **Equation 2.40**.

Table 2.7 gives the solubility products of the different ferric oxyhydroxide mineral phases.

$$Fe(OH)_3 \longleftrightarrow Fe^{3+}+3OH^- \quad 2.39$$

$$K_s=\left[Fe^{3+}\right]\left[OH^-\right]^3 \quad 2.40$$

Taking the logarithms of both sides of **Equation 2.40**, the solubility becomes:

$$pK_s=pFe^{3+}+3pOH^- \quad 2.41$$

Table 2.7: Solubility of the different iron oxyhydroxide mineral phases (Schwertmann and Cornell, 2000)

Mineral phase	**Solubility product** as pFe^{3+} + $3pOH^-$
Ferrihydrite	37-39.4
Hematite	42.2-43.3
Lepidocrocite	40.6-42.5
Goethite	43.3-44

The dependence of Fe removal from solution upon the solubility product is presented by (Hove, 2008) (**Figure 2.5**). Although maximum removal of Fe occurs at pH 8, it can be inferred from the figure that it is thermodynamically feasible to reduce the Fe concentration to 0.5 mg/L by precipitating it as a hydroxide at pH range 5-7. Arden (1951) determined that when a sodium hydroxide is added to a ferric sulphate solution, it gives an unstable solution containing high concentrations of the basic ions. When the OH^-: Fe(III) molar ratio exceeds 0.5, a precipitate of $2Fe_2O_3.SO_3$ is formed. When more base is added, it leads to the formation of $Fe(OH)_3$. The precipitation is only complete when the ratio is 2.5. The study by Cornell et al. (1989) showed that the nature of the precipitate formed depends on the OH^-, Fe(III) molar ratio as well as aging. When the molar ratio is more than 3, a mixture of ferrihydrite and amorphous hematite is formed while at a ratio of 0.5-1.0, crystalline phases are formed. Many other studies have been conducted to determine the phase transformation and final precipitate product formed. For example, Domingo et al. (1994) formed lepidocrocite under slightly acidic conditions with a Fe(II):OH^- ratio of ≥ 0.5.

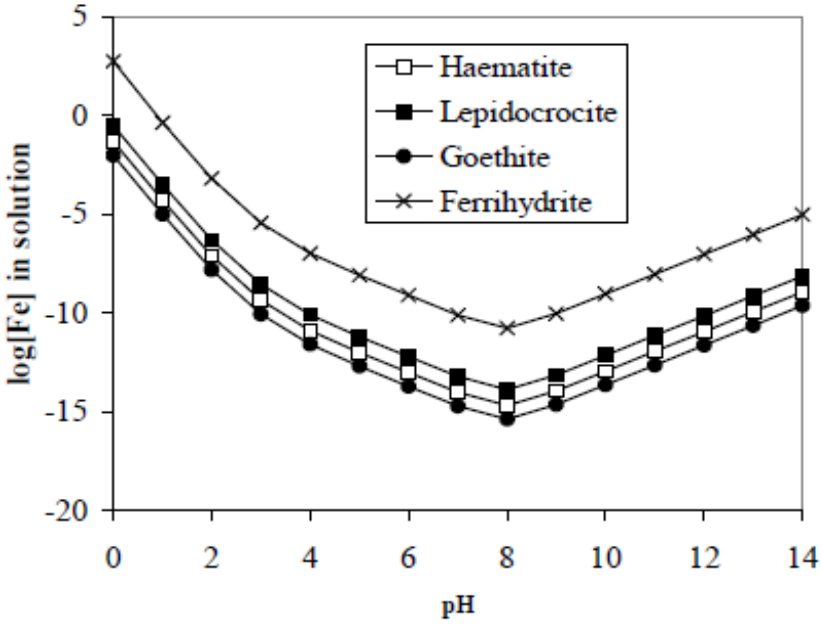

Figure 2.5: Concentration of Fe(III) remaining in solution after hydrolysis as a function of pH (Hove, 2008)

2.2.6.2 Hydrolysis of Al^{3+}

The precipitation of $Al(OH)_3$ from an acidified aqueous solution may be presented by the following process steps (De Hek et al., 1978):

$$Al(H_2O)_6^{3+} + 3OH^- \longrightarrow Al(OH)_3(H_2O)_{(s)} + 3H_2O \qquad 2.42$$

$$Al(OH)_3(H_2O)_3 \longrightarrow Al(OH)_s + 3H_2O \qquad 2.43$$

Equation 2.42 is the base displacement reaction that yields a hydrated precipitate followed by the hydration step. It has been established that at low pH values and thus OH/Al ratios, the major contributors to the total Al^{3+} concentration are the monomeric ($Al(OH)^{2+}$) and dimeric ($Al_2(OH)_2^{4+}$) solute species. These can be represented by the following hydration reactions:

Table 2.8: Hydrolysis of Al^{3+}

Species	Reaction	Equilibrium constant (K)
Al^{3+}-free		
$Al(OH)^{2+}$	$Al^{3+} + H_2O \longrightarrow Al(OH)^{2+} + H_3O^+$	log K_1 = 4.89
$Al(OH)_2^{4+}$	$2Al^{3+} + 4H_2O \longrightarrow Al(OH)_2^{4+} + 2H_3O^+$	log K_2 = 5.38

On introducing the solubility product, the following thermodynamic relationships are obtained:

$$\log K_s = \log[Al^{3+}] + 3pH - 3K_w \qquad 2.44$$

$$\log K_s = \log\left[Al(OH)^{2+}\right] - \log\left[Al^{3+}\right] - pH \quad (2.45)$$

$$\log K_s = \log\left[Al_2(OH)_2^{4+}\right] - 2\log\left[Al^{3+}\right] - 2pH \quad (2.46)$$

The actual Al concentrations at a pH and time can be calculated from these equations. For example, Lydersen (1990) calculated the distribution of dissolved inorganic Al at pH 5 and obtained 36% Al^{3+} , 37% $Al(OH)^{2+}$, 26% $Al(OH)_2^{+}$ and 1% $Al(OH)_3^{0}$.

The initial precipitation products are amorphous in nature with no definite ordered structure. As the precipitate age, they evolve into identifiable crystalline phases (Rubin and Hayden, 1973). Gibbsite forms very slowly at normal temperatures and acidic media. In alkaline media, a mixture of boehmite, bayerite and possibly nordstrandite form. A detailed discussion on the formation of these crystalline phases is presented by Schoen and Roberson (1970). The values of the solubility products of these phases are presented in **Table 2.9**.

Table 2.9: Summary of solubility products of aluminium hydroxide (Rubin and Hayden, 1973)

Phase	**Log K_{sp}**
Boehnite (Pseudo)	-32.90
Bayerite	-32.95
Gibbsite	-32.65

2.2.7 Iron and aluminium recovery from AMD/hydrometallurgical solutions

The composition and the physical nature of the Fe and Al precipitation products depend upon kinetic and equilibrium relationship of the precipitation reaction. The two most important parameters that determine the nature of the precipitate are temperature and pH. The removal of metals such as Fe(III) and Al(III) from the solution is usually required to obtain a purified solution for other extraction processes or purification of the wastewater. Fe(III) and Al(III) can easily be removed with selective hydroxide precipitation techniques as shown in **Figure 2.6**. As shown in **Figure 2.6,** the relationship between pH and the main equilibrium phases shows that Fe(III) and Al(III) concentrations in the solution is directly related to pH such that at lower pH values the equilibrium solubilities of Fe(III) and Al(III) are higher and decreases with an increase in solution pH.

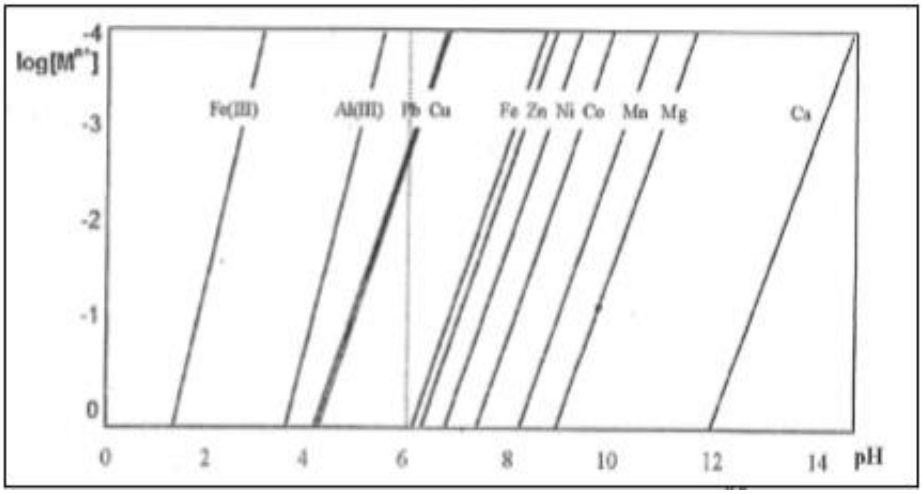

Figure 2.6: Equilibrium Concentration of Metal Hydroxides (Ngatenah et. al, 2010)

Babcan (1971) determined the main equilibrium Fe phases during the hydrolysis of 0.5 M ferric sulphate solution. The relationship between pH, temperature and the main equilibrium phases is shown in **Figure 2.7**. The figure shows at a pH < 2, the equilibrium solubility of Fe (III) is higher forming Fe^{3+} ions. Therefore, at higher pH values excess Fe will rapidly precipitate. This rapid precipitation leads to the formation of metastable or poorly crystalline phases such as ferrihydrite or schwertmannite. As discussed in

Section 2.2.4, ferrihydrite is known to be the precursor for the more crystalline ferric oxyhydroxide minerals during Fe(III) precipitation (Grundl and Delwiche, 1993; Murad and Schwertmann, 1980). However, **Figure 2.7** does not show ferrihydrite or schwertmannite regions as these are metastable phases that transform to more stable phases upon ageing. Ferrihydrite is expected to transform to more stable goethite and/or hematite. Ferrihydrite has the general formula $5Fe_2O_3 \cdot 9H_2O$. A number of other formulae have been suggested such as $2FeOOH \cdot 2.6H_2O$ (Russell, 1979) and $Fe_5HO_8 \cdot 4H_2O$ (Towe and Bradley, 1967). The name ferrihydrite commonly refers to a range of poorly crystalline iron oxide/hydroxide phases of which 2-line (exhibiting 2 broad XRD peaks) ferrihydrite and 6-line (exhibiting 6 broad XRD peaks) ferrihydrite are most common (Javed, 2017).

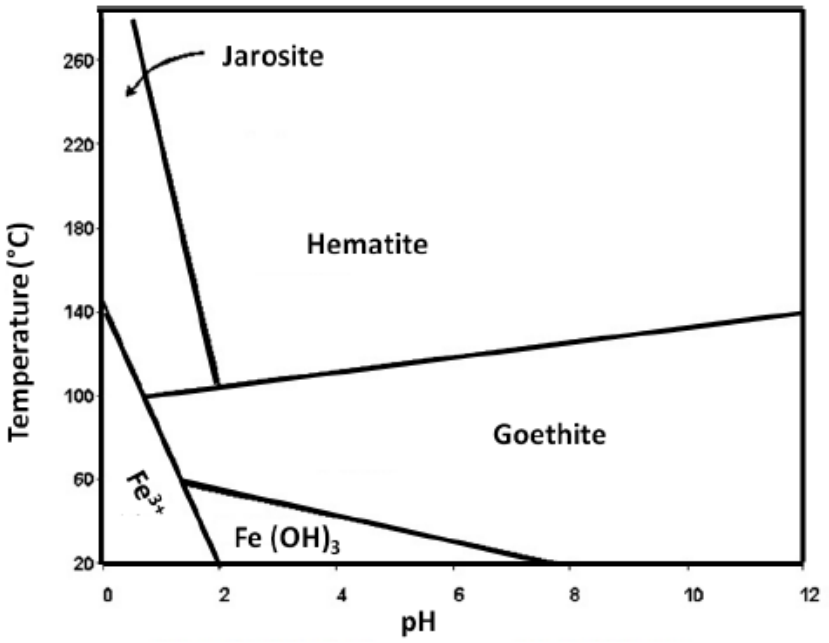

Figure 2.7: Stability regions of various compounds in the Fe-S-O system (Babcan, 1971)

Jambor and Dutrizac (1998) established that hat ferrihydrite is not strictly amorphous but has poor long-range order and very small crystallite size (2–6 nm). It is also known to have a higher tendency to adsorb divalent cations such as copper and nickel and

therefore increases contamination or loss of metal to the precipitate (Cornell et al., 1989; Dyer et al., 2012; Sahu and Asselin, 2011). The high sorbent capacity is due to very high (200-300 m^2/g) BET (Brunauer-Emmett-Teller) surface area (Cornell and Schwertmann, 2003). The precipitation of Fe(III) as ferrihydrite depends on the sulphate concentration of the solution. In concentrated ferric sulphate solutions of pH 2 to 4, a similarly structured schwertmannite, $Fe_8O_8(OH)_6SO_4$ is a more common phase than ferrihydrite (Bigham et al., 1996). Schwertmannite is a complex hydroxy ferric sulphate with poorly crystalline nature with some workers suggesting that it is nothing but ferrihydrite with high sulphate values (Claassen, 2006).

Fe(III) has been precipitated as ferrihydrite in several hydrometallurgical systems. In the zinc process, a paragoethite process residue consisted of approximately 40-50% ferrihydrite with the remaining fraction being other iron oxyhydroxides (Loan et al., 2006). Similarly, a study by Claassen (2006) produced a residue containing approximately 50% of the Fe associated with ferrihydrite, schwertmannite and a third unknown phase. Dyer et al. (2012) also identified ferrihydrite in their study of the Caron leach residue.

In AMD, Fe and Al have been recovered either separately or together for possible use in several applications. Two-step processes have been implemented to recover Fe and Al separately by raising the pH value to 4.5, thus precipitating the Al and removing the sludge. This is followed by removal of Fe(II), which does not precipitate at pH less than 7, using an electrolysis unit (Hajar and Riefler, 2013). Seo et al. (2017) developed a process for recovering dissolved metals from AMD. The AMD from Samma-Taejeong coal mine, South Korea was neutralized by adding neutralizing agents and an oxidant, hydrogen peroxide, to evaluate the recovery of metals and their purities. The water chemistry contained dissolved Fe, Al, and Mn, and these were precipitated under two conditions, 1) only neutralization by sodium hydroxide and 2) neutralization after oxidation with hydrogen peroxide. They found that both Al and Fe were concurrently precipitated at pH 4.5 with neutralization after oxidation. The recovery sequence was Fe, Al, then Mn for oxidation of AMD while with neutralization alone it was Al, Fe, and Mn. Wei and Viadero (2007) conducted selective precipitation of Fe, Al, Mn and Ca using precipitation. Their objective was to use chemical treatment of AMD to recover high

purity metals. They determined that Fe could be recovered at pH 3.5-4.0 then Al at pH 6.0-7.0 with purities of >93.4% and >92.1%, respectively. Wei and Viadero (2007) also determined that sodium hydroxide, sodium carbonate, ammonia hydroxide, calcium oxide, and calcium hydroxide (lime) all were sufficient for Fe and Al recovery, but unreacted lime may pose a purity issue in a full-scale process.

Hedrich and Johnson (2012) selectively precipitated Fe from Al, Cu, Mn and Zn by employing a bio-oxidation modular system. The raw AMD contained 280 mg/L Fe entering the first reaction module and was rapidly oxidized by 90% using Ferrovu, myoxofaciens. The pH was increased to 3.5 in the second module using sodium hydroxide caused the Fe(III) to precipitate. The recovery of Fe, Al, Cu, Zn, and Ni as a function of equilibrium solution pH was simulated by Park et al. (2015) using Visual MINTEQ. They used the optimal precipitation pH values of the different elements from the simulation. The recovery of Fe, Al, Cu, Zn, and Ni was 99.6, 86.8, 71.9 and 77.0 for Fe, Al, Cu and Zn, respectively. Other workers that have recovered Fe and Al from AMD include Tabak et al. (2003) and Sahinkaya et al. (2009) who studied the recovery of the dissolved metals by selective precipitation as metal sulphides via biological methods. Flores et al. (2012) reported that Fe was recovered as goethite which was then evaluated as an adsorbent or catalyst. Wang et al. (2013) studied the combination of sulfidation and lime neutralization for the selective precipitation of dissolved metals from AMD. However, the pH range for the selective precipitation was not determined and additional experiments were recommended.

2.2.8 Summary

- Precipitation involves 2 fundamental steps: nucleation and growth. Growth controlled precipitation results in better quality precipitates. Supersaturation is the driving force of precipitation. Lower supersaturation is desirable to produce high quality precipitates (relatively pure and ease solid–liquid separation). In hydrometallurgical solutions and wastewater, supersaturation can be mainly controlled by carefully controlling the solution pH, temperature or by inducing secondary nucleation using seeding technique.

- This section focused much on the precipitation and characterization of the Fe minerals phases. This is so because Fe is the major constituent of AMD and Al(III) precipitation on the other hand is studied in the context of inclusion co-precipitation.

- The high pH values rapidly oxidize and precipitate Fe(III). The rapid precipitation leads to the formation of metastable or poorly crystalline phases such as ferrihydrite or schwertmannite. These mineral phases are expected with precipitation of Fe(III) and Al(III) in the pH range 5.0-7.0.

- The most applied method of metal recovery from wastewater is precipitation. Fe and Al have been recovered by several researchers using sodium hydroxide for pH control. However, ferric hydroxide precipitation, at high supersaturation, induces primary nucleation which leads to the formation of finer precipitate particles. This reduces the rate of settling and solid/liquid separation and thus requires longer periods of time or special equipment to speed up the separation. It was, therefore, as the objective of this study to experimentally study the seeded co-precipitation of ferric hydroxide and aluminium hydroxide and see if this method offers any improvement in the precipitate quality, and subsequent settling and dewatering capacity.

References

Arden, T., 1951. 78. The hydrolysis of ferric iron in sulphate solution. Journal of the Chemical Society (Resumed) 350–363.

Babcan, J., 1971. Die Synthese von Jarosit KFe 3 (SO 4) 2 (OH) 6. Geol Zbornik Geol Carpath 22, 299–304.

Barnes, A., 2008. Rates and mechanisms of Fe (II) oxidation in a passive vertical flow reactor for the treatment of ferruginous mine water. Cardiff University (United Kingdom).

Barry, R.C., Schnoor, J.L., Sulzberger, B., Sigg, L., Stumm, W., 1994. Iron oxidation kinetics in an acidic alpine lake. Water Research 28, 323–333. https://doi.org/10.1016/0043-1354(94)90270-4

Batley, G.E., 1989. Trace Element Speciation Analytical Methods and Problems. CRC Press.

Bigham, J., Schwertmann, U., Traina, S., Winland, R., Wolf, M., 1996. Schwertmannite and the chemical modeling of iron in acid sulfate waters. Geochimica et Cosmochimica Acta 60, 2111–2121.

Blesa, M.A., Matijević, E., 1989. Phase transformations of iron oxides, oxohydroxides, and hydrous oxides in aqueous media. Advances in Colloid and Interface Science 29, 173–221.

Chmielewski, T., Charewicz, W.A., 1984. The oxidation of Fe(II) in aqueous sulphuric acid under oxygen pressure. Hydrometallurgy 12, 21–30. https://doi.org/10.1016/0304-386X(84)90045-8

Claassen, J.O., 2006. Characterisation and optimisation of the Zincor iron removal process.

Cornell, R.M., Giovanoli, R., Schneider, W., 1989. Review of the hydrolysis of iron (III) and the crystallization of amorphous iron (III) hydroxide hydrate. Journal of Chemical Technology & Biotechnology 46, 115–134.

Cornell, R.M., Schwertmann, U., 2003. The iron oxides: structure, properties, reactions, occurrences and uses. John Wiley & Sons.

Davison, W., Seed, G., 1983. The kinetics of the oxidation of ferrous iron in synthetic and natural waters. Geochimica et Cosmochimica Acta 47, 67–79. https://doi.org/10.1016/0016-7037(83)90091-1

De Hek, H., Stol, R., De Bruyn, P., 1978. Hydrolysis-precipitation studies of aluminum (III) solutions. 3. The role of the sulfate ion. Journal of Colloid and Interface Science 64, 72–89.

Demopoulos, G., 2009. Aqueous precipitation and crystallization for the production of particulate solids with desired properties. Hydrometallurgy 96, 199–214.

Demopoulos, G.P., Zinck, J.M., Kondos, P.D., 1997. Multiple stage precipitation of heavy metals from acidic aqueous solution.

Dirksen, J., Ring, T., 1991. Fundamentals of crystallization: kinetic effects on particle size distributions and morphology. Chemical Engineering Science 46, 2389–2427.

Domingo, C., Rodríguez-Clemente, R., Blesa, M., 1994. Morphological properties of α-FeOOH, γ-FeOOH and Fe3O4 obtained by oxidation of aqueous Fe (II) solutions. Journal of colloid and interface science 165, 244–252.

Dyer, L., Su, B., Asselin, E., 2012. Cobalt loss due to iron precipitation in ammoniacal carbonate solutions. Hydrometallurgy 125, 144–147.

Flores, R.G., Andersen, S.L.F., Maia, L.K.K., José, H.J., Moreira, R. de F.P.M., 2012. Recovery of iron oxides from acid mine drainage and their application as adsorbent or catalyst. Journal of Environmental management 111, 53–60.

Flynn Jr, C.M., 1984. Hydrolysis of inorganic iron (III) salts. Chemical Reviews 84, 31–41.

George, P., 1954. The oxidation of ferrous perchlorate by molecular oxygen. Journal of the Chemical Society (Resumed) 4349–4359.

Grundl, T., Delwiche, J., 1993. Kinetics of ferric oxyhydroxide precipitation. Journal of Contaminant Hydrology 14, 71–87. https://doi.org/10.1016/0169-7722(93)90042-Q

Haber, F., Weiss, J., 1934. The catalytic decomposition of hydrogen peroxide by iron salts. Proceedings of the Royal Society of London. Series A-Mathematical and Physical Sciences 147, 332–351.

Hajar, A., Riefler, G., 2013. Selective precipitation of aluminium and iron in acid mine drainage. Presented at the National Association of Abandoned Mine Land Programs Conferebce, Daniel WV, pp. 206–222.

Hedrich, S., Johnson, D.B., 2012. A modular continuous flow reactor system for the selective bio-oxidation of iron and precipitation of schwertmannite from mine-impacted waters. Bioresource technology 106, 44–49.

Hove, M., 2008. The kinetics and mechanisms of the oxidation and precipitation of iron : the high density sludge (HDS) process.

Hove, M., Van Hille, R.P., Lewis, A.E., 2007. The effect of different types of seeds on the oxidation and precipitation of iron from homogeneous solutions. BIWIC 2007 14th Internationa workshop on idustrial crystallysation.

Huffman, R.E., Davidson, N., 1956. Kinetics of the Ferrous Iron-Oxygen Reaction in Sulfuric Acid Solution. Journal of the American Chemical Society 78, 4836–4842. https://doi.org/10.1021/ja01600a004

Hustwit, C.C., Ackman, T.E., Erickson, P.M., 1992. Role of Oxygen Transfer in Acid Mine Drainage Treatment 24.

Jackson, E., 1986. Hydrometallurgical extraction and reclamation. Chichester: Horwood; New York et al.: Wiley.

Jambor, J.L., Dutrizac, J.E., 1998. Occurrence and constitution of natural and synthetic ferrihydrite, a widespread iron oxyhydroxide. Chemical reviews 98, 2549–2586.

Javed, T., 2017. Iron precipitation and associated metal loss from simulated process solutions.

Kobe, K.A., Dickey, W., 1945. Oxidation of Ferrous Sulfate Solutions with Oxygen. Industrial & Engineering Chemistry 37, 429–431. https://doi.org/10.1021/ie50425a014

Kolthoff, I., 2002. Theory of coprecipitation. The formation and properties of crystalline precipitates. The Journal of Physical Chemistry 36, 860–881.

Kubota, N., Onosawa, M., 2009. Seeded batch crystallization of ammonium aluminum sulfate from aqueous solution. Journal of Crystal Growth 311, 4525–4529. https://doi.org/10.1016/j.jcrysgro.2009.08.014

Lamb, A.B., Elder, L.W., 1931. The electromotive activation of oxygen. Journal of the American Chemical Society 53, 137–163.

Loan, M., Newman, O., Cooper, R., Farrow, J., Parkinson, G., 2006. Defining the Paragoethite process for iron removal in zinc hydrometallurgy. Hydrometallurgy 81, 104–129.

Lydersen, E., 1990. The solubility and hydrolysis of aqueous aluminium hydroxides in dilute fresh waters at different temperatures. Hydrology Research 21, 195–204.

Mathews, C., Robins, R., 1972. The oxidation of aqueous ferrous sulphate solutions by molecular oxygen. Presented at the Proc. Aust. Inst. Min. Met, pp. 47–56.

McBain, J., 2002. Oxidation of ferrous solutions by free oxygen. The Journal of Physical Chemistry 5, 623–638.

Millero, F.J., 1985. The effect of ionic interactions on the oxidation of metals in natural waters. Geochimica et Cosmochimica Acta 49, 547–553. https://doi.org/10.1016/0016-7037(85)90046-8

Minegishi, T., Asaki, Z., Higuchi, B., Kondo, Y., 1983. Oxidation of ferrous sulfate in weakly acidic solution by gas bubbling. METALLURGICAL TRANSACTIONS B 8.

Morgan, B., Lahav, O., 2007. The effect of pH on the kinetics of spontaneous Fe(II) oxidation by O2 in aqueous solution – basic principles and a simple heuristic description. Chemosphere 68, 2080–2084. https://doi.org/10.1016/j.chemosphere.2007.02.015

Murad, E., Schwertmann, U., 1980. The Möessbauer spectrum of ferrihydrite and its relations to those of other iron oxides. American Mineralogist 65, 1044–1049.

Myerson, A., 2002. Handbook of industrial crystallization. Butterworth-Heinemann.

Ngatenah, S.N.I., Kutty, S.R.M. and Isa, M.H., 2010. Optimization of heavy metal removal from aqueous solution using groundwater treatment plant sludge (GWTPS).

Ostwald, W., 1886. Lehrbuch der allgemeinen Chemie. W. Engelmann.

Park, S.-M., Yoo, J.-C., Ji, S.-W., Yang, J.-S., Baek, K., 2015. Selective recovery of dissolved Fe, Al, Cu, and Zn in acid mine drainage based on modeling to predict precipitation pH. Environmental Science and Pollution Research 22, 3013–3022.

Pitzer, K.S., Mayorga, G., 1973. Thermodynamics of electrolytes. II. Activity and osmotic coefficients for strong electrolytes with one or both ions univalent. The Journal of Physical Chemistry 77, 2300–2308.

Pound, J.R., 1939. The Oxidation of Solutions of Ferrous Salts. Journal of Physical Chemistry 43, 955–967.

Rönnholm, M.R., Wärnå, J., Salmi, T., Turunen, I., Luoma, M., 1999. Kinetics of oxidation of ferrous sulfate with molecular oxygen. Chemical Engineering Science 54, 4223–4232. https://doi.org/10.1016/S0009-2509(99)00117-7

Rubin, A.J., Hayden, P.L., 1973. Studies on the Hydrolysis and Precipitation of Aluminum (III).

Ruiz, M.C., Jerez, O., Padilla, R., 2016. Kinetics of the Cupric Catalyzed Oxidation of Fe^{II} by Oxygen at High Temperature and High Pressure. Mineral Processing and Extractive Metallurgy Review 37, 160–167. https://doi.org/10.1080/08827508.2016.1168412

Russell, J., 1979. Infrared spectroscopy of ferrihydrite: evidence for the presence of structural hydroxyl groups. Clay minerals 14, 109–114.

Sahinkaya, E., Gungor, M., Bayrakdar, A., Yucesoy, Z., Uyanik, S., 2009. Separate recovery of copper and zinc from acid mine drainage using biogenic sulfide. Journal of Hazardous Materials 171, 901–906.

Sahu, S., Asselin, E., 2011. Characterization of residue generated during medium temperature leaching of chalcopyrite concentrate under CESL conditions. Hydrometallurgy 110, 107–114.

Schoen, R., Roberson, C.E., 1970. Structures of aluminum hydroxide and geochemical implications. American Mineralogist: Journal of Earth and Planetary Materials 55, 43–77.

Schwertmann, U., Cornell, R.M., 2000. Iron oxides in the laboratory. Wiley Online Library.

Seo, E., Cheong, Y., Yim, G., Min, K., Geroni, J., 2017. Recovery of Fe, Al and Mn in acid coal mine drainage by sequential selective precipitation with control of pH. Catena 148, 11–16.

Singer, P.C., Stumm, W., 1970. Oxygenation of ferrous iron. Water Poll. Cont. Res. Ser 14010–06169.

Snoeyink, V.L., Jenkins, D., 1980. Water chemistry. John Wiley.

Söhnel, O., Garside, J., Principles, P., 1992. Industrial Applications.

Stauffer, T.E., Lovell, H.L., 1968. The oxygenation of iron (ji) - relationship to coal mine drainage treatment 167.

Stumm, W., Lee, G.F., 1961. Oxygenation of Ferrous Iron. Industrial & Engineering Chemistry 53, 143–146. https://doi.org/10.1021/ie50614a030

Stumm, W., Morgan, J.J., 2012. Aquatic chemistry: chemical equilibria and rates in natural waters. John Wiley & Sons.

Sung, Windsor., Morgan, J.J., 1980. Kinetics and product of ferrous iron oxygenation in aqueous systems. Environmental Science & Technology 14, 561–568. https://doi.org/10.1021/es60165a006

Tabak, H.H., Scharp, R., Burckle, J., Kawahara, F.K., Govind, R., 2003. Advances in biotreatment of acid mine drainage and biorecovery of metals: 1. Metal precipitation for recovery and recycle 14.

Tamura, H., Goto, K., Nagayama, M., 1976a. Effect of anions on the oxygenation of ferrous ion in neutral solutions. Journal of Inorganic and Nuclear Chemistry 38, 113–117. https://doi.org/10.1016/0022-1902(76)80061-9

Tamura, H., Goto, K., Nagayama, M., 1976b. The effect of ferric hydroxide on the oxygenation of ferrous ions in neutral solutions. Corrosion Science 16, 197–207. https://doi.org/10.1016/0010-938X(76)90046-9

Towe, K.M., Bradley, W.F., 1967. Mineralogical constitution of colloidal “hydrous ferric oxides.” Journal of Colloid and Interface Science 24, 384–392.

Truesdell, A.H., Jones, B.F., 1973. A computer program for calculating chemical equilibrium of natural waters. https://doi.org/10.3133/wri7613

Turnbull, D., Vonnegut, B., 1952. Nucleation catalysis. Industrial & Engineering Chemistry 44, 1292–1298.

Verbaan, B., Crundwell, F., 1986. An electrochemical model for the leaching of a sphalerite concentrate. Hydrometallurgy 16, 345–359.

Wang, L.P., Ponou, J., Matsuo, S., Okaya, K., Dodbiba, G., Nazuka, T., Fujita, T., 2013. Integrating sulfidization with neutralization treatment for selective recovery of copper and zinc over iron from acid mine drainage. Minerals Engineering 45, 100–107.

Wehrli, B., 1990. Redox reactions of metal ions at mineral surfaces. IN: Aquatic Chemical Kinetics: Reaction Rates of Processes in Natural Waters. Environmental Science and Technology Series. John Wiley & Sons, New York. 1990. p 311-336. 9 fig, 4 tab, 58 ref.

Wei, X., Viadero, R.C., 2007. Synthesis of magnetite nanoparticles with ferric iron recovered from acid mine drainage: Implications for environmental engineering. Colloids and Surfaces A: Physicochemical and Engineering Aspects 294, 280–286. https://doi.org/10.1016/j.colsurfa.2006.07.060

3 Solvent extraction of iron and aluminium

3.1 Theory of solvent extraction

The SX, sometimes referred to as liquid-liquid separation, is one of the favored separation technique because of its simplicity, speed and wide scope (Kislik, 2012). SX involves the distribution of a solute or solutes between two immiscible liquids or phases owing to the difference in their solubility. This technique rests on a strong scientific foundation and is considered to be an ideal method for separating trace elements from multi element solutions (Rydberg, 2004). The method is of major commercial importance to the metallurgical, chemical and biochemical industries for its ability to separate valuable products or waste from a complex matrix of species.

The transfer of solute from one liquid phase to another involves extraction reactions, which permit the establishment of liquid-liquid distribution equilibria. The distribution of a solute A, equilibrated between an aqueous phase and an organic solvent may be described by an equilibrium equation (Rydberg, 2004);

$$A_{(aq)} \Leftrightarrow A_{org} \qquad 3.1$$

If concentration of the solute in one phase is constant, the concentration of the solute in the other phase is also fixed. The distribution coefficient is used to quantitatively measure the performance of a SX system. The relationship between the concentrations of solute in each of the phases led to Nernst's formulation of the distribution law (Kislik, 2012). This is the ratio of the solubility of a solute in the organic phase with its solubility in the aqueous phase. This is expressed mathematically by **Equation 3.2**.

$$D=\frac{A_{org}}{A_{aq}} \qquad 3.2$$

Where D is the distribution coefficient, A_{org} is the concentration of the solute in the organic phase, whereas A_{aq} is the concentration of the solute in the aqueous phase (Goto and Smutz, 1965). The D value is temperature dependent since solubility and equilibrium rates are greatly affected by the heat present in the solution. For metals species M, it can be written as;

$$D=\frac{[M]_{t,org}}{[M]_{t,aq}} \qquad 3.3$$

Where $[M]_t$ is the metal concentration.

A high distribution coefficient designates a high extractability of metal ions from the aqueous phase. However, in SX practice, the distribution coefficient is less informative than percentage extraction, S given by;

$$S=\frac{100D}{(1+D)} \qquad 3.4$$

The extraction curves are particularly useful for designing separation schemes. Another important parameter is the measure of the ability of the system to separate one species from another. This is called the separation factor, SF and is the ratio of the distribution of species to another. This is represented mathematically as;

$$SF=\frac{D_{M_a}}{D_{M_b}} \qquad 3.5$$

Where SF is the separation factor, D_{M_a} is the distribution coefficient of metal species M_a and D_{M_b} is the distribution coefficient of metal species M_b.

3.2 Extraction

Extraction of metal species can be achieved by using different extraction systems. These are classified as;

i. Chelate extraction

ii. Organic acid extraction

iii. Neutral or solvating extraction

iv. Ion-pair extraction

v. Ligand substitution extraction

vi. Synergetic extraction

However, some metal extractants belong to more than one class.

3.2.1.1 Extraction by chelation:-

Chelate refers to "claw", which can be described as a way in which the organic extractant binds a metal ion. A chelate is a metal complex which results from the interaction between central metal ions with a poly functional organic molecule giving rise to stable ring compound. Chelates have at least two donor atoms in the molecule which gives rise to ring formation. In many cases, upon bonding with the metal ion, the extractant releases a hydrogen ion into the aqueous solution from which the metal gets extracted. **Figure 3.1** shows a hydroxyquinoline complex with Al(III) (Clarke, 1991). The complex resulting from chelation is soluble in the organic phase. The general case of chelation may be represented by **Equation 3.6**.

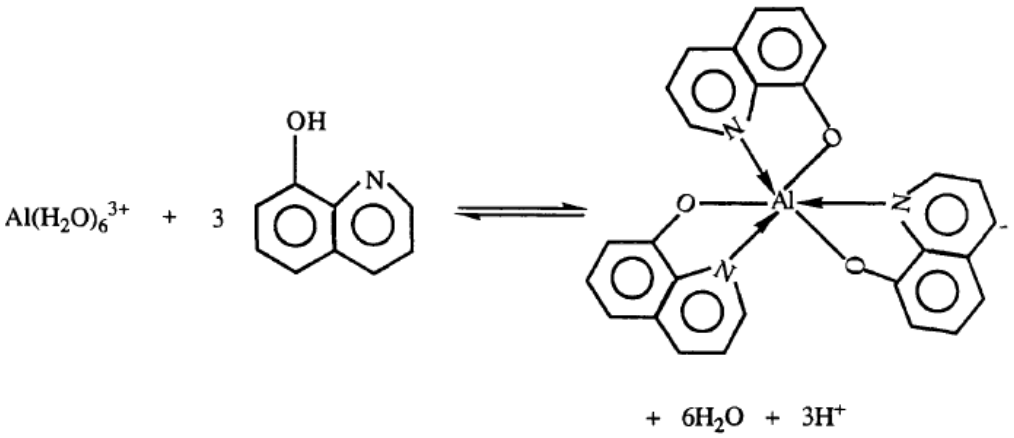

Figure 3.1: Example of complexation of Al(III) by chelation(Clarke, 1991)

$$M^{n+}_{(aq)} + nHA_{org} \rightleftharpoons MA_{n(org)} + nH^{+}_{(aq)} \qquad 3.6$$

Where M = metal and HA = extractant.

Chelates are classified according to the type of basic groups and charge present. If basic groups are uncharged, this results in a formation of the positively charged metal chelate. If the basic groups are anionic, then neutral chelate results while cationic reagents result in the formation negatively charged chelates. The cationic chelates pair with anion like perchlorate to form uncharged extractable species. Examples of commercially available chelating extractants include but not limited to 2-hydroxybenzophenone oximes, 8-hydroxyquinolines, thenoyltrifluoroacetone (HTTA), 1-benzoyl acetone (Clarke, 1991; Classen et al., 1954; Gao et al., 2015; Jordanov et al., 2002; Tamhina and Herak, 1976).

3.2.1.2 Acid extractants

Acid extractants are similar in much respect to chelating extractants in the sense that they are both expressed by the basic extraction equilibrium according to **Equation 3.6**. However, acid extractants are affected more by the solvent phase properties than chelating extractants. Self-association to form dimers and polymers by hydrogen

bonding is common with acid extractants, although this does not happen at high metal loading. The acid extractants operate by a cation exchange mechanism where the extractant proton is substituted by a metal. Examples of acid extractants include carboxylic acids e.g., PP′-di(2-ethylhexyl) methane diphosphonic acid (H2DEH[MDP]), phosphorus acids such as mono 2-ethyl hexyl phosphoric acid (H2MEHP) and phosphoric acids such as 2-ethylhexyl-phosphonic acid (HEHEHP).

3.2.1.3 Extraction by solvation:

Extractions by solvation has been reported by many authors (Barkat et al., 2001; Soldenhoff, 1987). Hydrated metal ions in aqueous solutions are extracted by adduct molecules containing donor sites and in such a case the extracted species gets solvated in the organic phase. In this way, the solvent itself participates in extraction of the complex. Extractants of this class are basic in nature and will coordinate to certain neutral metal complexes by replacing water of hydration, thereby causing the resulting organo-metal complex to become organic soluble and aqueous insoluble. The two types of extractants employed in solvation extraction are ones involving oxygen bonded to carbon or those involving oxygen bonded to phosphorous. Examples of the oxygen bonded to carbon species include esters and ketones while the oxygen bonded to phosphorous include species such as trialkyl phosphates(I), tributyl butylphosphonate, trialkyl phosphine oxides(IV).

3.2.1.4 Extraction by ion pair formation:

Extraction by ion-pair is based on the principle of ion association where a large, positively charged organic moiety causes the extraction of an anionic metal complex into the organic phase. It occurs through the formation of neutral uncharged species, which in turn get extracted in the organic phase. Usually long chain alkyl or aryl amines in acid media extract anionic metal complexes through ion pair formation. Alkyl or aryl group is responsible for organophilicity while positive charge of nitrogen favors ion pair formation (Katsuta et al., 2000; Nakai et al., 2004).

3.2.1.5 Ligand substitution extraction

Ligand substitution extraction is like neutral or solvating extraction in that extractant donates an electron pair to a metal ion, but they are different in that these extractants form inner shell complexes with metals and, in doing so, will displace other ligands

3.2.1.6 Synergism extraction

The term synergism was first used by Blake Jr et al. (1958) in the year 1958. It is the extraction term that describes the working together of two (or more) extractant molecules to transfer metal ions from aqueous medium to organic phase. The distribution ratio for the combination of extractants is greater than the largest individual distribution ratio e.g., D12 >> D1 + D2. In this way two extractants cooperate to increase the extraction.

For metal extraction to be successful, the synergist should have the following characteristics (Blake Jr et al., 1958);

i. It should have the capability to displace water molecules from the metal complex rendering it less hydrophilic

ii. It should form less stable complex than the primary ligand

iii. It should favor the maximum co-ordination number of the metal.

The extent of synergism is given by **Equation 3.7** (Rydberg, 2004; Siekierski and Taube, 1961);

$$\Delta D = D_{mix} - \left(D_I + D_{II}\right) \qquad 3.7$$

Where ΔD is the extent of synergism, D_{mix}, D_I and D_{II} denote the distribution ratios of a metal ion with mixture of extractants (I + II), extractant I and extractant II, respectively, in binary liquid system. The extent of synergism is determined by the synergistic

coefficient (S.C) for the combination of the two extractants and is defined by **Equation 3.8** (Rydberg, 2004; Siekierski and Taube, 1961);

$$S.C=\log\left[\frac{D_{mix}}{D_I-D_{II}}\right] \qquad 3.8$$

Where S.C is the synergistic coefficient.

Synergism will only occur when S.C and ΔD have positive values. When both S.C and ΔD have negative values, there is a decrease in synergism extraction. This phenomenon is known as antagonism (Anyun, 2001). Any of the following combination of extractants can be used in synergism extraction;

i. Acidic and neutral extractants

ii. Two acidic extractants

iii. Two neutral extractants

iv. Anionic and neutral extractants

v. Cationic and anionic extractants

vi. Two anionic extractants.

3.3 Solvent extraction of Fe(III) and Al(III) from acidic sulphate solutions

Section 3.1 and **3.2** discussed the general principles of SX. However, in the context of this study, it is pertinent to discuss the extraction and stripping of Fe(III) and Al(III), as well as the associated metal species found in AMD.

The separation and recovery of Fe(III) and Al(III) by SX has been studied by several researchers under different operating conditions and in the matrix of other metal species. Meyer et al. (1980) recommended the use of acidic extractants such as acidic organophosphorus to extract both Fe(III) and Al(III) from acidic solutions. Since then,

acidic organophosphorus extractants have been used to extract Fe(III) and Al(III). Senapati et al. (1994) studied the extraction of Fe(III) using 0.2 M -bis(2,4,4-trimethylpentyl) phosphinic acid (Cyanex 272) as the extractant from sulfate solution. After Fe(III) recovery through SX, the raffinate still contained 0·25 g/L of Fe(III) which was quantitatively separated by a lime precipitation technique. Deep et al. (2006) studied the separation of Fe(III) and Al(III) from a tannery filtrate using Cyanex 272. The solvent was found to be efficient for the extraction of Fe(III) and Al(III) with the possibility of the solvent's easy regeneration using dilute sulfuric acid. In another study, Deep et al. (2007) used a mixture of partially neutralized Cyanex 272 and tributyl phosphate (TBP) for the extraction of Fe(III) from the sulfuric acid medium containing high Fe content. They observed that during Fe(III) extraction by the solvent, a proportional amount of H^+ ion was released in to the aqueous phase thus stopping further mass transfer. Consequently, the solvent was partially neutralized to circumvent the problem. An equivolume addition of TBP in the extractant solution was required to attain satisfactory phase separation characteristics. The proposed extractant mixture extracted Fe(III) over a fairly wide range of the aqueous phase pH with a good loading capacity.

Figure 3.2 shows pH-dependence of metal cation loading by Cyanex 272 with the loading sequence of Fe(III) > Zn(II) > Al(III) > Mn(II) > Mg(II) > Ca(II) (Aguilar and Cortina, 2008). These are the cations that are mostly found in AMD.

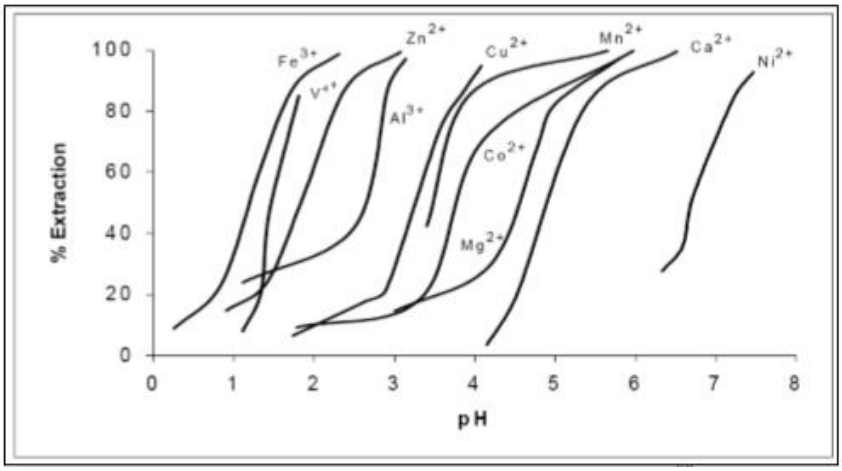

Figure 3.2: Typical Cyanex 272 extraction curves at different pH values (Aguilar and Cortina, 2008)

Ichlas and Ibana (2017) proposed a process consisting of two SX steps but with only one extractant - Cyanex 272, used in both steps. The first extraction step involved the removal of Al(III) and Zn(II), whereas the second extraction step involved the separation of Co along with Mg from Ni. The experimental results showed essentially quantitative removal of Al(III) (>97%) and Zn(II) (>99%) in a single extraction stage using 20vol% Cyanex 272 at pH 2.1. Ajgaonkar and Dhadke (1997) developed a rapid method for the SX separation of Fe(III) and Al(III) from multicomponent mixtures using Cyanex 302 in chloroform. The Fe(III) and Al(III) were quantitatively extracted at pH 2.0-2.5 and 3.0-4.0 using 0.005 M and 0.001 M Cyanex 302 in chloroform, respectively. Mishra and Dhadke (1998) examined the separation of Al(III) and Be(II) using Cyanex 921 diluted in cyclohexane for the separation of Be(II) and Al(III) by pH adjustment. Al(III) was first selectively extracted in the pH range 4.5 – 5.5. Thereafter, the pH was raised to between 8 and10 where Be(II) was selectively extracted. In another study, Deep et al. (2006) proposed the separation of Fe(III) and Cr(III) by SX with 0.50 M Cyanex 923. Fe(III) was selectively extracted from the mixed sulhuric acid and sodium chloride medium leaving pure Cr(III) in the raffinate.

Other organophosphorus acids have also been used to extract mostly Fe(II) from different process solutions. Demopoulos and Pouskoulell (1989) reported on the innovative use of H2MEHP as a selective extractant of Fe(III) from concentrated sulphuric acid solutions. In a mixture with a long-chain alcohol as modifier and an aliphatic diluent, the extractant was found to extract Fe(III) at high rates and loadings from feed liquors of varying sulphuric acid concentrations (up to 150 g/l), thus effectively eliminating the need for pH control. Xue et al. (1999) conducted studies for the removal of Fe(III) from a Zn sulfate solution using Eichrom’s Dipex extractant, H2DEH[MDP]. They found that 99% of Fe(III) can be extracted effectively and selectively using this extract from a highly acidic solution. The separation factor of Fe/Zn, was 106. Fortes and Benedetto (1998) carried out separation of Fe(III) from indium in sulfuric acid media using di-(2-ethylhexyl) phosphoric acid (D2EHPA) diluted in isoparafin. The results showed that D2EHPA can be effectively used to separate Fe(III) and In(II) from acid solutions.

Carboxylic acids have also been used to extract Fe(III) and Al(III). For example, Mühl et al., (1980) conducted a study of the separation of Fe(III) and Al(III) by SX using carboxylic acid tributyl phosphate, amines and aliphatic monocarboxylic acids. The Fe(III) was extracted from both the chloride and sulfate leach liquors of aluminosilicate leaching. The effect of pH, chloride ion, temperature Fe(III) and Al(III) concentrations on the separation efficiency were reported. Fe(III) was reduced from about 5–10 g/L in the leach liquor to less than 0.1 g/L. Fletcher et al. (1965) used tertiary aliphatic carboxylic acid and versatic 911 for the removal of Fe(III) from base metal solution at pH of about 2. It was reported that the hydrolyzed species were extracted as either $Fe(OH)L_2$ or $Fe(OH)_2L$.

Other reported studies especially on Fe(III) extraction used chelate extractants to separate Fe(III) from other metal species. Simpson et al. (1996) studied the SX of Fe(III) by means of the commercial salicyaldoxime LIX 860 and its influence on Cu(II) extraction in sulfuric acid media. Extraction experiments were carried out at varying equilibrium time, temperature, extractant concentration, pH of the aqueous phase, and concentration of Fe(III) and Cu(II) ions in the solution. Since LIX 860 is an acidic extractant, the extraction reaction for Fe(III) is expressed as;

$$Fe^{3+}_{(aq)} + 3HR_{(org)} \Leftrightarrow FeR_{3(org)} + 3H^{+}_{(aq)} \qquad 3.9$$

Thermodynamically, this reaction was found to be endothermic with $dH_o = 8.6$kJ/mol.

To improve the SX extraction kinetics, synergism extractants have also been employed to separate Fe(III) and Al(III) from process solutions. A synergism extraction study was conducted by Demopoulos et al. (1993) to extract Fe(III) from a solution containing 30-150 g/L sulphuric acid using a mixture of 7-alkylated 8-hydroxy quinoline (Kelex 100) with dialkyl phosphorus (HR) acids: D2EHPA, 2-ethylhexylester (PC-88A), or Cyanex 272. The results obtained showed synergism extraction with all the extractant mixtures apart from a Kelex 100-M2EPHA mixture. This was attributed to the formation of mixed metal-Kelex100-HR-sulfate complexes. Demopoulos and Gefvert (1984) reported on the

use of a mixed reagent consisting of Kelex 100 and (D2EHPA) for Fe(III) removal from sulfuric acid solution (50 < H_2SO_4 < 200 g/L). Synergism was observed both in terms of Fe(III) loading and extraction rate. In another study, Demopoulos and Pouskoulell (1989) expanded on synergism experimentation by testing a mixture of Kelex 100 with other alkyl phosphorous acid namely H2MEHP, HEHEHP, PC- 88A, and Cyanex 272. During experimentation, M2EHPA was found as an excellent extractant for Fe(III).

A kinetic study of Fe(III) extraction from sulfate solutions with primary amine N1923 and TBP was performed by Meng and Yu (1996) using a modified RDC after cell calibration. The result showed that the rate-limiting step in the extraction process is chemical reaction at the interfaces. Yu et al. (1989) established synergism was found in the extraction of Fe(III) by the addition of tertiary amine to HEHEHP or HR in the organic phase as solvent. The amount of sulphuric acid that was needed to trip Fe(III) was also found to reduce when mixed solvent was used. Jiayong et al. (1992) observed that a mixed solvent system consisting of a mixture of primary and secondary amines with neutral donor solvents such as 2-octanol and TBP enhanced the extraction and the stripping of Fe(III) from the sulfate system. With the addition of TBP in the primary amine solution, Fe is extracted as $(FeOHSO_4)(RNH_3)_2SO_4 \cdot TBP$, which is schematically shown in **Figure 3.3**. For a primary amine alone as the solvent, the extraction species is $Fe(SO_4)_3(RNH_3)_3$. Thus, Fe is extracted as an unhydrolysed iron sulfate complex $FeSO_4$ with the dissociated amine sulfate.

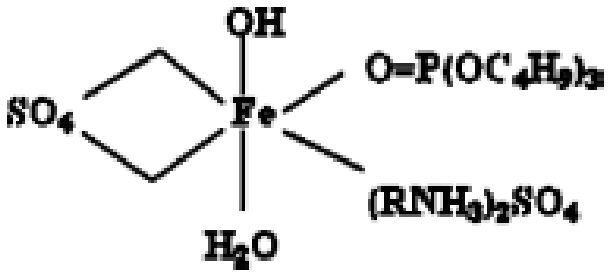

Figure 3.3: Schematic representation of the proposed extraction species of Fe(III) with primary amine and TBP (Jiayong et al., 1992)

3.4 Solvent extraction of other metals associated with AMD

Although SX of Fe(III) and Al(III) has been employed with considerable success, the solution chemistry of AMD means considerable attention should be given to the other metal species that are found in AMD. The two other metal cations found in substantial concentrations in coal AMD are Mn and Mg. Aguilar and Cortina (2008) established that pH-dependence of metal cation loading by Cyanex 272 with the loading sequence of Fe(III) > Zn(II) > Al(III) > Mn(II) > Mg(II) > Ca(II) (shown in **Figure 3.2**). (Aguilar and Cortina, 2008). Therefore, it becomes pertinent to understand the behavior of these elements during Fe(III) and Al(III) extraction.

In the two-step process developed by Ichlas and Ibana (2017) to extract Al(III) and Zn(II) from a nitric leach solution, Co and Mn were co-extracted in four extraction stages at staggered pH values of 4.0, 4.4, 4.5, and 4.0 in the first, second, third, and fourth stages, respectively, using also 20vol% Cyanex 272. Tsakiridis and Agatzini-Leonardou (2005) conducted SX of Al(III) in the presence of Co, Ni and Mn from sulphate solution with 0.63 M Cyanex 272 in the pH range 2.0-3.0. The Co and Mg co-extraction did not exceed 0.5%.

3.5 Methods of extraction

The two commonly applied methods of solvents extraction batch wise extraction, commonly applied with lab scale test work and multistage countercurrent extraction.

3.5.1 Batch wise single stage extractions:

This is commonly used on the small scale in chemical labs. It is normal to use a separating funnel. Batch extraction is the simplest one consisting of extracting the solute from one immiscible layer until equilibrium is attained, after which layers can settle and the two phases would then be separated. This method is mostly used for analytical separation. This extraction method was adopted in this study.

3.5.2 Multistage counter current continuous processes:

These are commonly used in industry for the processing of metals such as the base metals, lanthanides etc. This is because the separation factors are so small that many extraction stages are needed to achieve the desired separation. In the multistage processes, the aqueous raffinate from one extraction unit is fed to the next unit as the aqueous feed, while the organic phase is moved in the opposite direction. Hence, in this way, even if the separation between two metals in each stage is small, the overall system can have a higher separation factor.

Chapter summary

This chapter gives an overview of the SX processes and a discussion of the extraction of metals from acidic sulphate solutions. In these types of solutions, there is a buildup of acidity and metal impurity. The nature of waste generated becomes very complex and hazardous. Hence, it becomes mandatory for industries to treat these solutions for either purification purposes for downstream processes or impurity removal before disposal. SX is a technique that can be used for environmental sustainability by recovering valuable metals from waste solutions thereby reducing the heavy metals that are ultimately discharge into the environment. The current practice of AMD neutralization and precipitation of the metallic contents as sludge leads to the loss of the metal value present, and the burden of sludge disposal remains (discussed in **Chapter 1**). Hence, the idea of the 3R's, i.e. recover-recycle-reuse, of these wastes has become the main focus of the research.

In this section, the various aspects on Fe(III) and Al(III) recovery from different sulphate solutions by SX methods have been discussed. Various types of solvents used for metal extraction such as chelating, acidic extractants, solvation, mixed solvents etc., been discussed. In the context of this study i.e., co-extraction of Fe(III) and Al(III), most of the researchers have reported good extraction efficiencies when Cyanex 272 has been used. More so, the stripping of the two species from the loaded organic solution has been reported to happen with relatively easy with sulphuric acid solution. As such, the decision of experimenting the SX of Fe(III) and Al(III) with Cyanex 272 in Shellsol D70 was arrived at.

References

Aguilar, M., Cortina, J.L., 2008. Solvent extraction and liquid membranes: Fundamentals and applications in new materials. CRC Press.

Ajgaonkar, H., Dhadke, P., 1997. Solvent extraction separation of iron (III) and aluminium (III) from other elements with Cyanex 302. Talanta 44, 563–570.

Anyun, Z., 2001. Study of the antagonistic extraction of palladium (II) with 1-phenyl-3-methyl-4-propionylpyrazolone-5-one and an organic amine. Solvent Extraction and Ion Exchange 19, 925–938.

Barkat, D., Derriche, Z., TAYEB, A., 2001. Synergistic Solvent extraction of zinc (II) and cadmium (II) from sulfate medium by a mixture of 1-phenyl-3-methyl-4-benzoylpyrazol-5-one and methyl-isobutyl ketone. Turkish Journal of Chemistry 25, 381–389.

Blake Jr, C., Baes, C., Brown, K., Coleman, C., White, J., 1958. PROC. UN INTERN. CONF. PEACEFUL USES AT. ENERGY, 2ND GENEVA 28, 289.

Clarke, P.A., 1991. Studies into the separation of the component metals of chrome residue.

Classen, A., Bastings, L., Visser, J., 1954. A highly selective procedure for the spectrophotometric determination of aluminium with 8-hydroxy-quinoline and its application to the determination of. Analytica Chimica Acta 10, 373–385.

Deep, A., Correia, P.F., Carvalho, J.M., 2006. Separation and recovery of Fe (III) and Cr (III) from a tannery filtrate using Cyanex 272. Industrial & engineering chemistry research 45, 3200–3206.

Deep, A., Correia, P.F., de Carvalho, J.M., 2007. Liquid− Liquid Extraction and Separation of a Macro Concentration of Fe3+. Industrial & engineering chemistry research 46, 5707–5714.

Demopoulos, G., Gefvert, D., 1984. Iron (III) removal from base-metal electrolyte solutions by solvent extraction. Hydrometallurgy 12, 299–315.

Demopoulos, G., Mihaylov, I., Pouskouleli, G., 1993. Synergistic Extraction of Iron (III) from Sulphuric Acid Solutions with Mixed Kelex 100-Alkyl Phosphorus Acid Extract ants. Solvent extraction and ion exchange 11, 67–89.

Demopoulos, G., Pouskoulell, G., 1989. Solvent extraction of iron (III) from acid sulphate solutions by mono (2-ethyl hexyl) phosphoric acid. Canadian Metallurgical Quarterly 28, 13–18.

Fletcher, A.W., Flett, D., Wilson, J., 1965. Solvent extraction of ferric iron by a carboxylic acid.

Fortes, M., Benedetto, J., 1998. Separation of indium and iron by solvent extraction. Minerals engineering 11, 447–451.

Gao, M.-W., Zhu, G.-R., Wang, X.-H., Wang, P., Gao, C.-J., 2015. Preparation of short channels SBA-15-PVC membrane and its adsorption properties for removal of uranium (VI). Journal of Radioanalytical and Nuclear Chemistry 304, 675–682.

Goto, T., Smutz, M., 1965. Separation factors for solvent extraction processes: The system of 1 M di-(2-ethyl-hexyl) phosphoric acid (in amsco 125-82)-Pr-Nd salts as an example. Journal of Inorganic and Nuclear Chemistry 27, 1369–1379.

Ichlas, Z.T., Ibana, D.C., 2017. Process development for the direct solvent extraction of nickel and cobalt from nitrate solution: aluminum, cobalt, and nickel separation using Cyanex 272. International Journal of Minerals, Metallurgy, and Materials 24, 37–46.

Jiayong, C., Shuqiu, Y., Huizhou, L., Xiquan, M., Zhichun, W., 1992. New mixed solvent systems for the extraction and separation of ferric iron in sulphate solutions. Hydrometallurgy 30, 401–416.

Jordanov, V., Atanassova, M., Dukov, I., 2002. Solvent extraction of lanthanides with 1-phenyl-3-methyl-4-benzoyl-5-pyrazolone. Separation Science and Technology 37, 3349–3356.

Katsuta, S., Yamada, H., Kudo, Y., Takeda, Y., 2000. Ion-pair formation in water and extraction into benzene of 18-crown-6–sodium ion complex with nitrated phenolate ions. Analytica chimica acta 416, 145–150.

Kislik, V.S., 2012. Solvent extraction: classical and novel approaches. Elsevier.

Meng, M.X., Yu, S., 1996. Kinetics of iron (III) extraction with primary amine and TBP using a modified rotating diffusion cell. Hydrometallurgy 41, 55–70.

Meyer, G.A., Fekete, S.O., Wicker, G.R., 1980. Selective extraction of iron and aluminum from acidic solutions.

Mishra, B., Dhadke, P., 1998. Solvent extraction separation of beryllium (ll) from aluminum (lll) by cyanex 921 (TOPO). Separation science and technology 33, 1681–1692.

Mühl, P., Gloe, K., Fischer, C., Ziegenbalg, S., Hoffmann, H., 1980. The application of liquid—liquid extraction for the separation of iron during the production of alumina. Hydrometallurgy 5, 161–178.

Nakai, T., Murakami, Y., Sasaki, Y., Fujiwara, I., Tagashira, S., 2004. Ion-pair formation of a copper (II)-ammine complex with an anionic surfactant and the recovery of copper (II) from ammonia medium by the surfactant-gel extraction method. Analytical sciences 20, 235–237.

Rydberg, J., 2004. Solvent extraction principles and practice, revised and expanded. CRC press.

Senapati, D., Chaudhury, G.R., Sarma, P.B., 1994. Purification of nickel sulphate solutions containing iron, copper, cobalt, zinc and manganese. Journal of

Chemical Technology & Biotechnology: International Research in Process, Environmental AND Clean Technology 59, 335–339.

Siekierski, S., Taube, M., 1961. General remarks on synergic effects in the extraction of uranium and plutonium compounds. Nukleonika (Poland) 6.

Simpson, J., Navarro, P., Alguacil, F.J., 1996. Iron (III) extraction by LIX 860 and its influence on copper (II) extraction from sulphuric solutions. Hydrometallurgy 42, 13–20.

Soldenhoff, K.H., 1987. Solvent extraction of copper (II) from chloride solutions by some pyridine carboxylate esters. Solvent Extraction and Ion Exchange 5, 833–851.

Tamhina, B., Herak, M., 1976. Solvent extraction of uranium (VI) by 3-hydroxy-2-methyl-1-phenyl-4-pyridone. Journal of Inorganic and Nuclear Chemistry 38, 1505–1507.

Xue, S., Gula, M., Horwitz, E., 1999. Solvent extraction of iron(III) from acid sulfate solutions with Eichrom's Dipix extractant. Presented at the 1999 SME Annual Meeting: Mining in a New Era, p. 72.

Yu, S., Chen, J., Chen, C.-Y., 1989. Synergistic extraction of ferric iron in sulfate solutions by tertiary amine and 2-ethylhexyl 2-ethylhexylphosphonic acid (HEHEHP) or dialkylphosphonic acid. Hydrometallurgy 22, 183–192.

4 Coagulation

Chemical coagulation is an essential part of drinking water and wastewater treatment. This section discusses the coagulation process of water treatment.

4.1 Coagulation process

Water pollution can be attributed to the discharge of untreated waste, dumping of industrial effluent, and the run-off from agricultural fields. Impurities in water are in colloids size and are negatively charged. Several methods have been used to remove colloidal impurities from water among which is coagulation and flocculation. Coagulation and flocculation processes are essential in a number of diverse disciplines including biochemistry, rubber manufacturing and in water and wastewater treatment (Bratby, 2006). Mer and Healy (1963) deplored the indiscriminate use of the terms coagulation and flocculation which is found to represent synonymous concepts. It was proposed that the term coagulation be based on colloidal destabilization where colloidal particles are united while flocculation is used for precipitation and co-precipitation mechanism. The enmeshment of colloidal particles in a precipitate has generally come to be known as sweep flocculation (discussed in **Section 4.4**). These processes are typically used in destabilizing, agglomerating and subsequent removal of particles. Coagulation is a physico-chemical process which neutralizes the colloidal particles in water by a chemical called coagulant. The neutralization forces the colloidal particles to join to form small aggregates called flocs which are easily filtered from the water. First, the repulsion force between particles must be overcome, a step that requires that the particles be destabilized; and, second, contact between the destabilized particles must be induced so that aggregation can occur. The destabilization step typically is achieved through the addition of chemicals to modify the electrochemistry properties on the particle surfaces, followed by thorough blending in rapid mix tanks. The aggregation step is accomplished through gentle stirring (slow mixing) in flocculation tanks. A representation of the coagulation process is shown in **Figure 4.1** (Bagwell et al., 2001).

4.2 Coagulation with Al(III) and Fe(III)

Coagulation and flocculation phenomena have been practiced from the earliest times using a variety of substances to treat water and wastewater. The widely used coagulants in water treatment are metal salts including aluminium sulphate $\left[Al_2(SO_4)_3.14.3H_2O\right]$, aluminium chloride $\left[AlCl_3\right]$, polyaluminium chloride $\left[(AlCl_3)_N\right]$, ferric sulphate $\left[Fe_2(SO_4)_3.5H_2O\right]$ and ferric chloride $\left[FeCl_3\right]$ (Saunders and Saunders, 1991).

When added to water, Al(III) and Fe(III) salts dissociate to their respective trivalent ions, Al^{3+} and Fe^{3+}, and then associate with water molecules to form hydroxy complexes, ($Al(H_2O)_6^{3+}$ and $Fe(H_2O)_6^{3+}$). These complexes then react with the water by replacing the H_2O molecules in the aquometal complex with OH^- ions. These subsequent reactions are called hydrolysis reactions. Hydrolytic reactions result in the formation of several soluble species, including monomeric, dimeric, and polymeric hydroxometal complexes. The typical hydrolysis reactions are presented in **Section 2.2.6**.

4.3 Coagulation with polymers

Apart from Al(III) and Fe(III) salts, synthetic organic polymers have been shown to be effective coagulants or coagulant aids. Polymers are long-chain molecules composed of many subunits called monomers. A polymer that is composed of only one type of monomer is termed a homopolymer and those comprised of different monomers are termed copolymers (Bagwell et al., 2001). The number and type of subunits or monomers can be varied to yield a wide range of polymers having different chemical characteristics (such as charge polarity and charge density) and molecular weights. A polymer is called a polyelectrolyte if its monomers consist of ionizable groups. Polyelectrolytes having a positive charge upon ionization are referred to as cationic polymers. Negatively charged polyelectrolytes are termed anionic polymers. Finally, polymers that do not contain ionizable groups are called nonionic polymers.

Cationic polymers have been shown to be effective in coagulating negatively charged clay particles (Ruehrwein and Ward, 1952). It has been hypothesized that electrostatic forces or ion exchange is the process by which the polymers become attached to the clay particles, which is then followed by bridging. Cationic polymers do not require a large molecular weight to be effective in destabilization. Low dosages of cationic polymer (0.1 to 1.5 mg/L) are usually sufficient to achieve coagulation. In contrast, 5 to 150 mg/L of alum or ferric sulphate/ chloride is often needed to obtain similar results.

Anionic particles generally are ineffective coagulants for negatively charged particles, and there is for the presence of divalent metal ions (such as Mg^{2+}) for anionic polymers to flocculate negative colloids (Ruehrwein and Ward, 1952). However, anionic polymers of large molecular weight or size can bridge the energy barrier between two negatively charged particles, thereby effectively enhancing the coagulation efficiency. The minimum polymer size depends on several factors, but limited data indicate that the minimum size is on the order of a molecular weight of one million. When anionic polymers are used in conjunction with an electrolyte such as NaCl or $CaCl_2$ or another coagulant such as alum, their coagulation efficiency is increased.

There are pros and cons to the use of either synthetic organic polymer coagulants or metal salts coagulants. The use of alum or ferric chloride can result in copious volumes of sludge that must be handled, whereas the sludge quantities are negligible when a polymer is used. On the other hand, a narrow bank exists for optimum polymer dosage with synthetic organic polymers. Overdosing or under dosing from this optimum dose will result in re-stabilization of the colloids and hence failure of the coagulation process. The control method for polymer feed systems must be precise and reliable to give satisfactory performance (Bagwell et al., 2001). On the contrary, there is a sizeable bank for optimal metal salt coagulant dosage.

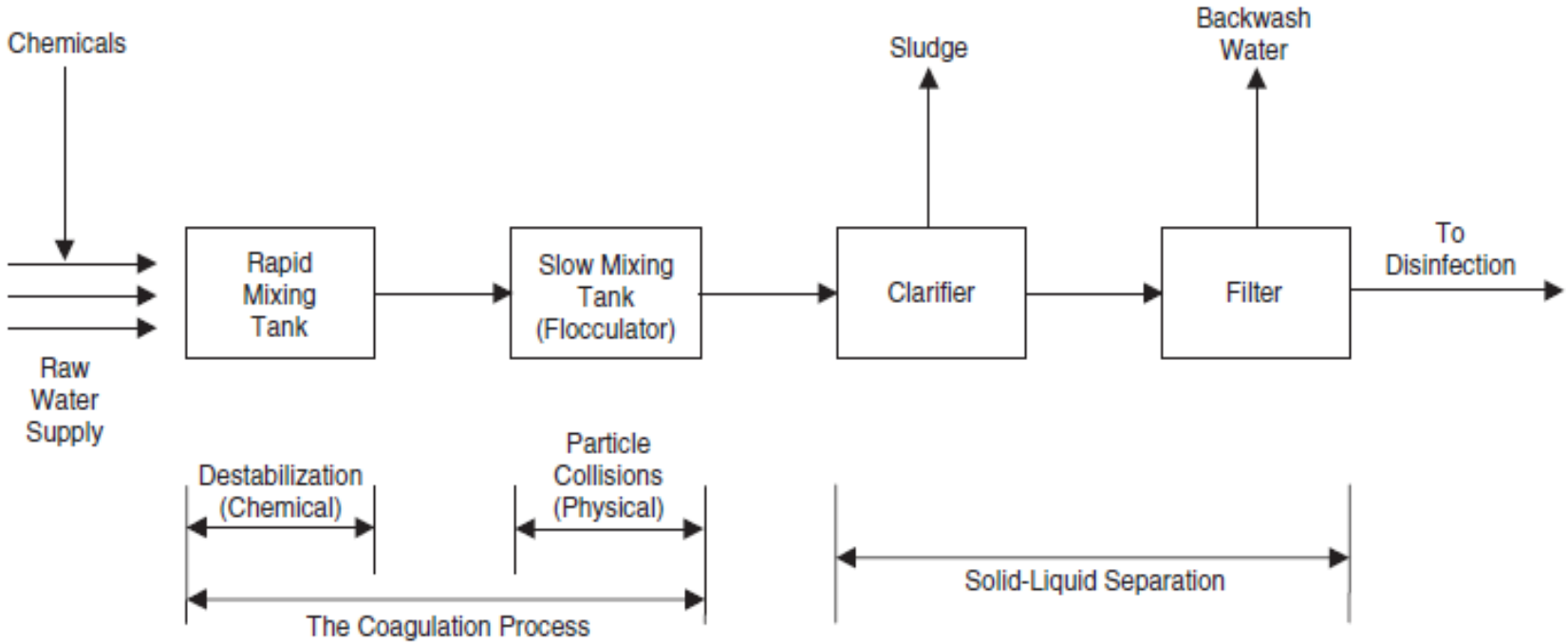

Figure 4.1: Schematic diagram of conventional coagulation / flocculation / sedimentation process (Bagwell et al., 2001)

4.4 Coagulation mechanisms

The exact mechanism of particle destabilization in water treatment is a complex process which involves many reactants and reactions. It was suggested by Stumm and O'Melia (1968) that coagulation is a time dependent process which include several reaction steps such as;

- hydrolysis and subsequent polymerization of multivalent metal ions to multiinuclear hydrolysis species (**discussed in Section 2.2.6**)
- adsorption of hydrolysis species at the solid-solution interface to accomplish destabilization of the colloid
- aggregation of destabilized particles by interparticle bridging involving particle transport and chemical interactions.
- aggregation of destabilized particles by particle transport and van der Waals forces.
- ‘’aging" of flocs, accompanied by chemical changes in the structure of M-OH-M (metal-hydroxide-metal) linkages, with concurrent change in floc stability and in the extent of floc hydration
- precipitation of the metal hydroxide.

Under certain conditions, these steps occur either sequentially, overlap or concurrently. It is reasonable to assume that different reaction steps may become rate controlling under different conditions (Stumm and O'Melia 1968).

Essentially, there are four coagulant mechanism by which coagulation in water treatment occur (Amitharajah and O'Melia, 1990; Langelier and Ludwig, 1949; Saunders and Roeder, 1991; Wei et al., 2015). These are;

1. Adsorption of hydrolysis species on the colloid causing charge neutralization

2. Enmeshment of the colloid to be coagulated by hydroxide precipitates of the coagulant metal ("sweep" coagulation)
3. Compression of the double layer
4. Adsorption to permit interparticle bridging

Double layer compression is a phenomenon that has been well studied and is mechanistically well understood (Capodaglio et al., 2011; Lyklema, 1978). Double layer compression is accomplished by additions of indifferent electrolytes (charged ions) which accumulates at the particle surface and are held there through attractive and electrostatic forces. The compact and fixed region of counter ions is known as the “stern layer”. Surrounding this is the “diffuse layer” of ions resulting from electrostatic attractions of ions of opposite charge to the particle and electrostatic repulsion of ions of the same charge as the particle. Together, the two layers form the “electrical double layer”. The destabilization by the double layer compression has not been considered an important mechanism in typical water treatment conditions. Thus, this mechanism will also not be discussed any further.

Adsorption and interparticle bridging mechanism is the case where polymers or synthetic organic types of coagulants specifically adsorb to the surface leading to charge neutralization. This mechanism has been used to explain the ability of synthetic organic polymer with high molecular weight, to coagulate a colloidal dispersion. However, since all the works in this study were performed using Fe(III) and Al(III) based coagulants, this mechanism will not be discussed further.

4.4.1 Adsorption and charge neutralization

Destabilization of colloids by charge neutralization requires collision between the colloids and the incipiently forming product of the hydrolysis reactions. Adsorption of charged species for neutralization has been documented as one of the key steps in the coagulation process. Adsorption of cations on negative surfaces may occur for simple electrostatic reasons or by some form of surface complex formation. The adsorbed

counter ions neutralize the colloidal surface charge, thereby reducing the repulsive energy barrier and encouraging rapid coagulation (Kang, 1994).

When adsorption continues beyond neutralization, this leads to reversal of the charge at colloidal surface. In this case, the repulsive energy barrier to coagulation is reestablished and the colloids are re-stabilized. O'Melia (1987) stated that although destabilization of colloids is a function of electrostatic colloidal surface properties, these properties are determined primarily by the chemistry of the system. The adsorption and hence, the destabilizing capacity is influenced by the chemical structure, the presence of certain functional groups, and the degree of hydrolysis of coagulants.

From the standpoint of coagulation, the total amount of soluble metal species is important. **Figure 4.2** shows the concentration of Fe(III) and Al(III) hydrolysis products, in equilibrium with the amorphous hydroxide, over a range of pH values. Although the species responsible for charge neutralization could be dissolved cationic hydrolysis products, it is clear from **Figure 4.2** that, for both Al(III) and Fe(III), such species are only minor components at around neutral pH and above. For example, at a pH of around 6, there is a minimum solubility (about 2 µM) for Al(III) with Fe(III) species showing a much lower solubility (around 20 nM). The Fe and Al(III) solubility calculations are significantly affected by the presence complexing cations. These include fluoride, phosphate, and sulphate, which can give increased solubility of the metals, especially at lower pH values (Reiber et al., 1995). As well as the effects on equilibrium species distribution, some anions can modify the rate of hydroxide precipitation. An important example is the sulphate, which can enhance precipitation of aluminium hydroxide (De Hek et al., 1978), essentially by association with highly charged polynuclear species, thereby reducing the free energy barrier to the formation of solid particles.

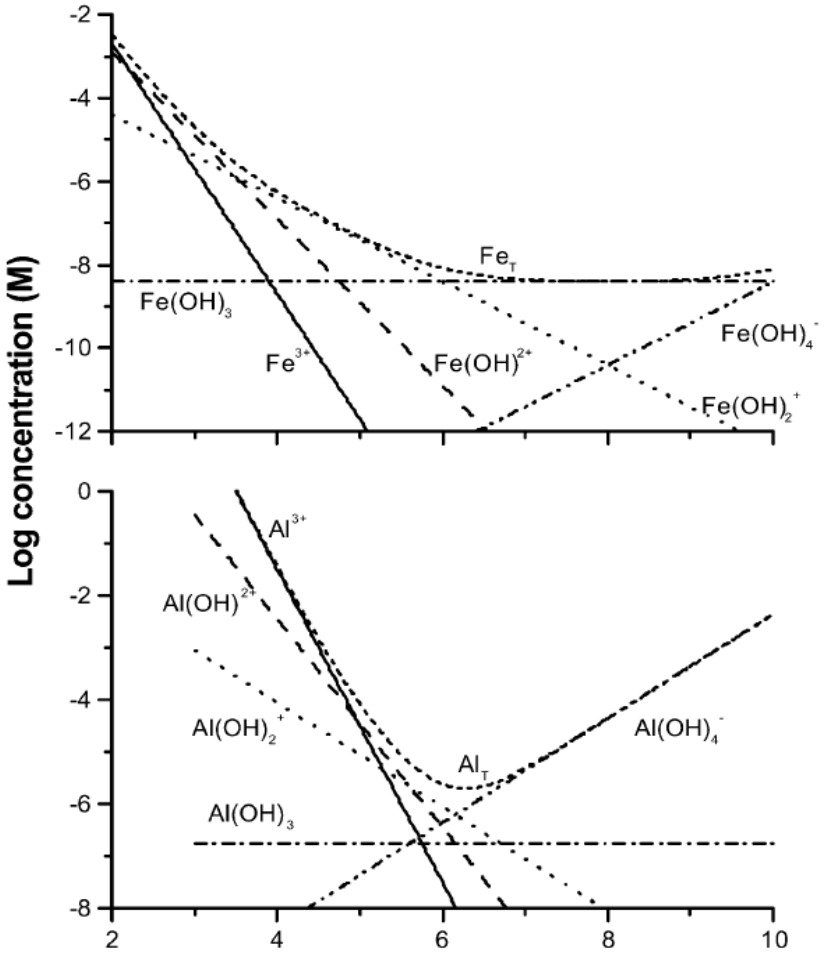

Figure 4.2: Concentration of soluble Fe and Al species in equilibrium with amorphous hydroxides. (Fe_T and Al_T represent total soluble species) (Peulen, T.O., 2007)

4.4.2 Sweep coagulation

Although particles may be effectively destabilized by charge neutralization, there are two disadvantages in water treatment (Gregory and Duan, 2001):

1. Quite precise control of coagulant dosage is needed to give optimum destabilization.

2. The particle collision rate and hence the coagulation rate depend on the square of the particle concentration and can be very low for dilute suspensions.

These problems can be avoided if higher coagulant dosages are used, since considerable quantities of amorphous hydroxide precipitate are then formed. When a metal salt such as alum or Fe(III) salt is added to water in concentration sufficiently high to cause precipitation of a metal hydroxide, colloidal particles can be enmeshed in these precipitates as they are formed and also collide with them afterward (Amitharajah and O'Melia, 1990). This process is often referred to as "sweep floc" removal.

Packham (1965) established that optimal removal of particles from water is achieved under conditions of rapid hydroxide precipitation. Although precise mechanisms are still not fully understood, it is clear that impurity particles are enmeshed. Sweep flocculation generally gives considerably improved particle removal than when particles are destabilized by charge neutralization only. At least part of the reason is the greatly improved rate of aggregation, owing to the increased solids concentration. Hydroxide precipitates tend to have a rather open structure, so that even a small mass can give a large effective volume concentration and hence a high probability of capturing other particles. It is also possible that binding of particles by precipitated hydroxide may give stronger aggregates. The different mechanisms outlined above have led to the definition of four zones of coagulant dosage, with the following consequences for negatively charged particles (Gregory and Duan, 2001);

Zone 1: Very low coagulant dosage; particles still negative and hence stable

Zone 2: Dosage sufficient to give charge neutralization and hence coagulate

Zone 3: Higher dosage giving charge neutralization re-stabilization

Zone 4: Still high dosage giving hydroxide precipitate and sweep flocculation

As mentioned in the previous section, the rate of precipitation is increased by the presence of anions in solution. Sulfate ions are particularly effective. Moreover, the colloidal particles themselves can serve as nuclei for the formation of the precipitate, so that the rate of precipitation increases with increasing concentration of the colloidal particles to be removed (Weber, 1972).

4.5 Effect of operating conditions on coagulation

Kinetic studies have shown that coagulation and flocculation happen at a fast rate. For example, Hahn and Stumm (1968) conducted kinetic studies and established that the kinetics of Al(III) hydrolysis and precipitation require diffusion times estimated at 10^{-5} to 10^{-3} s for hydroxo-aluminum complexes to reach optimum destabilization. The reaction rates are so fast that to achieve the desired results, there is a need to control the parameters that affect coagulation and flocculation. The coagulation and flocculation processes can be affected by many factors including interacting constituents, surrounding environment, kinetics of coagulant hydrolysis and precipitation. The factors that affect coagulation are classified as controllable and uncontrollable parameters.

4.5.1 Controllable parameters

These are the parameters that can be manipulated to overcome any change in raw water characteristics. These include coagulant dosage, coagulant aid dosage, mixer type, coagulation mixing intensity and reaction time.

4.5.1.1 Coagulant dose

Regardless of the type of the coagulant used in coagulation, dose can be increased or decreased according to the incoming turbidity type and level to achieve the desired results. The general trend is an increase in the dose with higher turbidities and low temperatures (Budd et.al, 1997). Increase of coagulant dose beyond the optimum does not necessarily increase the performance. For example, if an excess dose of alum is applied, then very slight or no improvement to turbidity removal may be observed (Morris and Knock, 1984). In addition, higher amount of coagulants produces the adverse effect by generating extra sludge that needs to be treated later (Ammary and Cleasby, 1995).

4.5.1.2 Coagulant aid dose

Coagulant aids are used to enhance and improve the coagulation process. Their main function is to establish the bridging mechanism, and therefore, it is more aiding flocculation rather than the coagulation stage (Ammary and Cleasby, 1995). Coagulant aids are added in small concentration. However, their effect on the final turbidity levels is considerable and can also lead to the reduction in the concentration for the main coagulant used. Several types of coagulant aids are used. A good example is activated silica which is made from sodium silicate. It can act as coagulant by itself or as a coagulant aid when used with alum of ferric sulphate, by establishing bridges (Steel and Terence, 1981). In addition, polyelectrolytes (polymers) are now widely used as coagulants aid because of their large molecule size. The bridging mechanism is effective, producing a floc size up to 100 times greater than those produced by using metal salt coagulants alone (Steel and Terence, 1981). The optimum combinations and/or ratios for coagulant to coagulant aid are not always known. This varies according to the nature of the chemicals and raw water characteristics, as well as their interactions.

4.5.1.3 Coagulation mixing intensity (rapid) & velocity gradient

Coagulation mixing intensity plays a significant role in the coagulation process because it is a parameter that can easily be changed and consequently alter the energy that is imparted to the water. Rapid mixing provides the required kinetic energy to particles to overcome the energy barrier and allow the collision between colloids. During rapid mixing, not only dispersion of the coagulant in the raw water is carried out, but it also brings about the initial stage of particle collisions and subsequent aggregation. These aggregates act as the nuclei for further growth. For every set of conditions there is an optimum rapid mixing intensity. A relation between the velocity gradient (G-value) and speed of mixing was developed by Ammary and Cleasby (1981) and is represented mathematically by **Equation 4.1**;

$$G=aS^{b} \qquad 4.1$$

Where G is the velocity gradient sec^{-1}; S is the speed of mixing in (rev/min); a and b are constants which temperature and impeller geometry dependent. However, Sajjad (1995) established that **Equation 4.1** was for a two-blade turbine impeller at 23°C. It was reported that G-values between 300 and 1000 sec^{-1} proved to be optimum for cationic polymers (Ghosh et.al, 1985) while Mc Bride et al. (1990) recommended 1000 sec^{-1} to be used with a combination of alum and cationic polymer. Hudson (1981) suggested various rapid mixing times varying from 0.5 – 5.0 minutes.

4.5.1.4 Coagulation mixing intensity (slow mixing or flocculation mixing) and mixing regime

Flocculation has already been defined as the successive collisions of destabilized colloids and/or microflocs required to promote particle growth. During this stage, sweep floc and bridging mechanisms take place and thus, the mixing speed is different from that for coagulation. The velocity typical G- values for conventional flocculation range between 10 -60 sec^{-1} (Alshikh, 2007).

4.5.1.5 Mixer type

In coagulation, mixing can be varied by either changing the mixing speed or mixer type. It has been established that different impeller geometry can make the flocculation process more efficient with respect to power input (Sajjad, 1995; Hanson and Cleasby, 1990). This has been explained by the relationship between the impeller shape and G-value imparted to the water.

4.5.2 Uncontrollable parameters

Certain parameters are influenced by the environment and thus, are difficult to control such as the characteristics of the raw water. The properties of the water are process and location dependent and can change widely from process to process and from one place to another. These are properties of the raw water such as alkalinity, pH, and turbidity.

Alkalinity is the measurement of the buffering capacity to neutralize any acidic solution added to water. Alkalinity may refer to the presence of bicarbonate (HCO_3^{-1}), carbonate (CO_3^{-2}) and (OH^{-1}) in natural waters. Since most coagulants and coagulant aids are acidic in nature, alkalinity is consumed and pH value decreases for two reasons, bicarbonate consumption and carbonic acid formation as shown in the reaction below ((Tseng et.al, 2000; Ravina, 1993);

$$AL_2\left(SO_4\right)_3 + 3Ca\left(HCO_3\right)_2 + 6H_2O \rightarrow 3CaSO_4 + 2Al\left(OH\right)_2 + 6H_2CO_3 \qquad 4.2$$

Turbidity is the measure of relative clarity of water caused by suspended and colloidal matter, such as clay, silt, and finely divided organic and inorganic matter. Also, it can include biological organisms such as algae, cyanobacteria, zooplankton, and filamentous or macro bacterial growths. Turbidity is not a direct measure of suspended particle concentration in the water, but it is rather the measure of the scattering effect that such particles have on light. Turbidity measurements are very widely used as a good indicator of water quality.

4.6 Chapter summary

This chapter discussed the conventional coagulants that are used in water treatment. The most widely used coagulants are Al(III) and Fe(II) metal salts. To a lesser extent, polymers have been used as coagulants in certain coagulation processes. However, it has been established that for effective performance of the polymer coagulants, there is a need for strict control of the pH as overdosing or under dosing from this optimum dose will result in re-stabilization of the colloids and hence failure of the coagulation process.

In addition, the factors that affect the coagulation process were discussed. Of importance to the coagulation process are the coagulant dose, coagulation mixing intensity and flocculation mixing intensity.

References

Alshikh, O., 2007. Parameters affecting coagulation/flocculation of drinking water under cold temperatures.

Amitharajah, A., O'Melia, C., 1990. Coagulation process: Destabilization, Mixing and flocculation. In water Quality and Treatment.

Bagwell, T., Henry, H., Kenneth, M., 2001. Handbook of public water systems. FIDÃ Engineering Inc., New York.

Bratby, J., 2006. Coagulation and flocculation in water and wastewater treatment. IWA publishing.

Capodaglio, A.G., Callegari, A., Sauvignet, P., 2011. Advanced separation technology application for NOM removal from a freshwater supply. Presented at the 2011 IWA Specialty Conference on Natural Organic Matter.

De Hek, H., Stol, R., De Bruyn, P., 1978. Hydrolysis-precipitation studies of aluminum (III) solutions. 3. The role of the sulfate ion. Journal of Colloid and Interface Science 64, 72–89.

Gregory, J., Duan, J., 2001. Hydrolyzing metal salts as coagulants. Pure and Applied Chemistry 73, 2017–2026.

Hahn, H.H., Stumm, W., 1968. Kinetics of coagulation with hydrolyzed AI (III): The rate-determining step. Journal of colloid and interface science 28, 134–144.

Kang, L.-S., 1994. Flocculation kinetics using Fe (III) coagulant in water treatment: the effects of sulfate and temperature.

Langelier, W.F., Ludwig, H.F., 1949. Mechanism of flocculation in the clarification of turbid waters. Journal (American Water Works Association) 41, 163–181.

Lyklema, J., 1978. Surface chemistry of colloids in connection with stability, in: The Scientific Basis of Flocculation. Springer, pp. 3–36.

Mer, V.K.L., Healy, T.W., 1963. The role of filtration in investigating flocculation and redispersion of colloidal dispersions. The Journal of Physical Chemistry 67, 2417–2420.

O'Melia, C.R., 1987. Particle-particle interactions. IN: Aquatic Surface Chemistry: Chemical Processes at the Particle-Water Interface. John Wiley and Sons, New York. 1987. p 385-403, 4 fig, 47 ref. NSF Grant.

Packham, R., 1965. Some studies of the coagulation of dispersed clays with hydrolyzing salts. Journal of Colloid Science 20, 81–92.

Peulen, T.O., 2007. Electoflotation of water containing Cd (II), Cu (II), and Pb (II) with aluminium electrodes.

Reiber, S., Kukull, W., Standish-Lee, P., 1995. Drinking water aluminum and bioavailability. Journal of the American Water Works Association 87.

Ruehrwein, R., Ward, D., 1952. Mechanism of clay aggregation by polyelectrolytes. Soil science 73, 485–492.

Saunders, F.M., Roeder, L.M., 1991. Coagulant recovery: A critical assessment. The Foundation.

Saunders, F.M., Saunders, F.M., 1991. Coagulant recovery: A critical assessment. The Foundation.

Stumm, W., O'Melia, C.R., 1968. Stoichiometry of coagulation. Journal-American Water Works Association 60, 514–539.

Weber, W.J., 1972. Physiochemical processes for water quality control.

Wei, N., Zhang, Z., Liu, D., Wu, Y., Wang, J., Wang, Q., 2015. Coagulation behavior of polyaluminum chloride: Effects of pH and coagulant dosage. Chinese Journal of Chemical Engineering 23, 1041–1046.

Experimental work

5 Oxidation and precipitation experimental methods and results

5.1 Hypothesis and objectives

The following hypothesis and objectives were studied in this part of the experimental program;

- It was established from the literature surveyed that the rate of Fe(II) is not affected by pH below a pH of 4.0. Therefore, the effect of pH on Fe(II) oxidation in the pH range (1.5-3) was not evaluated. On the other hand, it was established from literature that there is a strong dependency of Fe(II) oxidation on pH in the pH range 5.0-8.0. Therefore, the objective of this part of the study was to determine the rate of Fe(II) oxidation in the pH range of interest (5.0-7.0).

- Literature suggested that different cations, such as Cu(II) and Co(II) affect the rate of Fe(II) oxidation. However, no information in open literature discussed the effect of Al(III) ions on the Fe(II) oxidation rate. In lieu of this, it was pertinent to study the effect of Al(III) ions on Fe(II) oxidation rate. Moreover, Al(III) ions exist together with Fe ions in AMD

- Literature also suggested that the rate of Fe(II) oxidation is affected by presence of metal (hydr)oxides. Therefore, the effect of metal (hydr)oxides (seeding material) on the rate of Fe(II) oxidation was explored.

- From the literature surveyed, it was established that unlike homogeneous precipitation, heterogeneous precipitation using specific seeding material promotes the formation of bigger particles of the targeted phases. This in turn translates into improved dewaterability of the precipitate during solid/liquid separation. Therefore, the effect of seeding on the co-precipitation of Fe(III) and Al(III), to improve the filterability of the precipitate, was studied.

5.2 Materials

For the Fe(II) oxidation, synthetic solution containing only Fe(II) and Al(III) was used to study the Fe(II) oxidation and the effect of Al(III) cations on the Fe(II) oxidation rate. The solution samples used in the study were prepared as described in **Appendix I**. The chemicals used during both oxidation and precipitation test work are presented in **Table 5.1.**

Table 5.1: Reagent grade chemicals used in oxidation and precipitation experiments

Name	Source	Physical form
Ferrous sulphate	Sigman Aldrich	Powder
Aluminium sulphate	Sigman Aldrich	Powder
Sodium hydroxide	Sigman Aldrich	Pellets
Sulphuric acid	Sigman Aldrich	Liquid
potassium dichromate solution	CC imelmann	Powder
phosphoric acid	CC imelmann	Liquid
Sodium diphenylamine	CC imelmann	Liquid

5.3 General experimental setup

All experiments – Fe(II) oxidation and precipitation - were conducted in a 2 L reactor shown in **Figure 5.1**. The agitator was fitted with a 2 radial blade impeller and a speed of 300 rev/min was used for all the experimental runs. To maximize mixing, the reactor was fitted with 4 equally spaced baffles. The reactor closure had ports for electrodes to measure pH and temperature. The experimental procedure involved oxidation of Fe(II) to (Fe(III) by aeration. The oxidation of Fe(II) to Fe(III) is essential to the precipitation of

Fe at low pH. The Fe(III) precipitates at the pH range of 3-4 while Fe(II) does not precipitate at a pH < 6 (Snoeyink and Jenkins, 1980).

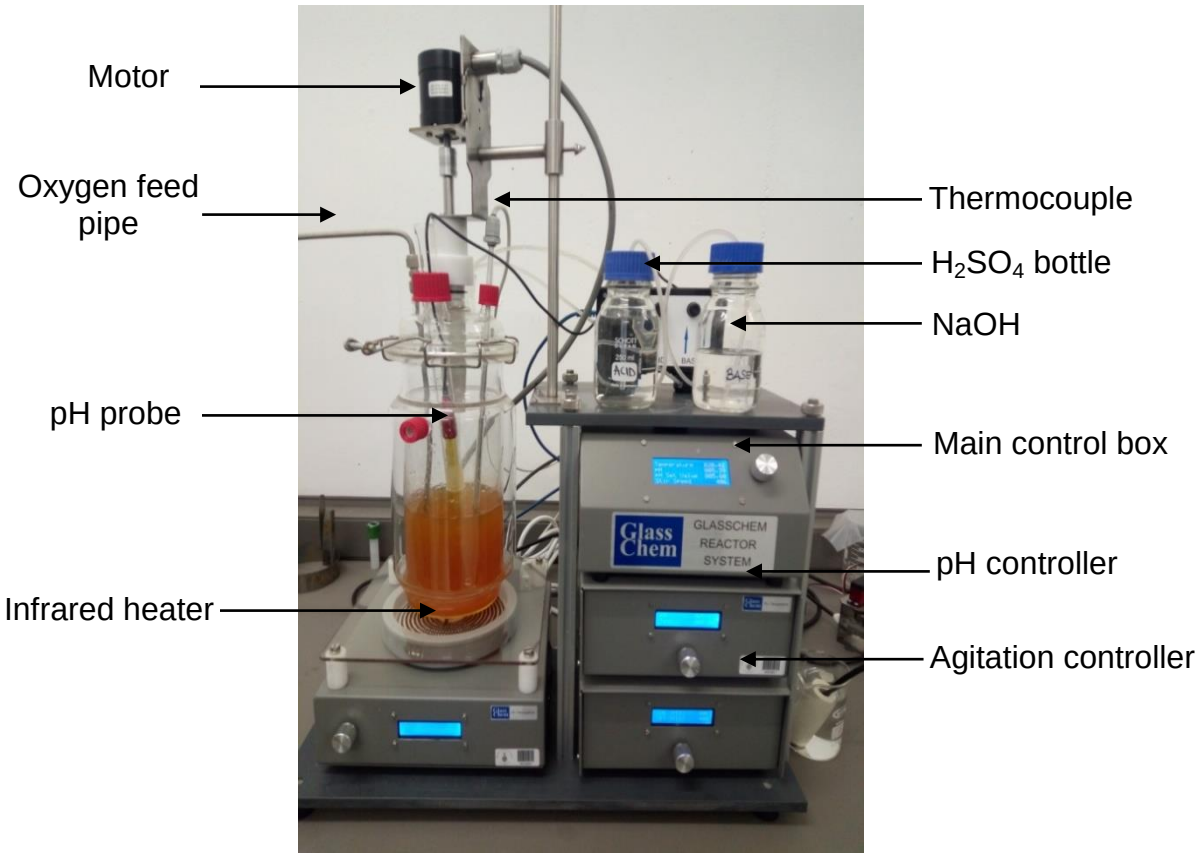

Figure 5.1: Fe(II) oxidation and precipitation experimental setup

5.4 Oxidation experimental procedure

The reactor was charged with the 1 L of deionized water and then heated to the required operating temperature (25˚C) using the infrared heater hotplate with the impeller stirring slowly. Once the required operating temperature was reached, the impeller speed was then increased to the setpoint value of 300 rev/min. The reactor was then charged with the right amount of Fe(II) and Al(III) salts using $FeSO_4 \cdot 7H_2O$ and $Al_2(SO_4)_3$, respectively. In experiments which required the addition of the seeding material, the relevant concentration of the seeding material was added at this point.

Thereafter, agitation was then increased to the required speed of 300 rev/min and the pH was adjusted by automatically injecting either 4.0 M sodium hydroxide or 0.1 M sulfuric acid using a GlassChem reactor system which has an automatic titrator. The accuracy of the pH control was 0.1 pH units. In order to ensure that the oxygen transfer was not limiting, air was injected at a constant rate of 15 L/min. The reaction proceeded for 4 hours and 10 mL samples were removed at 15 minutes intervals via the sampling tube attached to a syringe. Before discharging, the samples were deoxygenated using nitrogen to stop oxidation. All experiments were performed in triplicates. **Table 5.2** summarizes the Fe(II) oxidation tests conditions.

The Fe(II) concentration was monitored by wet chemistry using potassium dichromate titration method (Mendham, 2006). 50 mL of deionized water was added into a 250 mL Erlenmeyer flask and about 5 mL of phosphoric acid was added to mask the Fe(III) in solution. An accurate 5 mL volume was then pipetted into a volumetric flask and titrated against a standardized (0.0017 M) potassium dichromate solution. Sodium diphenylamine was used as the indicator to make a purple titration end point. The redox titration equation and calculations are described in **Appendix II**.

The concentration of the amount of Fe(II) remaining was calculated according to **Equation 5.1** :

$$\left[\mathrm{Fe(II)}\right] = \frac{\left(\mathrm{Vol}K_2Cr_2O_7 \times \mathrm{Normality}\right) \times \mathrm{rmm}_{\mathrm{Fe}}}{\mathrm{Volsample}} \qquad 5.1$$

Where Vol $K_2Cr_2O_7$ is the volume of potassium dichromate, rmm_{Fe} is the molar mass of Fe, vol sample is the volume of the sample (5 mL in this case). A similar experimental procedure was followed to study the effect of seeding on the Fe(II) oxidation rate. The only difference was that recycle sludge, at concentrations C_s = 0, 0.5, 1 and 2, which acted as a seeding material, was added to the Fe(II) containing solution prior to oxidation.

Table 5.2: Summary of Fe(II) oxidation test conditions

Parameter	Value			
pH	5.0		6.0	7.0
Reaction temperature, °C	25		25	25
Fe(II) concentration, mg/L	1000		2000	3000
Al(III) concentration, mg/L	200		400	600
Seed concentration, C_s	0.0	0.5	1	2
Air flowrate, L/min	15		15	15

5.5 Fe and Al co-precipitation experimental procedure

The Fe(III) and Al(III) precipitation studies were conducted using real AMD solution. Real AMD was used in this part of the study to determine the co-precipitation of other impurities found in the AMD. **Table 5.3** presents a summary of the experimental conditions for Fe(III) and Al(III) precipitation using real AMD. Just like the Fe(II) oxidation experiments, precipitation experiments were also performed in triplicates. The experimental procedure involved maintaining the temperature of the reactor contents at ambient temperature (25°C) using the infrared heater. The seeding material at the appropriate concentration was then added. The agitation was then increased to the 300 rev/min and the pH was adjusted by automatically injecting either 4.0 M sodium hydroxide or 0.1 M sulfuric acid using a GlassChem reactor system which has an automatic titrator. The volume of sodium hydroxide necessary to reach a required pH was determined from the titration curve of AMD with 4.0 M sodium hydroxide. The accuracy of the pH control was 0.1 pH units. After attaining the required pH, the experiment was allowed to proceed for a period of two hours as this is sufficient time for precipitation to take place. The precipitate was separated from the effluent by vacuum filtration followed by washing of the precipitate with deionized water to remove any

entrained effluent solution. The precipitate was then left in the oven for 24 hours at 80°C to dry.

Table 5.3: Factors and values selected for co-precipitation of Fe and Al

Parameter	Value
pH	5.0, 6.0, 7.0
Seed concentration, C_s	0.5, 1.0, 2.0
Reaction temperature, ˚C	25
Type of oxidant	Air
NaOH concentration, M	4.0
H_2SO_4 concentration, M	0.1
Time, h	2.0
Agitation, rev/min	300

5.6 Settling tests

After precipitation was completed, settling tests were conducted by pouring the slurries in 1 L glass measuring cylinders and allowed to settle for a period of 24 hours while recording the mudline.

5.7 Analytical methods

1. All solution and precipitate samples were analyzed for Fe, Al, Ca, Mn, Mg, Cu, Zn, Ni and Co using inductive coupled plasma mass spectroscopy (ICP-MS). The concentration of the sulphate was determined using ion chromatography. Metal recovery (*R*), was calculated according to **Equation 5.2**;

$$R = \frac{C_o - C_1}{C_o} \times 100 \qquad 5.2$$

Where C_0 is the concentration of a particular metal species in raw AMD (mg/L), C_1 is the concentration of a metal species in the effluent (mg/L) after precipitation. Tabak et al., (2003) defined the precipitate purity as the ratio of a desired precipitated metal species to the sum of all the metal species precipitated. Based on this definition, the precipitate purity (*P*) was calculated according to **Equation 5.3**;

$$P=\frac{C_i}{\sum_j^n C_j}\times 100\% \qquad 5.3$$

Where C_i is the concentration of the individual or sum of the species of interest (%), n is the total number of metal species while C_j is the concentration of all the metal species precipitated (%). In this case, C_i was regarded as the total concentration of Fe and Al in the precipitate.

2. Scanning electron microscopy (SEM) can singularly be used as an effective tool to study and deduce solid reaction products. This is made possible by utilizing its energy dispersive X-ray, backscattered electron imaging and X-ray mapping. Specifically, X-ray mapping can give clear and exact positions of elemental composition of the material and thereby suggesting the compounds present at specific sites on the sample (Chen and Dutrizac, 1990). In this study, SEM analysis was used to study the morphology of the precipitates. In order to determine the possible compounds produced during precipitation, X-ray mapping was used. The X-ray maps were also used to get an indication of the distribution of the Fe and Al, as well as other metal species in the precipitate samples. This was performed using a MA 15 EVO SEM ZEISS instrument with accelerating voltage of 20KV. This instrument uses INCA software to identify the compositions of the samples.

3. X-ray powder diffraction (XRD) can conclusively be used to qualitatively and quantitatively identify the crystalline phases present in a material and also give an indication of the degree of amorphousness of the material (Schwertmann and Cornell, 2000). In this study, XRD analyzes of the precipitates produced was used to identify and

quantify the precipitate phases. XRD analyzes of the samples were conducted on a Bruker D8 Advance diffractometer equipped with an energy dispersion Sol-X detector with cobalt radiation.

4. To understand the distribution of particles, aggregates and agglomerates, and therefore get a better understanding of solid–liquid separation, particle size distribution (PSD) was conducted using the Marven 3000 Mastersizer.

5.8 Oxidation and precipitation experimental results

The following sections present the oxidation and precipitation experimental results.

5.8.1 Fe(II) oxidation kinetics results and discussion

For homogeneous chemical reactions, the rate of reaction depends on the concentration of reactants in the solution. A rate model was initially chosen which follows a general relationship as observed by other researchers (Mathews and Robins, 1972) and is represented by;

$$r=k\left[Fe(II)\right]^{a}\left[O_2\right]^{b}\left[OH^{-}\right]^{c} \qquad 5.4$$

Where k is the rate constant and a, b and c are reaction orders.

When pH and oxygen concentrations are held constant, **Equation 5.4** reduces to a pseudo first order rate expression given by;

$$r=k\left[Fe(II)\right]^{a} \qquad 5.5$$

Where $k_1=k\left[O_2\right]^{b}(OH^{-})^{c}$

The linear plot of the logarithm of Fe(II) vs time in **Figure 5.2** showed that the reaction rate is first order with respect to Fe(II) for all the pH levels considered in this study. The findings from this study agree with what has been reported by other studies (Stumm and Lee, 1961; Stumm and Morgan, 2012b; Tamura et al., 1976b, 1976a). The gradient of each slope in **Figure 5.2** gives the value of the reaction rate at that particular pH. The reaction rate of oxidation at pH 5.0, 6.0 and 7.0 was 2.157, 4.97, and 7.73 mg/L/min. The increase in the oxidation rate with pH is due to the change in the Fe speciation. This can be explained using **Figure 5.3,** which shows a steep rise in the concentration of $FeOH^{+}$ and $Fe(OH)_2^{0}$. Since these species (especially $Fe(OH)_2^{0}$) are far more readily oxidized than Fe^{2+}, it is expected that an increase in the concentration of these species

would result in an increase in the oxidation rate with increase in pH (Jones et al., 2014; Morgan and Lahav, 2007; Millero, 1985; Lowson, 1982).

Jones et al. (2014) explained the pH dependency of Fe(II) oxidation by conducting electrochemical studies during Fe(II) oxidation. It was established that the Fe(III)/Fe(II) redox couple below pH of 2.5 has a potential of 0.77 V. However, as the pH increases and the Fe speciation changes, the Fe species $Fe(OH)^{+2}$ and $Fe(OH)_0^2$ couple predominate and possesses a more negative reduction potential of -0.02 V. This value indicates that Fe(II) becomes a better reducing agent and is therefore more readily oxidized. Morgan and Lahav (2007) showed that the hydrolyzed Fe(II) species are more readily oxidized than non-hydrolyzed ferrous species in the following order $Fe(OH)_2^0{}_{(aq)}$ >> $Fe(OH)^+$ >> Fe^{2+}. This is because the OH^- ligands donate the electron density to the reduced metal ion thereby increasing the reducing power and stabilizing the Fe^{2+} (Morgan and Lahav, 2007). The reactivity of $Fe(OH)_2^0$ over $FeOH^+$ and Fe2+ was also reported by Millero (1985) who showed that the rate constant for the oxidation of $Fe(OH)_2^0$ is 5 orders of magnitude higher than the rate constant for $FeOH^+$ which in turn is 5 orders of magnitude greater than the rate constant of Fe^{2+} (Lowson, 1982).

The reaction rate can be plotted against pH to obtain the order of reaction with respect to OH^-. This is represented in **Figure 5.4**. From the plot, the order of the reaction is 1.35 with respect to $[OH]^-$. This doesn't agree with what has been reported by several other researchers, (Stumm and Lee, 1961; Tamura et al., 1976b, 1976a) who reported a reaction order of 2. The disagreement could be because under the test conditions applied in this study, both homogeneous and heterogeneous oxidation was taking place and thus the depletion of Fe(II) was due to both mechanisms.

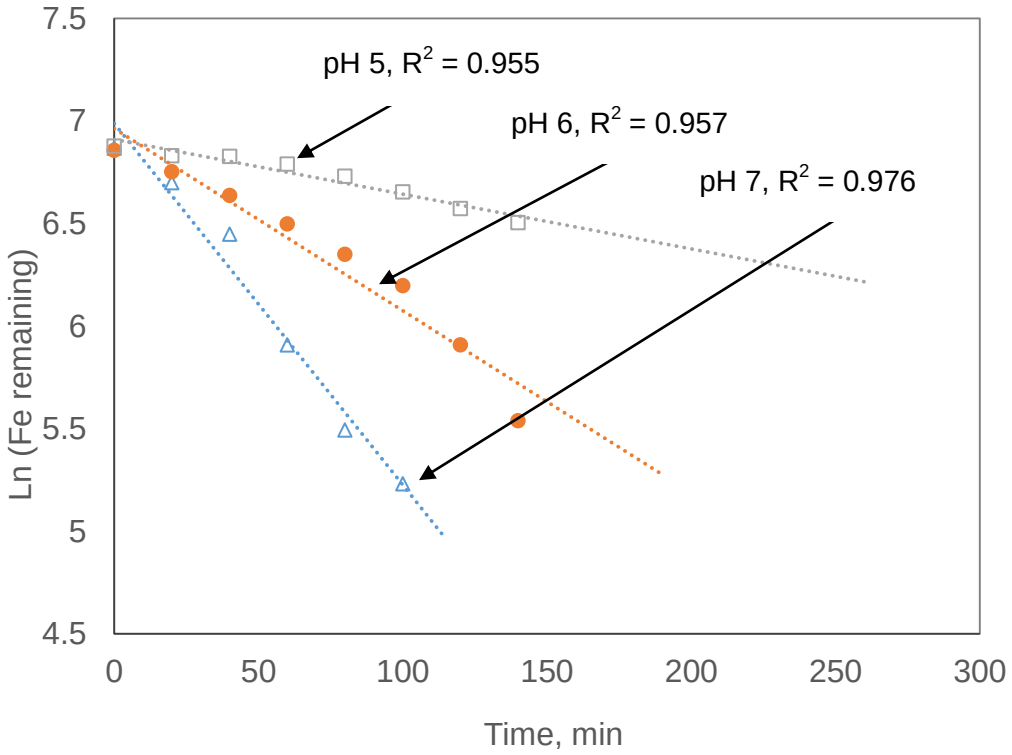

Figure 5.2: Change in ferrous Fe(II) concentration with time

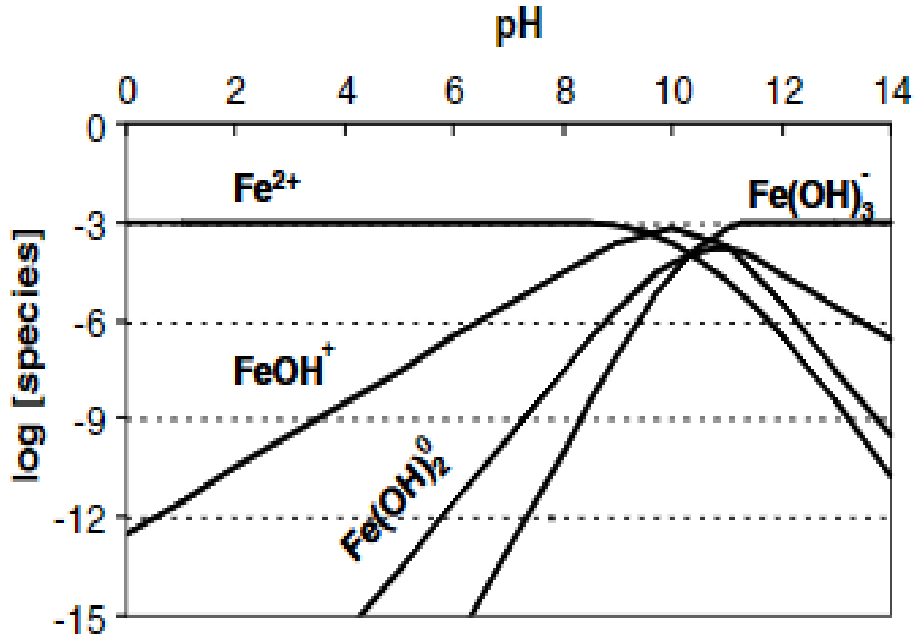

Figure 5.3: Log species – pH diagram of soluble ferrous hydroxide species(Morgan and Lahav, 2007)

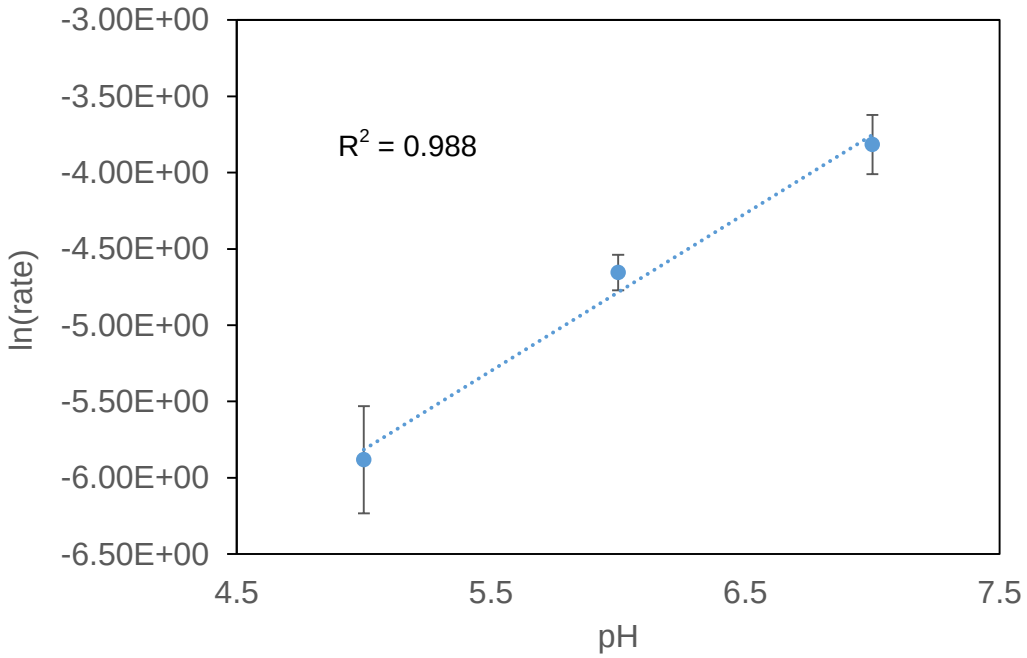

Figure 5.4: Change of reaction rate constant with pH during Fe(II) oxidation

5.8.2 Effect of seeding on Fe(III) oxidation

The study showed that seeding had a profound effect on the oxidation rate (see **Figure 5.5**). For example, the oxidation reaction rate increased from 2.157 mg/L/min in unseeded experiment to 2.7 mg/L/min at pH 5 for Cs= 0.5 test. A further increase in the seed concentration to C_s = 1 did not result in a significant increase in Fe(II) oxidation rate. However, it could not be explained at present why the oxidation rate did not increase with further increase in seed concentration. Tamura et al. (1976b) established that the presence of ferric hydroxide solids accelerated the Fe(II) oxidation rate. In the presence of oxide surfaces, the adsorption of Fe(II) onto the oxide particles alters the co-ordination environment around the metal center, effectively hydrolyzing Fe(II) and thereby altering its speciation (Jones et al., 2014). This makes Fe(II) a better reducing agent (discussed in **Section 5.8.1**), increasing its potential to reduce target species. The other dominant hypothesis for the observed trend is that there is electron transfer between the adsorbed species and the solid thereby making Fe(II) easily oxidizable (Gorski et al., 2016).

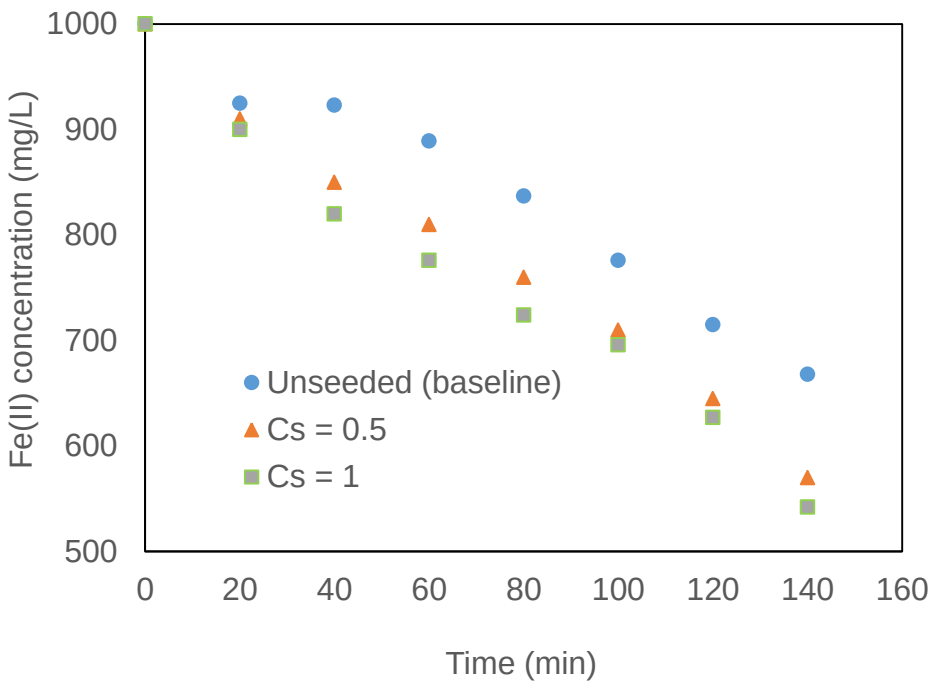

Figure 5.5: Effect of seeding on Fe oxidation (Fe(II) = 1000 mg/L, pH = 5)

5.8.3 Effect of Al(III) cations on Fe(II) oxidation rate

Figure 5.6 displays average results obtained during the study of the effect of Al(III) on Fe(II) oxidation rate. The base solution contained about 1000 mg/L Fe(II) and 200 or 400 mg/L Al. The error bars represent the deviation of experimental data points from the calculated average. The deviation of experimental data points from the calculated averages are within the range of 2%. In the current study, the Fe(II) oxidation rate was not found to be affected by the Al(III) cations as the oxidation rates remained marginally similar. As can been seen from the figure, the Fe(II) remaining in solution at a particular time is almost the same regardless of the Al(III) concentration. This shows that unlike other metal cations such as Cu(II) and Co(II) which hasten the decomposition of hydrogen peroxide (**Equation 2.3**) in the presence of Fe(II), thereby accelerating the Fe(II) oxidation rate, the effect of Al(II) on the oxidation rate of Fe(II) was almost negligible (Mathews and Robins, 1972; Stumm and Lee, 1961),.

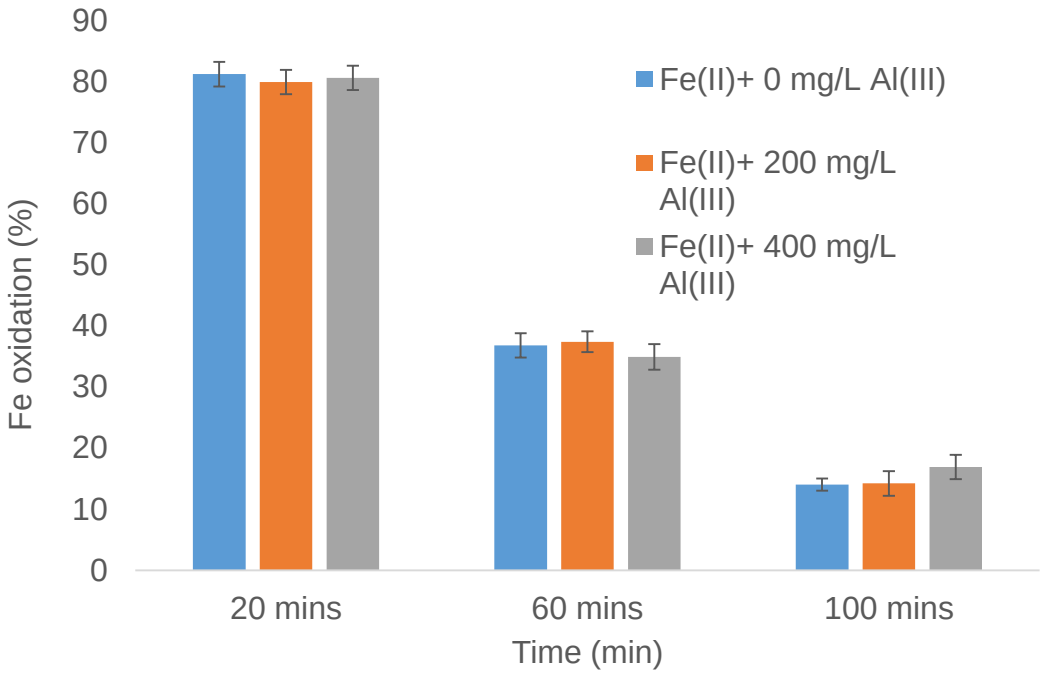

Figure 5.6: Effect of Al(III) on the oxidation of Fe(II)

5.8.4 Fe-Al precipitation results

5.8.4.1 Titration curve

The Fe(III) and Al(III) were recovered from the AMD by oxidation and selective precipitation process. To determine the amount of sodium hydroxide, with a particular concentration, needed to quickly raise the pH to the required value, a titration curve analysis was conducted. A titration curve, shown in **Figure 5.7,** of pH vs volume of 4M sodium hydroxide, was determined in a traditional way according to Jenke and Diebold (1983). Based on the results, the pH of the solution was then increased to and maintained at the required pH, with the addition of a volume of 4M sodium hydroxide solution to precipitate the Fe(III) and Al(III) as ferric and aluminium hydroxide. Roughly about 90 mL of sodium hydroxide was required to raise the pH to 5 while about 130 mL was required to raise the pH to 7.

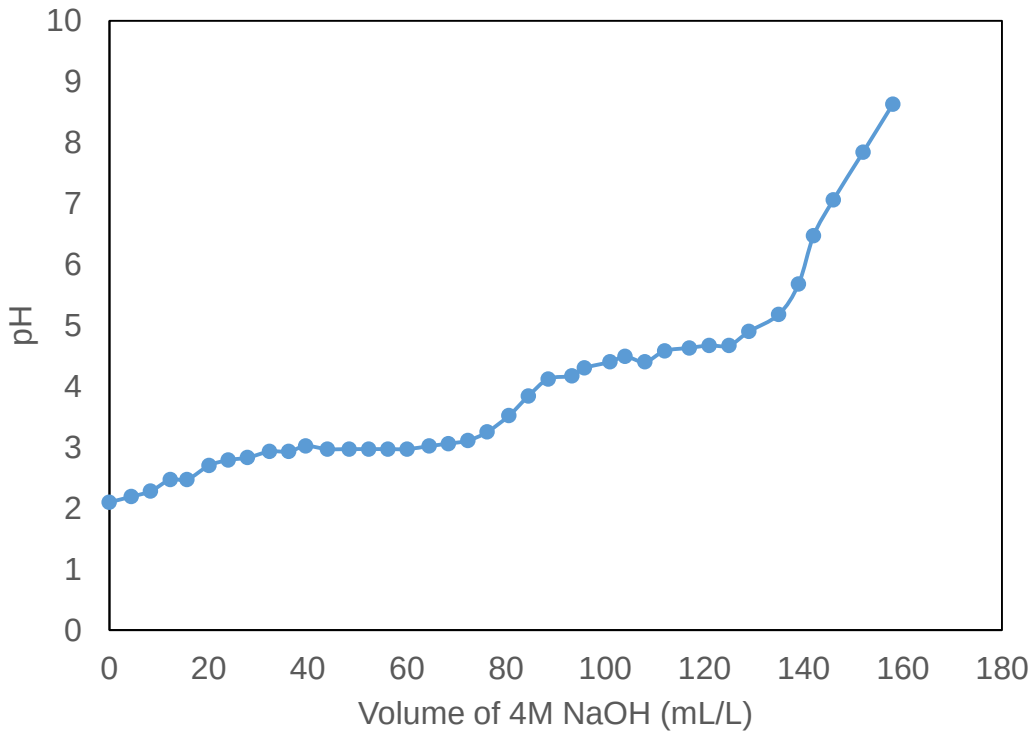

Figure 5.7: Titration curve of AMD with 4 M NaOH

5.8.4.2 Characterisation of acid mine drainage

The general characteristic of the raw AMD is presented in **Table 5.4**. The characteristics of the AMD is typical of the South African coal AMD solutions (Gitari et al., 2018; Petrik et al., 2017). As can be seen from the table, this included high concentration of Fe, Al, Ca, Mg, and Mn with minor concentrations of Ni, Zn, Cu and Co. The total Fe composition in the raw AMD was 80% as Fe(II) and 20% as Fe(III). The table also shows the South Africa (SA) standard for wastewater discharge into a receiving water body. The table further shows the chemical composition of the effluents obtained in this study at different precipitating pH values. As can be seen from the table, the concentrations of Fe and Al(III) in AMD are 4290 mg/L as 396 mg/L, respectively. The concentrations of the heavy metals especially Fe, is way above the SA discharge limits. Fe in AMD was 4290 mg/L compared to 0.3 mg/L discharge limit. The discharge standards for the other heavy metal which are in substantial concentration such as Al, Mg, Mn, Ca etc., are not given by the gazette.

5.8.4.3 Effect of pH on Fe(III) and Al(III) precipitation

The effect of pH on Fe(III) and Al(III) precipitation for C_s = 0, is shown in **Table 5.4**. When the pH was raised to 5.0, the Fe(III) and Al(III) concentrations were 2.7 and 14.0 mg/L in the effluent, respectively. This translated to 99.9 and 96.5% Fe and Al removal, respectively, as calculated using **Equation 5.2**. These recoveries, which are averages of the triplicate results, are depicted in **Figure 5.8** with the error bars related to the standard deviation (SD). An increase in pH to 7.0 resulted in Al(III) concentration of 3.7 mg/L in the effluent and the recovery being 99.1% but the Fe(III) recovery remained at 99.9%. Other studies have also found similar results (Park et al., 2015; Wei et al., 2005; Wei and Viadero, 2007). For example, during the synthesis of magnetic nanoparticles from AMD, Wei and Viadero, (2007) reduced Fe(III) from 169 mg/L at pH 2.6 to 0.09 mg/L at pH 6.7 and Al(III) from 71 mg/L to 0.2 mg/L under the same pH conditions. This represented 99.94% and 99.71% Fe(III) and Al(III) recovery, respectively.

Table 5.4: Summary of the chemical composition of raw AMD and effluents after precipitation

	Metal concentration, mg/L									
	pH	Fe (Total)	Al	Ca	Mg	Mn	Zn	Ni	Co	Cu
Raw AMD	2.1	4290.0	396.0	503.0	474.0	93.9	14.3	1.7	1.4	0.5
SA effluent standard[1]	5.5-9.5	0.3	NA	NA	NA	0.1	0.1	NA	NA	0.01
Effluent after precipitation	5.0	2.7	14.0	500.0	454.0	89.3	14.1	1.6	1.4	0.5
SD	-	0.03	1.50	2.01	9.53	2.10	2.13	-	-	-
	6.0	2.1	9.0	501	461.0	86.7	13.3	1.6	1.4	0.5
SD	-	0.04	0.92	1.15	3.60	3.10	1.67	-	-	-
	7.0	2.1	3.7	500	457.0	83.6	13.9	1.6	1.4	0.5
SD	-	0.03	0.67	2.02	4.58	1.87	3.87	-	-	-

[1](National Gazette, 2013); SD = Standard deviation; NA = Not applicable

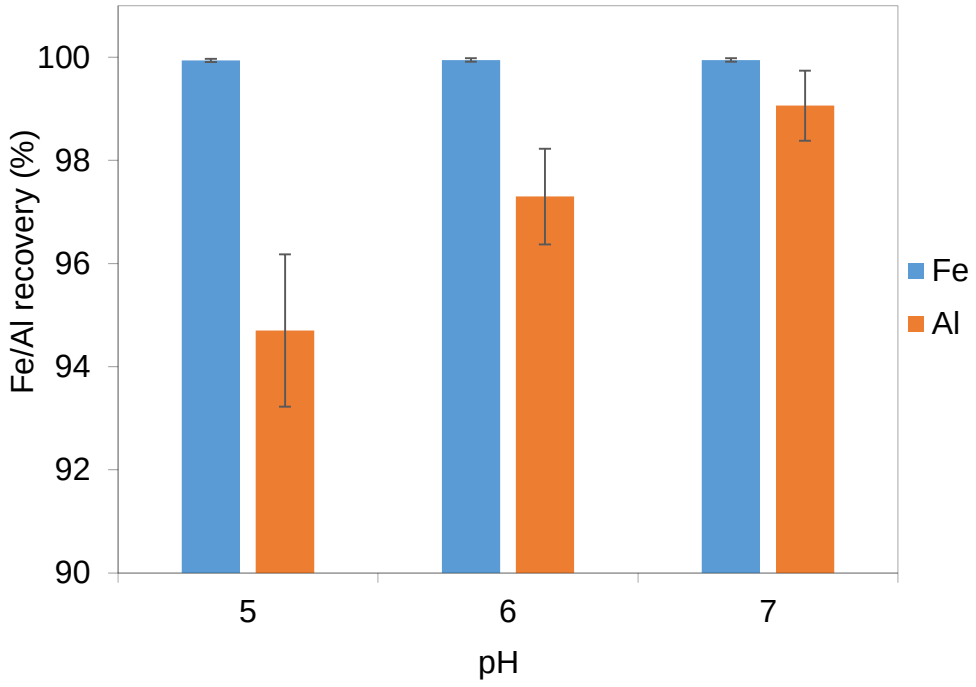

Figure 5.8: Effect of pH on Fe(III) and Al(III) recovery through precipitation of the AMD 25°C

Figure 5.9 presents the effect of pH on the solubility of the other major heavy metals. The results show that the precipitation of Ca is almost negligible in the tested pH range. However, Mn and Mg effluent concentration were reduced from 93.9 mg/L to 83.6 mg/L and 474.0 mg/L to 457 mg/L, respectively. This represented 10.9% and 3.6% co-precipitation of Mn and Mg, respectively. Other minor elements, including Zn, Cu and Co did not precipitate under the pH range studied. The precipitate purity was calculated using **Equation 5.3** and gave 99.0, 99.0 and 98.0 % for pH 5.0, 6.0 and 7.0, respectively. The results obtained in the study are comparable with results obtained by other researchers. Michalková et al. (2013) obtained less than 0.05% of Zn, Co, Cu and Ni in the AMD precipitated using sodium hydroxide at pH 6.9. In a study by Wei and Viadero (2007), the precipitation of Ca, Mg, Mn and Ni during neutralization at pH 6.7 was 6.02, 5.57, 16.67 and 37.27, respectively.

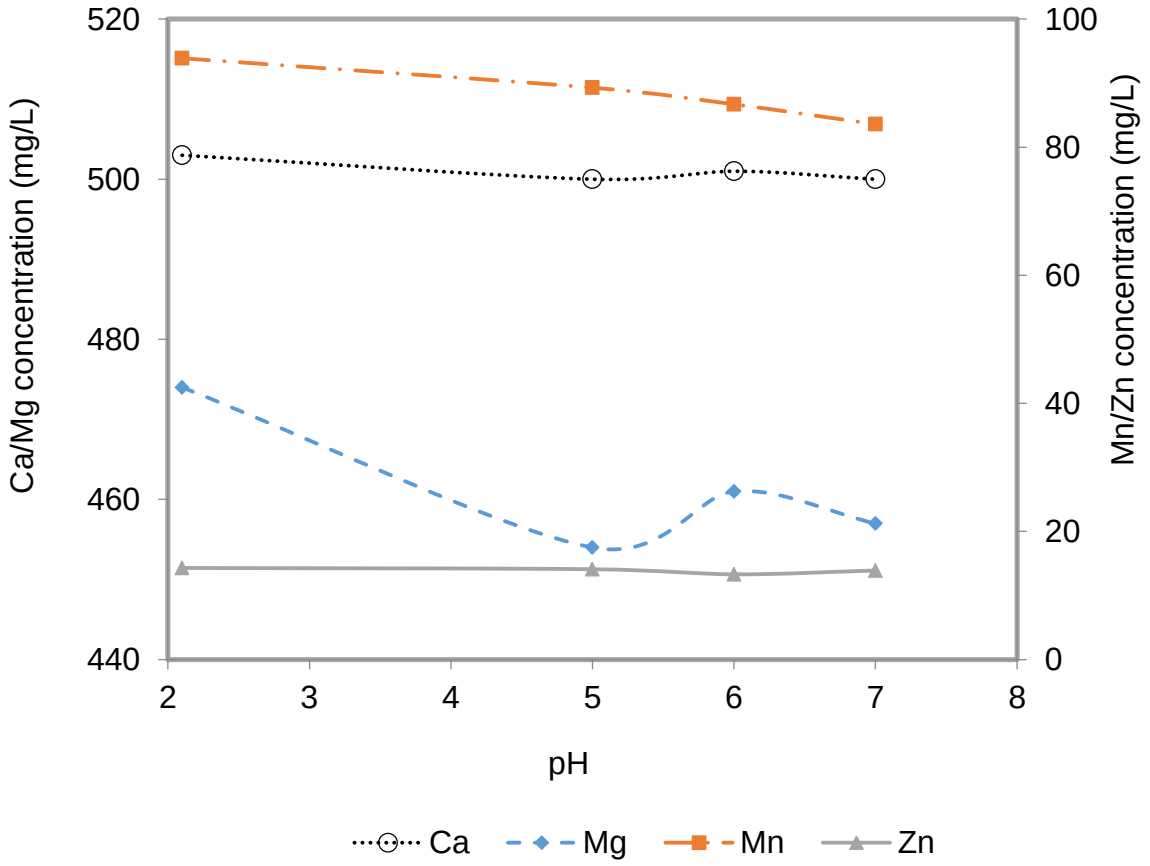

Figure 5.9: Solubility of the major heavy metals as a function of pH during Fe(III) and Al(III) precipitation at 25°C

5.8.4.4 Effect of seeding on precipitation

The recoveries of Fe(III) and Al(III) and the precipitation of other impurities at different pH and seed concentrations were examined. Presented in **Table 5.5** are the results obtained at pH 7. At this pH, precipitation of other heavy metals is expected to be substantial as compared to pH 5.0 and 6.0. This is according to the discussion in **Section 2.2.7** (**Figure 2.6**) on the effect of pH on the solubilities of metal hydroxides. Therefore, pH 7.0 offers a better comparison of the effect of seeding on precipitation of metals.

The recoveries of Fe(III) and Al(III) remained the same regardless of the seeding concentration. For example, at C_s =0, Fe(III) and Al(III) recoveries were 99.2 and 99.1%, respectively. An increase in the seed concentration to C_s = 2.0 resulted in Fe(III) and Al(III) recoveries of 99.7 and 99.1%, respectively.

Hove et al. (2009b) reported that seeding favors formation of larger, more pure and more stable particles at the expense of the smaller, impure and kinetically unfavorable particles. However, from the results obtained in this study, it can clearly be seen that seeding did not affect the precipitation of other impurities. Although the results of the precipitation of Ca, Mn, Mg and Zn are sporadic without showing any trend, the percentage precipitation varies within very small margins. As such, it can safely be concluded that seeding did not affect the precipitation of these elements.

Table 5.5: The effect of seeding on precipitation at pH 7

	Recovery/precipitation (%)			
Element	C_s = 0	C_s = 0.5	C_s = 1.0	C_s = 2.0
Fe(III)	99.2	99.5	99.3	99.7
Al(III)	99.1	98.7	99.4	99.0
Ca(II)	0.6	1.1	0.8	1.6
Mn(II)	11.0	8.7	9.4	12.3
Mg(II)	3.6	4.5	2.7	3.5
Zn(II)	0.4	0.8	0.7	0.4

5.8.4.5 Morphology of the precipitate

Chen and Dutrizac (1989) reported that SEM can be used to suggest the nature of the compounds present in a material by utilizing images and maps. To understand the nature of the precipitate formed at different operating conditions, precipitate samples taken for the single pass (C_s = 0), C_s = 1.0 and C_s = 2.0 were analyzed by SEM. Two images of each of the precipitates generated by the sodium hydroxide precipitation are presented (A_1, B_1, C_1 = x10 magnification and A_2, B_2, C_2 = x50 magnification). The scale line is also overlaid on each image for reference purposes. **Figure 5.10** shows the images of the precipitates formed at pH 5. It can be seen from the images that the particles were fluffy flocs or coagulates. The figure also shows that with seeding, the aggregations appear to become more compact and dense in nature. **Figure 5.10 A** shows precipitate from single pass experiment with less compact aggregates. An increase in the seeding material concentration (**Figure 5.10 B and C)** results in more compact, denser aggregations, with large aggregations formed by the clumping together of the smaller aggregations. This finding can be explained by the seeded precipitation theory as presented in Section 2.2.4, in which the growth of bigger size crystals can be achieved by reducing the supersaturation through introduction of seed crystals (Hove et al., 2007). Similar SEM results at other pHs are presented in **Appendix III**.

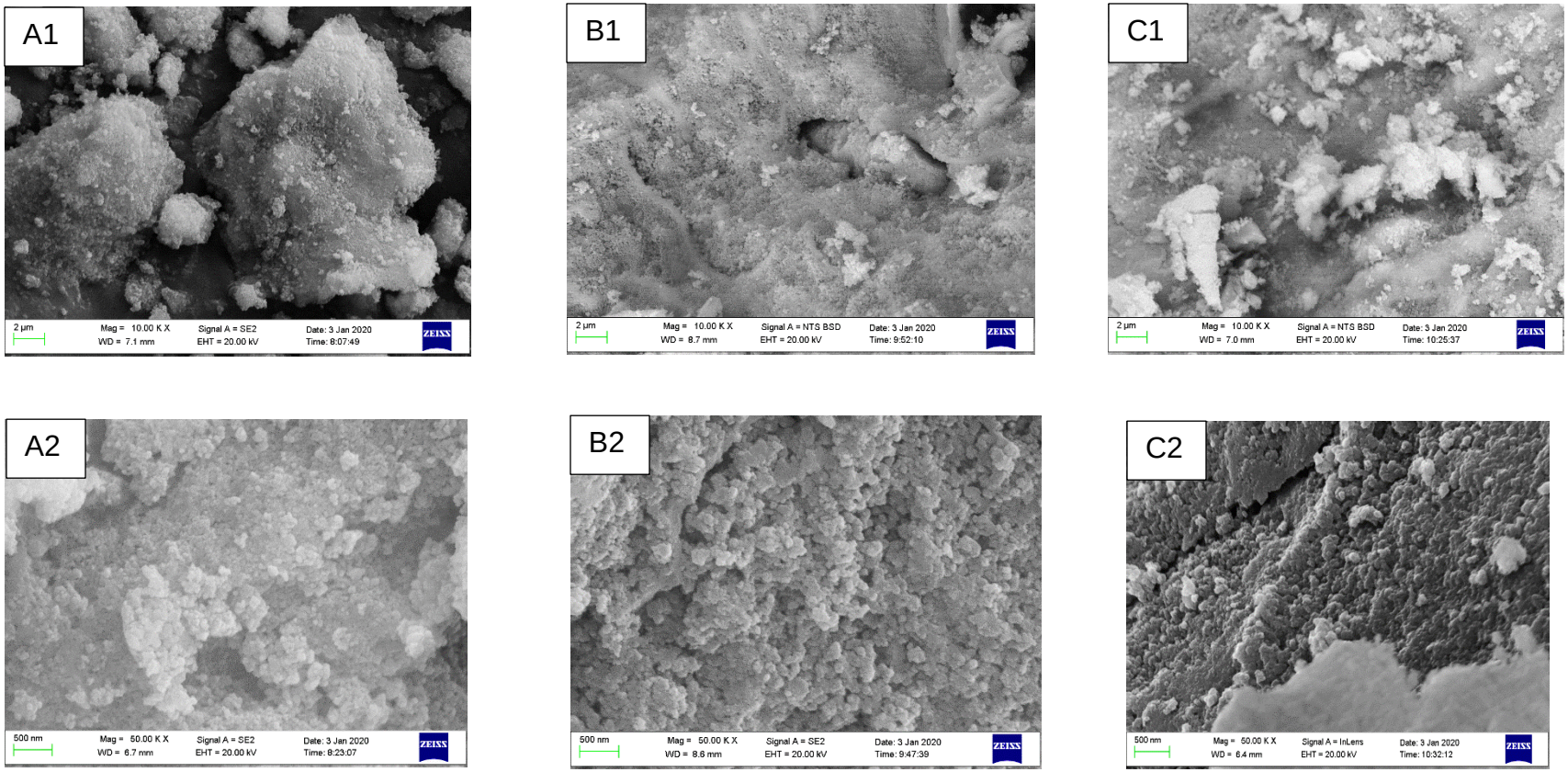

Figure 5.10: SEM micrographs of the precipitates formed at pH 5; 25°C; A = C_S 0; B = Cs 0.5; C = Cs 1.0

5.8.4.6 X-ray diffraction analysis

In **Figure 5.11**, the XRD results for seeded and unseeded precipitates formed at 25°C and different seed concentrations are presented. The precipitates produced at all conditions tested were reported to be largely amorphous. Ferric oxyhydroxides are formed upon rapid hydrolysis of Fe(III) solutions at temperatures of 20-30ºC. The XRD resulting from the precipitation have peaks that are not always definitive, except on occasions when a few broad reflections indicate that there is some crystalline character, not dissimilar to the naturally formed iron oxide ferrihydrite (Florence, 2015). As expected, ferrihydrite was the major phase identified in the precipitate forms at pH 5-7. Similar phases were identified regardless of the seed concentration. This meant that seeding did not affect the mineral phase produced from precipitation. Ferrihydrite and goethite are common phases identified in AMD precipitates and the phase generated depends on the aging (Rhoton et al., 2002). Lintnerova et al. (2006) identified ferrihydrite and schwertmannite as the principal phases in the precipitates generated from the AMD effluent at pH 5-8. The ferrihydrite pattern from this study (see **Figure 5.11**) contains essentially 1 broad, poorly defined peak position [°2θ] = 40.

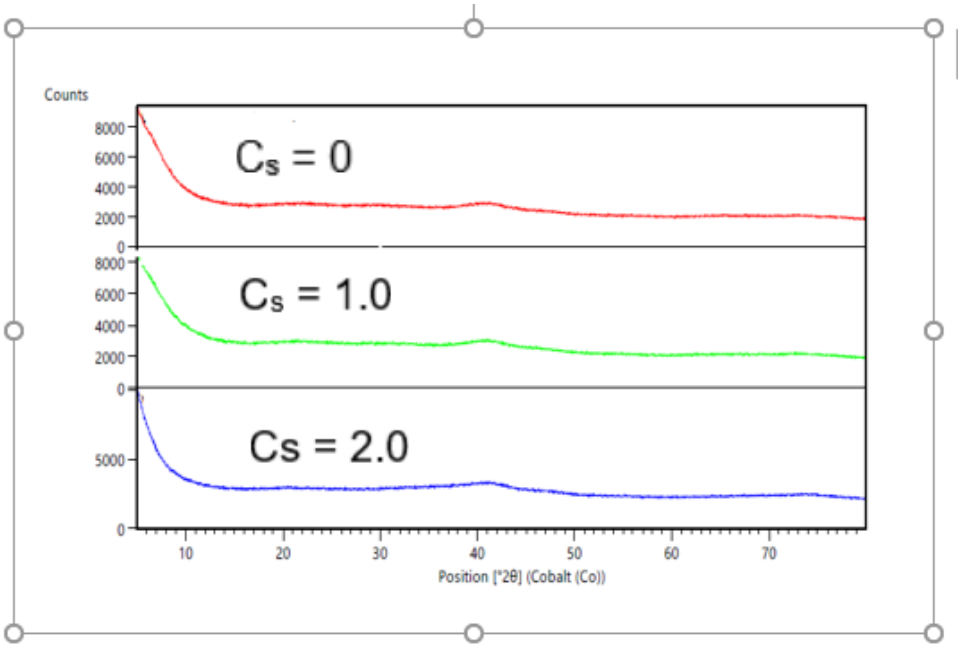

Figure 5.11: X-ray powder diffraction pattern of the precipitate formed in the recycled solids experimental system at pH 5, 25°C and different seed concentration.

Figure 5.11 compares well with the results obtained by other researchers who established that a poorly defined amorphous ferrihydrite precipitate is formed from AMD precipitation using sodium hydroxide (Lintnerova et al., 2006; Rhoton et al., 2002; Gan et al., 2005).

5.8.4.7 Particle size distribution, BET surface area and settling rate

The study of the effect of operating conditions on the Brunauer-Emmett-Teller (BET) surface area, particle size and particle settling rate was also conducted. **Figure 5.12** shows that the BET specific surface area decreased from 250 m^2/g for the single pass (C_s = 0) precipitate to 208 m^2/g and 100 m^2/g for C_s =0.5 and C_s = 1.0 systems, respectively. However, a further increase in seed concentration to C_s = 2.0 resulted in an increase in BET surface area of 123 m^2/g. At this point, it is not exactly clear what could have caused the increase in BET surface area. Lintnerova et al. (2006) obtained specific surface areas of AMD-precipitates in the range 150 to 400 m^2/g.

In addition to the BET surface area, the particle sizes of the precipitate particles, which are the average particle sizes (D_{50}) were measured. This is also presented in **Figure 5.12**. The particle size of the single pass precipitate was 1.5 µm as compared to 2.2 µm for C_s = 0.5 and 3.5 µm for C_s = 1.0. However, just like the BET surface area, an increase in the seed concentration from C_s = 1.0 to C_s = 2.0 resulted in a slight decrease in the average particle size from 3.5 µm to 3.4 µm, respectively.

The BET surface area and the average particle size results support the observation made from the SEM micrographs (discussed in **Section 5.8.4.4**) which showed that seeding resulted in the formation of compact, dense and large aggregates formed by the clumping together of the smaller aggregations.

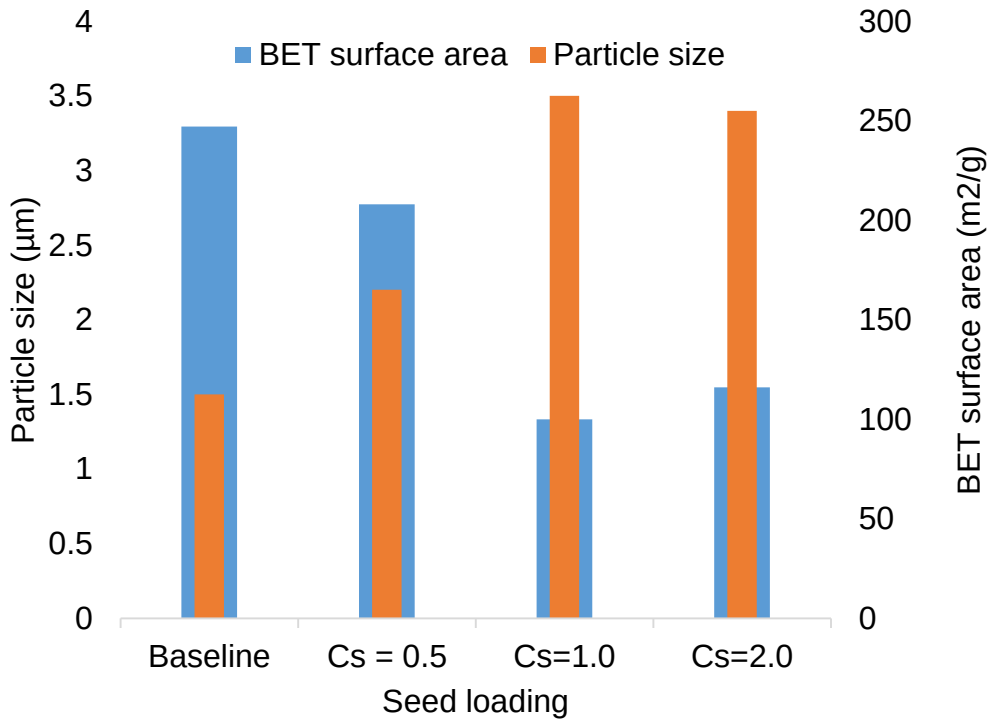

Figure 5.12: BET surface area and PSD of precipitate at pH 5

In order to further validate the observations made with the BET surface area and particle sizes, the particle settling rates were determined using the mudline test method. The particle settling rates were conducted in a 1 L measuring cylinder, shown in **Figure 5.13**, with the initial settling rates measured in the first 30 minutes. The 30 minutes is the typical time used in the determination the sludge settleability (Molman, 1934). The results showed that artificial seeds had a positive effect on the settling properties of the precipitates. The initial settling rates, as presented in **Table 5.6**, increased from 4.8 cm/min for the unseeded experiment to 6.7 cm/min for C_s = 0.5. When the precipitation seed concentration was increased to C_s = 2.0, the settling rate also increased to 7.9 cm/min. The settling profiles are represented in Figure 5.14. These findings are supported by the study conducted by Seckler (1995). The study stated that the metal removal efficiency, and subsequent precipitate characteristics during seeded precipitation, is a function of the quantity of material precipitated onto the seeds due to fine-grain aggregation and/or settling due to fines aggregation (Seckler, 1995).

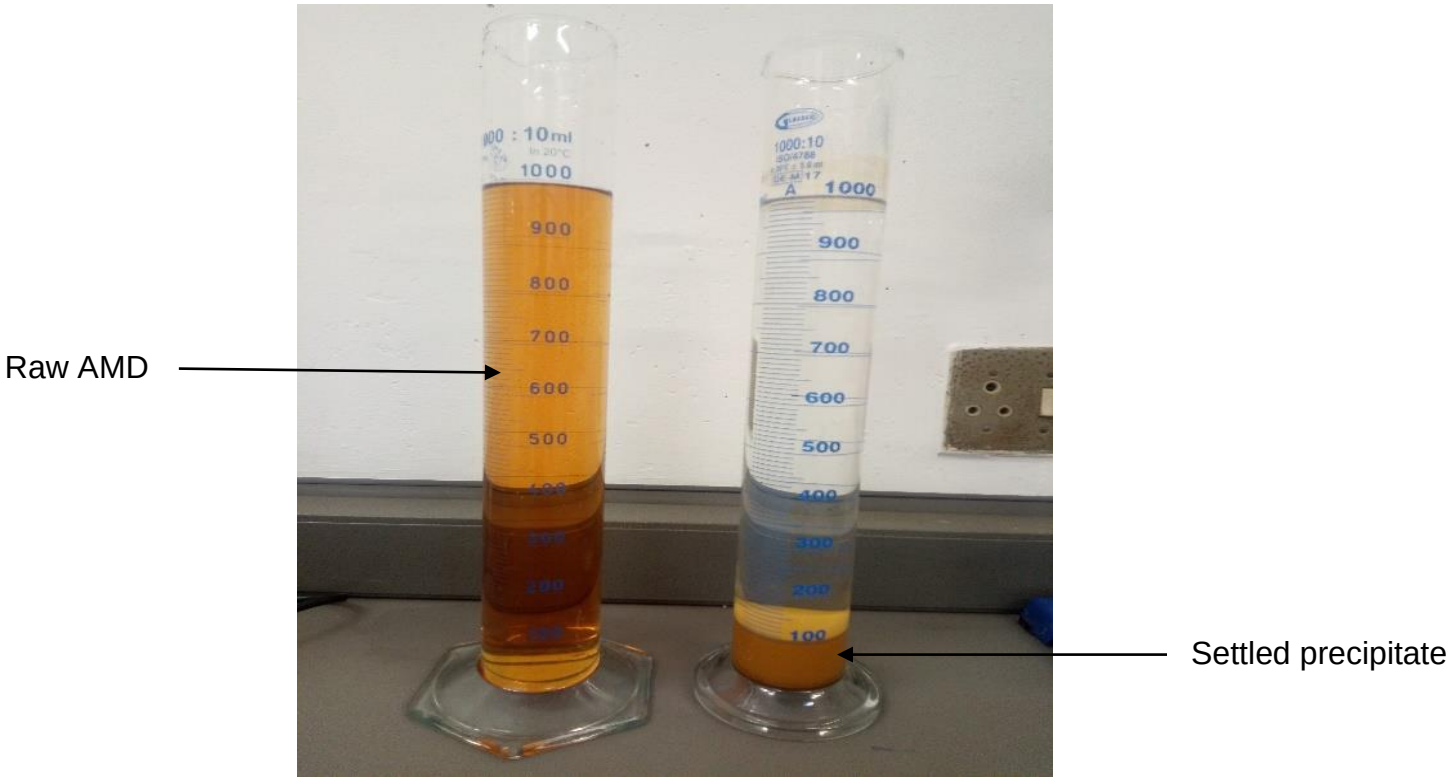

Figure 5.13: Figure showing raw and settled precipitate (C_s = 2.0) after 120 min of settling

Table 5.6: Effect of seeding on the particle settling rates

	Time, min	Height, cm	Initial settling rate (cm/min)
C_s = 0	30	144	4.8
C_s = 0.5	30	210	6.7
C_s = 1.0	30	225	7.5
C_s = 2.0	30	237	7.9

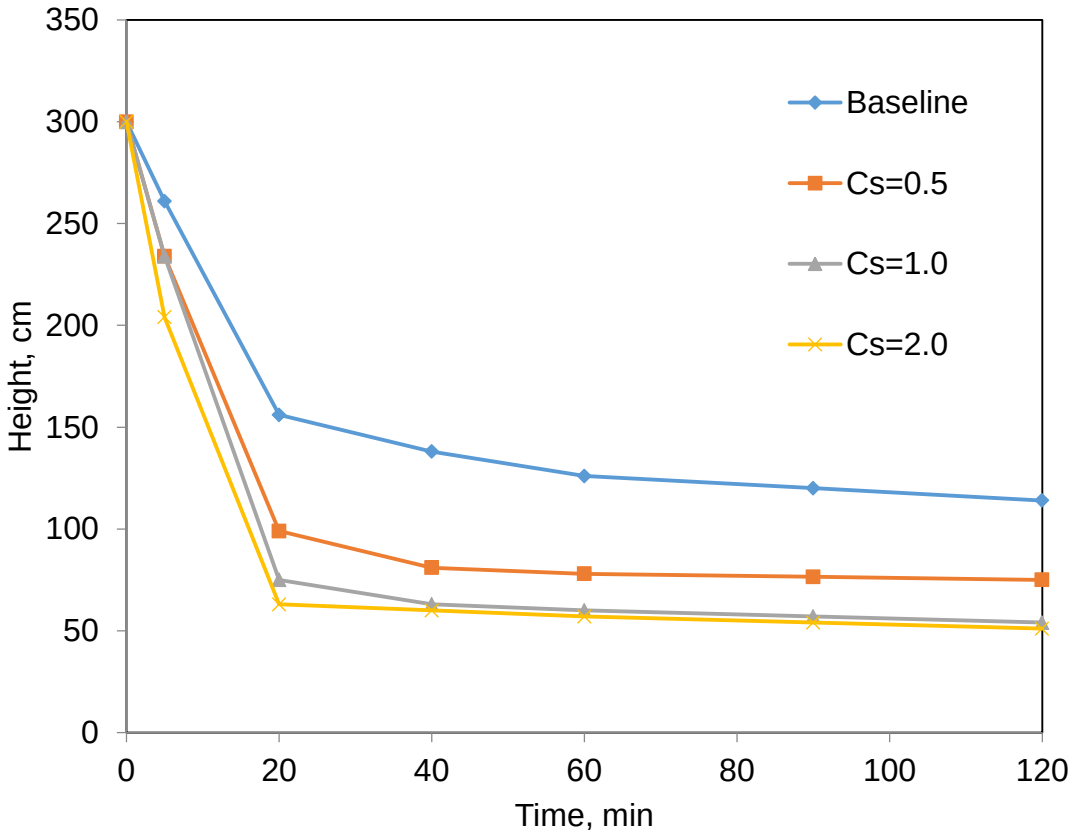

Figure 5.14: Settling rate of precipitate at different seed loading fraction

5.9 Conclusion

5.9.1 Fe(II) oxidation

The importance of Fe(II) oxidation rate during AMD treatment cannot be over emphasized as it determines the concentration of Fe(III) is solution, and subsequently the level of supersaturation during precipitation. In addition, the Fe(II) oxidation is one of the factors that determines the overall time required to treat the AMD. As such, it was important to study the kinetics of Fe(II) oxidation in the pH range of interest.

Kirby and Brady (1998) observed that there is no consensus on how to model kinetics of Fe(II) oxidation. This is due to the complexity of the solution chemistry, especially AMD, and the dependency of the oxidation rate on the hydrodynamics, type of oxidizing agent, and the nature of the alkalinity providing species. Nevertheless, this work tried to study the kinetics of ferrous sulphate oxidation and the effect of Al(III) cations on the oxidation rate. It is concluded from the results obtained that pH has a profound effect on the rate of Fe(II) oxidation. At high pH, the oxidation rate increases which results in shorter reaction time. The use of different concentrations of iron oxyhydroxides under different operating conditions increased the oxidation rate of Fe(II) to varying degrees. The Al(III) cations were not found to affect the oxidation rate. The oxidation precipitation of Fe(II) from ferrous solutions, at pH range 5.0-7.0 can be summarized as consisting of rapid initial homogeneous oxidation of Fe(II) followed by heterogeneous oxidation as a result of the instantaneous formation of primary particles (nucleation) from Fe(III) (Blesa and Matijević, 1989).

In the pH range of 5.0-7.0, the oxidation rate law agreed with what has been reported by several researchers with a first order dependency of Fe(II) while the 1.35 dependency of OH^- did not agree with most reported values. Due to the complexity nature of Fe(II) oxidation, other workers have reported contradictory results e.g., Wajon et al. (1985) who reported rate laws which do not show first order dependency on Fe(II) while operating in similar conditions to this study.

5.9.2 Fe(III) and Al(III) precipitation

The results obtained showed that 99.9 and 96.5% of Fe(III) and Al(III) can be recovered from AMD by precipitation at pH 5.0 using sodium hydroxide. At pH 7.0, the recovery for Al(III) increased to 99.1% while that of Fe(III) remained 99.9%. The precipitate purity was calculated and gave 99.0, 99.0 and 98.0 % for pH 5.0, 6.0 and 7.0, respectively

High supersaturation solutions have been known to produce precipitates with significantly smaller particle size distributions due to higher nucleation rates (Heffels and Kind, 1999). This can be countered by reducing supersaturation through the introduction of seeding. The results obtained in this study showed that seeded precipitation increased the particle size while reducing the BET surface area of the precipitates. The BET surface area and particle size results were confirmed by conducting the settling tests which showed that seeding improved the particle settling rates. Characterizations of the precipitate showed that the precipitates formed by precipitation Fe(III) and Al(III) in the pH range 5.0-7.0 are amorphous in nature with ferrihydrite being the dominant phase. The results obtained in this study agree with other studies such as Gan et al. (2005), Lintnerova et al. (2006) and Rhoton et al. (2002) which reported that the product of the high density sludge process is amorphous ferrihydrite.

These results have profound impacts for the wastewater treatment process in that optimum operational conditions will need a balance among the desired metal removal rate i.e., oxidation rate and precipitation and sedimentation and filterability of precipitate.

References

Blesa, M.A., Matijević, E., 1989. Phase transformations of iron oxides, oxohydroxides, and hydrous oxides in aqueous media. Advances in Colloid and Interface Science 29, 173–221.

Chen, T., Dutrizac, J., 1989. Practical mineralogical techniques for the characterization of hydrometallurgical products. Process Mineralogy IX: Applications to Mineral Beneficiation, Metallurgy, Gold, Diamonds, Ceramics, Environment and Health 289–309.

Florence, K., 2015. Mechanisms of the removal of metals from acid and neutral mine water under varying redox systems.

Gan, W.Y., Selomulya, C., Tapsell, G., Amal, R., 2005. Densification of iron (III) sludge in neutralization. International Journal of Mineral Processing 76, 149–162.

Gitari, W.M., Petrik, L.F., Akinyemi, S.A., 2018. Treatment of Acid Mine Drainage with Coal Fly Ash: Exploring the Solution Chemistry and Product Water Quality, in: Akinyemi, S.A., Gitari, M.W. (Eds.), Coal Fly Ash Beneficiation - Treatment of Acid Mine Drainage with Coal Fly Ash. InTech. https://doi.org/10.5772/intechopen.69741

Gorski, C.A., Edwards, R., Sander, M., Hofstetter, T.B., Stewart, S.M., 2016. Thermodynamic characterization of iron oxide–aqueous Fe2+ redox couples. Environmental science & technology 50, 8538–8547.

Heffels, S.K., Kind, M., 1999. Seeding technology: an underestimated critical success factor for crystallisation. IChemEUniversity of Cambridge

Hove, M., Van Hille, R.P., Lewis, A.E., 2009. The effect of different types of seeds on the oxidation and precipitation of iron. Hydrometallurgy 97, 180–184. https://doi.org/10.1016/j.hydromet.2009.03.001

Jenke, D.R., Diebold, F.E., 1983. Recovery of valuable metals from acid mine drainage by selective titration. Water research 17, 1585–1590.

Jones, A.M., Griffin, P.J., Collins, R.N., Waite, T.D., 2014. Ferrous iron oxidation under acidic conditions–The effect of ferric oxide surfaces. Geochimica et Cosmochimica Acta 145, 1–12.

Kirby, C.S., Brady, J.A.E., 1998. Field determination of Fe2+ oxidation rates in acid mine drainage using a continuously-stirred tank reactor. Applied Geochemistry 13, 509–520.

Lintnerova, O. T. I. L. I. A., Sottnik, P. and Soltes, S., 2006. Dissolved matter and suspended solids in the Smolnik Creek polluted by acid mine drainage (Slovakia). Geologica Carpathica'Brastislava–, 57(4), p. 311.

Lowson, R.T., 1982. Aqueous oxidation of pyrite by molecular oxygen. Chemical reviews 82, 461–497.

Mathews, C., Robins, R., 1972. The oxidation of aqueous ferrous sulphate solutions by molecular oxygen. Presented at the Proc. Aust. Inst. Min. Met, pp. 47–56.

Mendham, J., 2006. Vogels textbook of quantitative chemical analysis. Pearson Education India.

Michalková, E., Schwarz, M., Pulišová, P., Máša, B., Sudovský, P., 2013. Metals Recovery from Acid Mine Drainage and Possibilities for their Utilization. Polish Journal of Environmental Studies 22.

Millero, F.J., 1985. The effect of ionic interactions on the oxidation of metals in natural waters. Geochimica et Cosmochimica Acta 49, 547–553. https://doi.org/10.1016/0016-7037(85)90046-8

Morgan, B., Lahav, O., 2007. The effect of pH on the kinetics of spontaneous Fe(II) oxidation by O2 in aqueous solution – basic principles and a simple heuristic description. Chemosphere 68, 2080–2084. https://doi.org/10.1016/j.chemosphere.2007.02.015

National Gazette, 2013. National Gazette No. 36820, 06 September 2013, Vol. 579 [WWW Document]. URL https://www.greengazette.co.za/documents/national-gazette-36820-of-06-september-2013-vol-579_20130906-GGN-36820.pdf (accessed 9.20.19).

Park, S.-M., Yoo, J.-C., Ji, S.-W., Yang, J.-S., Baek, K., 2015. Selective recovery of dissolved Fe, Al, Cu, and Zn in acid mine drainage based on modeling to predict precipitation pH. Environmental Science and Pollution Research 22, 3013–3022.

Petrik, L.F., Fatoba, O.O., Missengue, R., Kalombe, R.M., Nyale, S., Madzivire, G., 2017. Treatment of mine water using a combination of coal fly ash and flocculants in a jet loop reactor system (No. WRC Report No.2129/1/18). Water Research Commission, South Africa.

Rhoton, F. E., Bigham, J. M. and Lindbo, DL., 2002. Properties of iron oxides in streams draining the loess uplands of Mississippi. Applied Geochemistry 17(4), pp. 409–419

Seckler, M.M., 1995. Calcium phosphate precipitation in a fluidized bed.

Snoeyink, V.L., Jenkins, D., 1980. Water chemistry. John Wiley.

Stumm, W., Lee, G.F., 1961. Oxygenation of Ferrous Iron. Industrial & Engineering Chemistry 53, 143–146. https://doi.org/10.1021/ie50614a030

Stumm, W., Morgan, J.J., 2012. Aquatic chemistry: chemical equilibria and rates in natural waters. John Wiley & Sons.

Tabak, H.H., Scharp, R., Burckle, J., Kawahara, F.K., Govind, R., 2003. Advances in biotreatment of acid mine drainage and biorecovery of metals: 1. Metal precipitation for recovery and recycle 14.

Tamura, H., Goto, K., Nagayama, M., 1976a. The effect of ferric hydroxide on the oxygenation of ferrous ions in neutral solutions. Corrosion Science 16, 197–207. https://doi.org/10.1016/0010-938X(76)90046-9

Tamura, H., Goto, K., Nagayama, M., 1976b. Effect of anions on the oxygenation of ferrous ion in neutral solutions. Journal of Inorganic and Nuclear Chemistry 38, 113–117. https://doi.org/10.1016/0022-1902(76)80061-9

Wajon, J.E., Ho, G.-E., Murphy, P.J., 1985. Rate of precipitation of ferrous iron and formation of mixed iron-calcium carbonates by naturally occurring carbonate materials. Water Research 19, 831–837.

Wei, X., Viadero, R.C., 2007. Synthesis of magnetite nanoparticles with ferric iron recovered from acid mine drainage: Implications for environmental engineering. Colloids and Surfaces A: Physicochemical and Engineering Aspects 294, 280–286. https://doi.org/10.1016/j.colsurfa.2006.07.060

Wei, X., Viadero, R.C., Buzby, K.M., 2005. Recovery of Iron and Aluminum from Acid Mine Drainage by Selective Precipitation. Environmental Engineering Science 22, 745–755. https://doi.org/10.1089/ees.2005.22.745

6 Solvent extraction experimental methods and results

6.1 Hypothesis and objectives

Although results discussed in **Chapter 5** results showed that Fe(III) and Al(III) can be recovered from AMD using precipitation with sodium hydroxide, it was decided upon to test a process that does not involve the cumbersome settling and filtration processes. The SX using Cyanex group of reagents has been applied with great success to separate either Fe(III) or Al(III) from different process solutions, over a wide range of process conditions. Cyanex 272 dissolved in different types of diluents has largely been used to extract both Fe(III) and Al(III). The two parameters that have been known to affect the extraction of metal cations are the extractant concentration and the pH. The extraction of Fe(III) and Al(III) has been shown to increase with an increase in both pH and Cyanex 272 concentration. Thus, the simultaneous extraction of Fe(III) and Al(III) with Cyanex 272 in Shellsol D70 was investigated under various conditions. The effect of both extractant concentration and pH were pursued. The objectives of this part of the study were set to;

- study the simultaneous extraction of both Fe(III) and Al(III) from AMD in the pH range 1.5-3.0
- determine the number of extraction stages required to extract more than 95% of each metal species
- study the stripping kinetics of both species using sulphuric acid

6.2 Materials used in the solvent extraction test works

The chemicals used during extraction and stripping experiments of Fe(III) and Al(III) are shown in **Table 6.1.** Cyanex 272 extractant was used to load the metal species with pH control achieved using a solution of either sodium hydroxide or sulphuric acid. After the extraction stage, the Fe(III) and Al(III) were stripped using sulphuric acid.

Table 6.1: Reagent grade chemicals in the extraction and stripping test work

Name	Source	Physical form	Role of chemical
Cyanex 272	Cytec Surface specialist	Liquid	Extractant
Shellsol D70	Cytec Surface specialist	Liquid	Solvent for extractant
Sodium hydroxide	Sigman Aldrich	Pellets	pH control
Sulphuric acid	Sigman Aldrich	Liquid	pH control/stripping

6.3 General experimental setup

Most of the work that has been conducted on SX of metals such as Fe, Al, Co, Ni etc., has been done using the batch process. The organic/aqueous dispersion has either been mixed via a wrist action flask shaker (Fortes and Benedetto, 1998; Gandhi et al., 1993) or with a mechanical agitator (Darvishi et al., 2005; Sato et al., 1985) while phase separation has been conducted using separation funnels. In the present work, a shaking water bath (see **Figure 6.1**) was used with 250 mL conical flasks to serve as mixing reactors. Phase separation was conducted using the separating funnels shown

in **Figure 6.2**. The pH measurement was achieved using the Hanna HI 9812-5 pH portable pH meter.

Figure 6.1: Organic/aqueous dispersion experimental setup with conical flasks

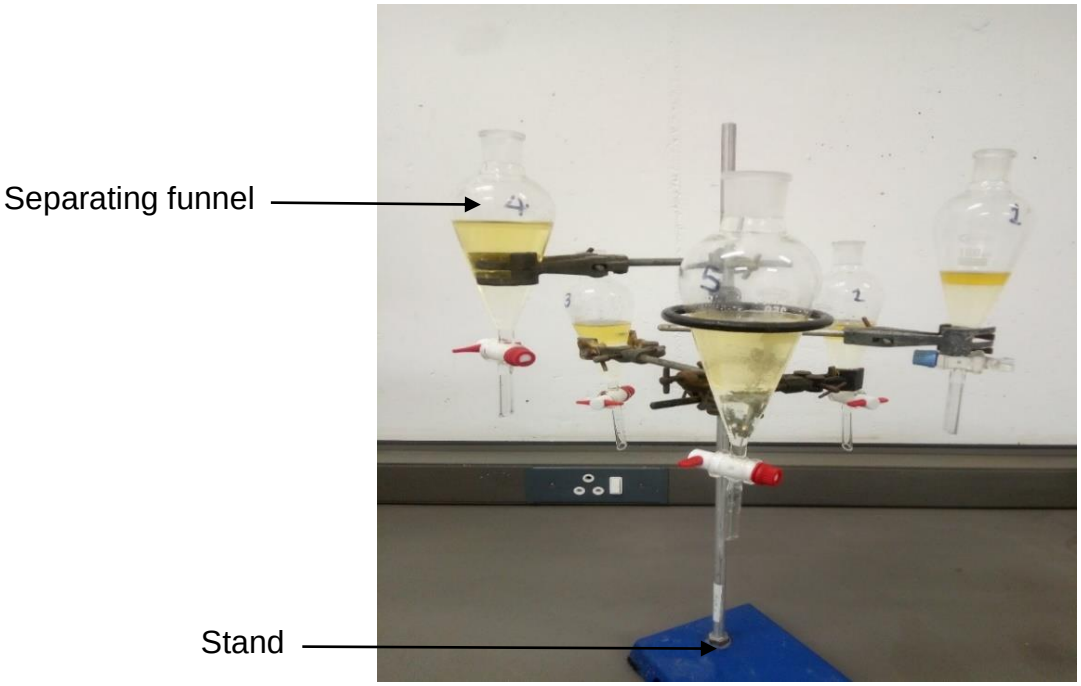

Figure 6.2: Separating funnels for phase separation

6.4 Extraction and stripping experimental procedure

The batch experiments of SX kinetic study were performed in the experimental set up shown in **Figure 6.1** and **Figure 6.2** while the experimental conditions are shown in **Table 6.2.** Initially, pipettes were used to transfer the organic and aqueous phases into the conical flasks. The aqueous and organic solutions were then preheated to the desired operating temperature, 25°C in this case, by using a water bath. This experimental temperature was chosen on the basis that it could be uneconomical to treat AMD at higher temperatures. A chemical dropper was used to add either 0.2 M sodium hydroxide or 0.2 M sulphuric acid to adjust the pH of the solution during agitation. The pH of the mixture was adjusted between 1.5 and 3.0. When the desired pH value was attained, the agitation continued for 15 minutes to ensure equilibrium.

After agitation was complete, the pH was measured, and the dispersion was transferred into 500 mL separation funnels and allowed to stand for 30 minutes for the two phases to separate. After complete phase separation in the separating funnels, a 10 mL sample of the aqueous solution was taken and diluted to the concentration range required for analysis. The metal content in the organic phase was determined via a mass balance from the analytical concentrations of the aqueous phase. Stripping experiments were conducted using the same experimental procedure.

Each loading isotherm was constructed at a particular pH. The highest O/A value was decided to be 5:1 while the lowest was 1:2. The resulting equilibrium loading curves accompanied by the operating lines using the McCabe–Thiele method led to the determination of the equilibrium counter-current stages required for the extraction of Fe(III) and Al(III) from the AMD. The organic phase samples were stripped by using 1.0, 2.0 or 3.0 M sulphuric acid. These are the typical sulphuric acid concentrations that have been used in the stripping of Fe(III) and Al(III) from organic solutions.

Table 6.2: Extraction and stripping experimental conditions

Parameter	Value
Cyanex 272 concentration, M	0.16, 0.32, 0.47, 0.63
pH	1.5, 2.0, 2.5, 3.0
Strip solution(H_2SO_4) concentration, M	1, 2, 3
Loading O/A ratio	0.5, 1.0, 1.5, 3, 5
Stripping O/A ratio	0.5, 1.0, 1.5, 3, 5
Reaction temperature, ˚C	25
Agitation, rev/min	200
Reaction time, min	15
Separation time, min 15	30

6.5 Analytical methods

The metal concentrations in the aqueous phase before and after each experimental run were measured by Inductively Coupled Plasma Optical Emission Spectrophotometry (ICP-OES) method using a Thermo-Scientific-IRIS Intrepid-II spectrometer accompanied by an ASX-520 Auto-sampler.

6.6 Experimental results and discussion

The study of the SX extraction kinetics was undertaken to determine the effect of Cyanex 272 concentration and pH on Fe(III) and Al(III) extraction from AMD.

6.6.1 Effect of Cyanex 272 concentration

The effect of Cyanex 272 concentration on the extraction of Fe(III) and Al(III) was examined at Cyanex 272 concentrations 0.16–0.63 M at 25ºC in the pH range 1.5-3.0. Presented in **Figure 6.3** and **Figure 6.4** are the results obtained at pH 1.5 and 2.5, respectively. The effect of pH is comprehensively discussed in **Section 6.6.2.**

Figure 6.3 shows that at pH 1.5, the extraction of Fe(III) increases steadily from 37.2% at 0.16 M to 70.0% at 0.47 M. A further increase in the extractant concentration to 0.63 M increased the Fe(III) extraction to 81.5%. Similarly, the extraction of Al(III) followed a similar trend. However, the maximum extraction of Al(III) at pH 1.5 was only 48.0% obtained with 0.63 M Cyanex 272. These results are in line with Aguilar and Cortina (2008) findings of the extraction curves of metals with Cyanex 272 at different pH values. The order of extraction for Cyanex 272 with increasing pH (discussed in **Section 3.3)** follows the sequence, Fe(III) > Zn(II) > Al(III) > Cu(II) > Mn(II) > Co(II) > Mg(II) > Ca(II) > Ni(II) (Cyanex 272, 2003). From the extraction sequence, it is clear that Cyanex 272 has a higher affinity for Fe(III) than Al(III) at lower pH. Thus, like the results shown in **Figure 6.3**, Fe (III) is expected to be extracted to a greater extent than Al(III) at pH 1.5.

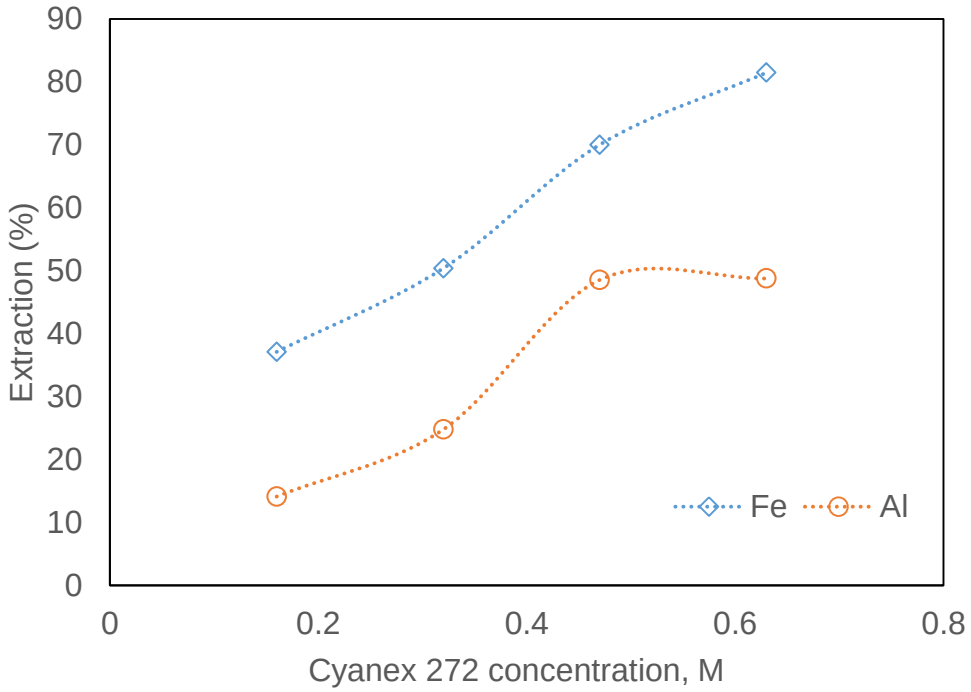

Figure 6.3: Effect of Cyanex 272 concentration on Fe(III) and Al(III) extraction. Experimental conditions: [Cyanex 272] = 0.06–0.63 M, [Al(III)] = 396 mg/L, [Fe(III)] = 4290 mg/L, O/A = 1:1, pH = 1.5, Temperature = 25 °C

The extraction curves summarized in **Figure 6.4** shows the results obtained for the effect of Cyanex 272 concentration to extract Fe(III) and Al(III) at pH 2.5. The figure shows that the extraction of Al(III) increased steadily with an increase in extractant concentration while the extraction of Fe(III) only increased moderately. For example, the percentage of Al(III) extracted increases from 45.2 to 91.7% when the extractant concentration increased from 0.16 to 0.47 M. Further increase in extractant concentration to 0.63 M did not significantly increase the extraction of Al(III). The extraction of Fe(III) shows a slightly different trend. Due to the high affinity of Cyanex 272 for Fe(III), the Fe(III) extraction increased from 79.1% to 92.9% when the extractant concentration was only increased from 0.16 to 0.32 M. A further increase in Cyanex 272 concentration did not result in any substantial increase in Fe(III) concentration. An important observation from the results obtained was that at pH 2.5, the Fe(III) and Al(III) extraction from AMD was marginally similar and further increase in the extractant

concentration did not increase the extraction of either species. Hence, 0.47 M was taken as the optimum concentration and used to study the stripping kinetics.

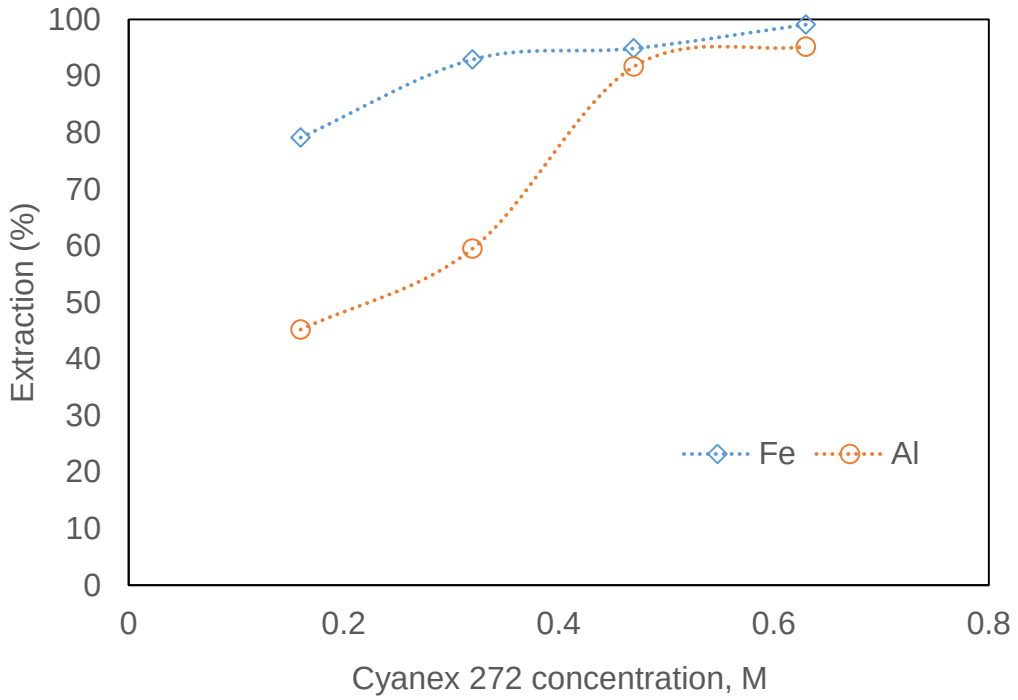

Figure 6.4: Effect of Cyanex 272 concentration on Fe(III) and Al(III) extraction. Experimental conditions: [Cyanex 272] = 0.06–0.63 M, [Al(III)] = 396 mg/L, [Fe(III)] = 4290 mg/L, O/A = 1:1, pH = 2.5, Temperature = 25 ± 2°C, Equilibrium time = 45 min.

6.6.2 Effect of equilibrium pH on extraction

The experimental results for the effect of pH on Fe(III) and Al(III) extraction are presented in **Figure 6.5**. The transfer of the metal ion to the extractant phase increases with the increasing pH of the aqueous medium, thus indicating an exchange of cations during the process. As can be seen from the figure, the extraction of Fe(III) at all pH values increased with increasing equilibrium pH reaching a maximum at a pH of around 2.5. The extraction increased from 37.1% to 79.1% when the pH was increased from 1.5 to 2.5 with 0.16 M Cyanex 272 concentration. Beyond a pH of 2.5, a dip in extraction was observed. The dip in extraction above pH 2.5 was similar with all the extractant concentrations. For example, at 0.47 M Cyanex 272 concentration and pH 1.5, the

extraction of Fe(III) was 70.0%. An increase in pH to 2.5 increased the extraction to 95.8%. However, beyond a pH of 2.5, the extraction extent reduced to 86.5%. The drop in extraction beyond pH 2.5 is possibly due to the hydrolysis of Fe(III) ion-pair complexes which indirectly promote competing equilibria. In addition, there is a possibility of the formation of ferric hydroxide precipitate.

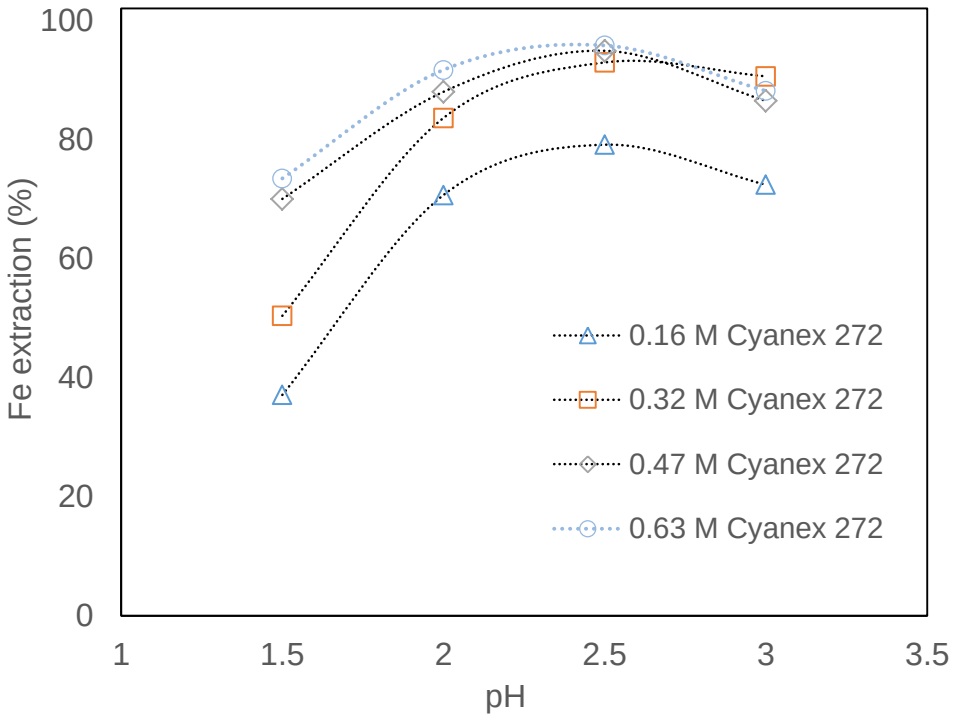

Figure 6.5: Effect of equilibrium pH on Fe(III) extraction by 0.47 M Cyanex 272. Experimental conditions: [Cyanex 272] = 0.47 M, [Al(III)] = 396 mg/L, [Fe(III)] = 4290 mg/L, O/A = 1:1, pH = 1.5–3.0, Temperature = 25 ± 2°C, Equilibration time = 45 min.

Figure 6.6 shows the effect of pH on Al(III) extraction. At all extractant concentrations, there was a steady increase in Al(III) extraction with pH. With 0.16 M Cyanex 272 concentration, the Al(III) extraction at pH 1.5 was 14.1%, increasing to 45.2% when the pH was increased to 2.5. A further increase in pH to 3.0 resulted in an increase in extraction to 54.3%. Similarly, extraction of 52.18 and 48.5% were obtained at pH 1.5 with 0.32 and 0.47 M Cyanex 272 concentration, respectively. The extractions increased to 45.2% and 91.1% at an operating equilibrium pH of 2.5 for 0.32 and 0.47 M

extractant concentrations, respectively. An Increase in pH to 3.0 increased the Al(III) extraction with all but 0.63 M concentration where the extraction extent remained the same as with 0.47 M.

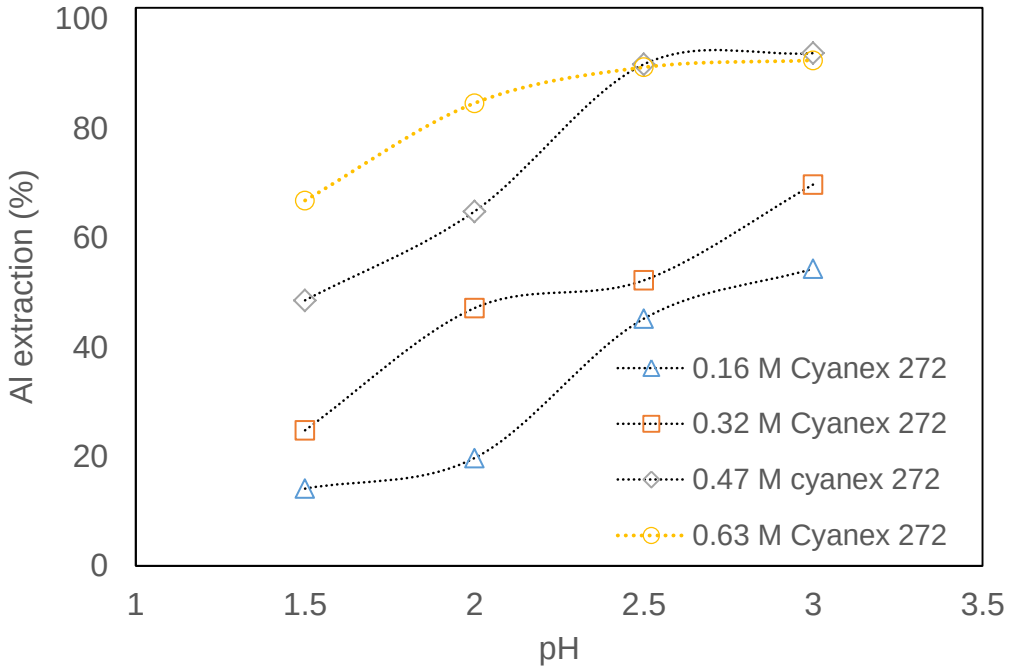

Figure 6.6: Effect of equilibrium pH on Al extraction by 0.47 M Cyanex 272. Experimental conditions: [Cyanex 272] = 0.47 M, [Al(III)] = 396 mg/L, [Fe(III)] = 4290 mg/L, O/A = 1:1, pH = 1.5–3.0, Temperature = 25 ± 2°C, Equilibration time = 45 min.

The optimal equilibrium pH for extraction of Fe(III) and Al(III) were 2.5 and 3.0, respectively. This agrees with reported values by some other researchers. For example, Mohapatra et al. (2007) concluded that the optimal pH for extraction of Al(III) using Cyanex 272 was between 2.2-3.6 when the study operated with a Cyanex 272 concentration of 0.3 M while Deep et al. (2006) determined an optimal pH of 2.3 for the extraction of Fe(III) from sulphate media. Other reported optimal equilibrium pHs for Fe(III) and Al(III) extraction using different extractants are presented in **Table 6.3**. It is clear from the table that the pH range for the extraction of Fe(III) is 1.8-2.5 and that for Al(III) is between a pH of 3.0 to 3.5 using Cyanex 272 dissolved in different diluents.

Table 6.3: Some reported optimal equilibrium pH for Fe(III) and Al(III) extraction by different authors.

Element	Extractant	Extractant conc; Temp	Diluent	Optimal pH range	Ref
Al(III)	Cyanex 272	0.05 M; 30°C	Toulene	3.2-3.6	1
Al(III)	Cyanex 272	0.05 M; 27°C	Kerosene	3.0-3.5	2
Al(III)	HDEHPA	0.3 M; 30°C	Kerosene	3.25-5.0	3
Al(III)	D2EHPA	0.3 M; 30°C	Kerosene	3.5-4.2	1
Al(III)	TOPO	0.3 M; 30°C	Kerosene	4.0-6.0	4
Fe(III)	Cyanex 272	0.2 M; 25°C	Escaid	1.8-2.2	5
Fe(III)	Cyanex 272	0.46 M; 25°C	Kerosene	2.0-3.0	6
Fe(III)	Lix 284	0.35 M; 25°C	Kerosene	2.0-3.0	6
Fe(III)	D2EHPA	0.27 M; 25°C	Kerosene	1.5-2.0	6

[1](Mohapatra et al., 2007); [2](Raji et al., 2020); [3](Phalke et al., 1996); [4](Zaki et al., 2005); [5](Deep et al., 2006); [6](Kul and Oskay, 2015)

6.6.3 Separation factor of Fe(III) over Al(III)

Further to the study of the effect of extractant concentration and equilibrium pH on the extraction of Fe(III) and Al(III), separation factors were calculated at every set of conditions tested to see the extractability of one species over the other. These results are presented in **Table 6.4**. The separation factors at all sets of conditions were low with the maximum of 3.46 obtained with 0.16 M Cyanex 272 concentration at pHs 2.5 and 3.0. At similar pH values but with 0.47 M Cyanex 272, the separation factors were 0.83 and 3.06. When the pH was increased to 2.5 and 3 at 0.47 M extractant concentration,

the separation factors reduced to 1.2 and 1.07 at pH 2.5 and 3, respectively. This finding supports the findings from **Sections 6.6.1** and **6.6.2** shows that at Cyanex 272 concentration of 0.47 M and pH above 2.5, both species are extracted to the same extent. As such, the 0.47 M loaded Cyanex 272 at pH 2.5 was used to conduct the stripping kinetic study (**discussed in Section 6.6.4**). The separation factor calculations also indicate that appropriate pH control is vital to achieve good Fe(III) and Al(III) co-extraction using Cyanex 272.

Table 6.4: Distribution coefficient and separation factor for Fe(III) and Al(III) at various Cyanex 272 concentrations and pH levels

Cyanex 272 conc	pH	$D_{Fe(III)}$	$D_{Al(III)}$	S.F
0,16 M	1,5	0.6	0.8	0.7
	2.0	2.4	0.9	2.7
	2,5	3.8	1.1	3.5
	3.0	4.1	1.2	3.5
0,32 M	1,5	1.9	2.1	0.9
	2.0	5.1	2.4	2.1
	2,5	13.1	4.2	3.1
	3.0	17.7	16.5	1.1
0,47 M	1,5	3.7	4.5	0.8
	2.0	7.3	2,4	3.1
	2,5	18.6	15.4	1.2
	3.0	24.7	23.0	1.1
0.63	1,5	4.2	4.1	1.0
	2.0	9.1	4.2	2.2
	2,5	22.3	17.6	1.3
	3.0	31.4	29.8	1.1

6.6.4 Theoretical number of stages required for extraction

To determine the theoretical number of stages required for complete extraction of Fe(III) and Al(III) from AMD, a McCabe-Thiele diagram was constructed by varying the A/O ratio from 5/1 to 1/2. The aqueous solutions were contacted with 0.47 M Cyanex 272. Presented in **Table 6.5** is the composition of the feed (raw AMD) and loaded organic. The metal content in the organic phase was determined via a mass balance from the analytical concentrations of the aqueous phase.

Table 6.5: Chemical composition of raw AMD and loaded organic (loaded using 0.47 M Cyanex 272 at pH 2.5 and O/A ratio 1:1).

		Metal concentration, mg/L								
	pH	Fe (Total)	Al	Ca	Mg	Mn	Zn	Ni	Co	Cu
Raw AMD	2.1	4290.0	396.0	503.0	474.0	93.9	14.3	1.7	1.4	0.5
Loaded organic		4210.0	391.2	61	72.3	50.2	9.6	-	-	-

The results are presented in **Figure 6.7** and **Figure 6.8**. Without having to change the pH (2.5), it can be seen that two stages of extraction at 0.47 M Cyanex concentration and O/A ratio of 1:1 are needed to recover Fe(III) by > 99.0% (>4210.0 mg/L) while one stage is required to extract Al(III) by > 92.0%. However, since the process is co-extraction of Fe(III) and Al(III), the two-stage extraction of Fe(III) means approximately 99.0% of Al(III) (>391.2 mg/L) is also recovered. Co-extraction of other impurities including Ca, Mg and 43.7 mg/L up to 12.2, 15.3 and 53.5% extraction, respectively is observed.

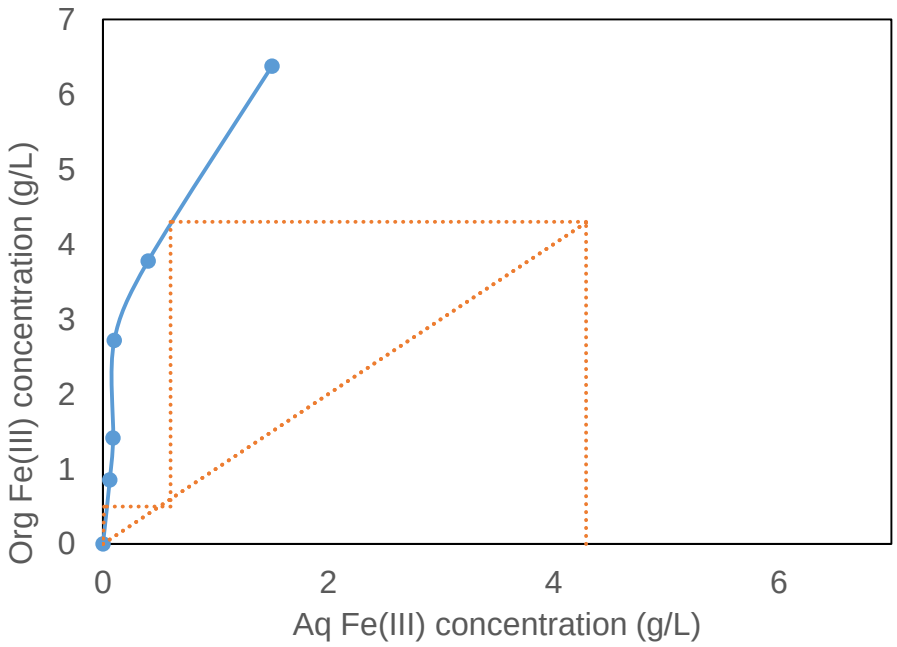

Figure 6.7: McCabe-Thiele diagram for the extraction Fe(III) by 0.47 M Cyanex 272. Experimental conditions: [Cyanex 272] = 0.47 M, [Al(III)] = 396 mg/L, [Fe(III)] = 4290 mg/L, O/A = 1:1, pH = 2, Temperature = 25 ± 2°C, Equilibration time = 45 min.

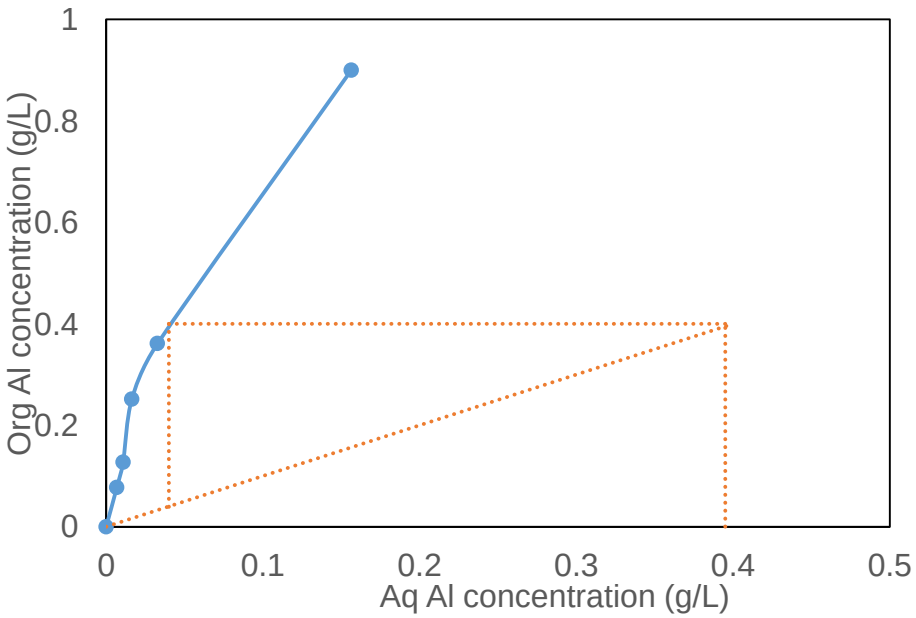

Figure 6.8: McCabe-Thiele diagram for the extraction Al(III) by 0.47 M Cyanex 272. Experimental conditions: [Cyanex 272] = 0.47 M, [Al(III)] = 396 mg/L, [Fe(III)] = 4290 mg/L, O/A = 1:1, pH = 2, Temperature = 25 ± 2°C, Equilibration time = 45 min.

6.6.5 Effect of sulphuric acid concentration on Fe(III) and Al(III) stripping

The stripping kinetics were investigated to determine the effect of sulphuric acid concentration on Fe(III) and Al(III) stripping from a 0.47 M Cyanex 272 loaded organic phase. The stripping kinetics were investigated by agitating the organic and either 1.0, 2.0 or 3.0 M sulphuric acid strip solution, at different O/A ratios. The mixture was agitated for 15 minutes to reach equilibrium. **Table 6.6** shows the composition of the loaded organic and strip solution at different sulphuric acid concentrations and O/A ratio 2:1. The results in **Figure 6.9** showed that at 1.0 M sulphuric acid, 89.1 and 84.1 % Fe(III) and Al(III) was stripped at.2:1 O/A ratio. An increase in the concentration of sulphuric acid increased the strip extraction of Fe(III) and Al(III) to 96.3 and 93.6%, respectively. Further increase in sulphuric acid concentration did not result in an increase in the recovery of either species. The strip liquor purity, from the analytical concentrations, was calculated according to **Equation 5.3** and gave >98.7 for all the sulphuric acid concentrations and O/A ratios.

Table 6.6: Chemical composition of loaded organic and strip solution (stripped using 2M sulphuric acid and 2:1 O/A ratio).

	Fe (Total)	Al	Ca	Mg	Mn	Zn	Ni	Co	Cu
Loaded organic	4210.0	391.2	61.0	72.3	50.2	9.6	-	-	-
Strip solution (1.0 M)	7504.7	676.0	7.6	64.0	74.8	-	-	-	-
Strip solution (2.0 M)	8141.0	732.0	8.9	59.2	78.0	-	-	-	-
Strip solution (1.0 M)	8165.7	736.0	13.4	56.4	75.0	-	-	-	-

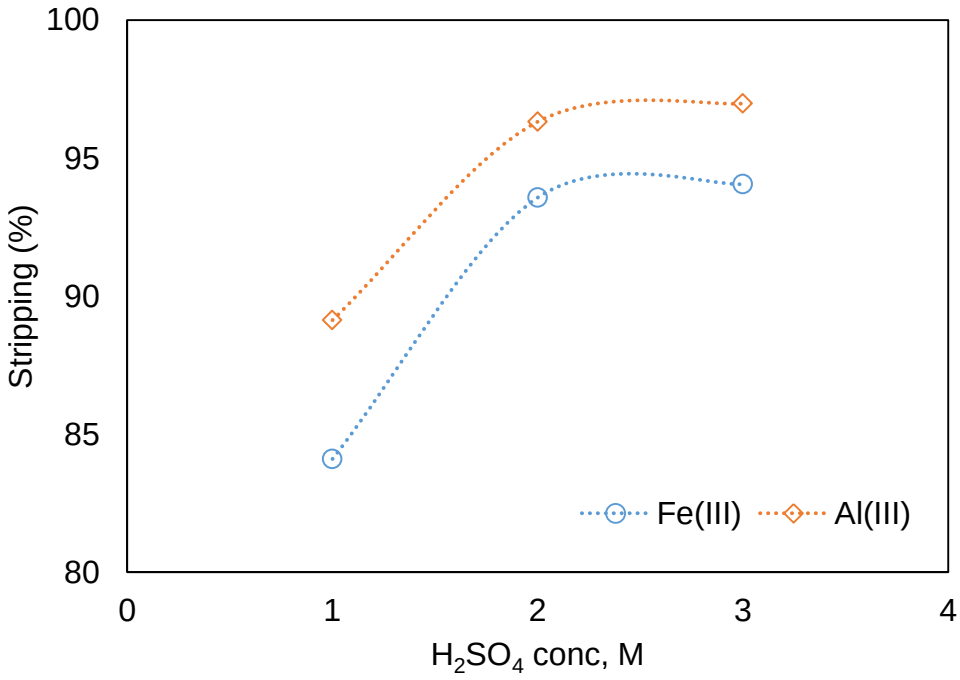

Figure 6.9: Effect of Sulphuric acid on Fe(IIII) and Al(III) stripping at 2:1O/A ratio

6.7 Conclusion

The separation of Fe(III) and Al(III) from AMD using SX was conducted. The main conclusions from the experimental findings can be summarized as follows:

- The Fe(III) and Al(III) can be co-extracted using Cyanex 272 with extraction efficiencies exceeding 94% at pH 2.5

- At a pH higher than 2.5, a drop in Fe(III) extraction was observed due to the hydrolysis of Fe(III) ion-pair complexes which indirectly promote competing equilibria.

- Extraction isotherms results showed that two stages are required to extract up to 99% while 1 stage is required to extract Al(III) up to 92.0%. However, the two-stage Fe(III) extraction means Al(III) also undergoes two stage extraction.

- When stripping the loaded phase, a 2 M sulphuric acid solution was used and this gave 96.3 and 94.0% Fe(III) and Al(III) recovery from the loaded organic at 2:1 O/A ratio. The strip liquor contained 8141.0 and 732 mg/L of Fe(III) and Al(III), respectively and the strip liquor purity was 98.8%.

References

Aguilar, M., Cortina, J.L., 2008. Solvent extraction and liquid membranes: Fundamentals and applications in new materials. CRC Press.

Darvishi, D., Haghshenas, D., Alamdari, E.K., Sadrnezhaad, S., Halali, M., 2005. Synergistic effect of Cyanex 272 and Cyanex 302 on separation of cobalt and nickel by D2EHPA. Hydrometallurgy 77, 227–238.

Deep, A., Correia, P.F., Carvalho, J.M., 2006. Separation and recovery of Fe (III) and Cr (III) from a tannery filtrate using Cyanex 272. Industrial & engineering chemistry research 45, 3200–3206.

Fortes, M., Benedetto, J., 1998. Separation of indium and iron by solvent extraction. Minerals engineering 11, 447–451.

Gandhi, M., Deorkar, N., Khopkar, S., 1993. Solvent extraction separation of cobalt (II) from nickel and other metals with Cyanex 272. Talanta 40, 1535–1539.

Kul, M., Oskay, K.O., 2015. Separation and recovery of valuable metals from real mix electroplating wastewater by solvent extraction. Hydrometallurgy 155, 153–160.

Mohapatra, D., Hong-In, K., Nam, C.-W., Park, K.-H., 2007. Liquid–liquid extraction of aluminium (III) from mixed sulphate solutions using sodium salts of Cyanex 272 and D2EHPA. Separation and purification technology 56, 311–318.

Phalke, P., Sherikar, A., Dhadke, P., 1996. Separation of beryllium (II) and aluminium (III) by solvent extraction using Bis-2 ethylhexyl phosphoric acid [HDEHP]. Separations Technology 6, 247–251.

Raji, M.A., Baba, A.A., Ibrahim, L., Alabi, A.G., Ghosh, M.K., Bale, R.B., 2020. Preparation of industrial alumina from a biotite-rich kaolinite (BRK) ore by Cyanex® 272. Indian Chemical Engineer 1–9.

Sato, T., Nakamura, T., Ikeno, M., 1985. The extraction of iron (III) from aqueous acid solutions by di (2-ethylhexyl) phosphoric acid. Hydrometallurgy 15, 209–217.

Zaki, E., Ismail, Z., Daoud, J., Aly, H., 2005. Extraction equilibrium of beryllium and aluminum and recovery of beryllium from Egyptian beryl solution using CYANEX 921. Hydrometallurgy 80, 221–231.

7 Coagulation experimental methods

7.1 Hypothesis and objectives

An investigation was conducted by Jiang and Graham (2003) to produce a pre-polymerized inorganic coagulant, poly-alumino–iron sulphate (PAFS) for drinking water treatment. An investigation of the conditions for preparing PAFS was conducted using chemical grade $Al_2(SO_4)_3.5H_2O$ and $Fe_2(SO_4)_3.5H_2O$. They hypothesized that a coagulant that contains both Fe(III) and Al(III) would perform in a wider pH range and possibly perform better that the conventional alum, ferric sulphate and ferric chloride coagulants. The PAFS coagulant was evaluated for the removal of color and dissolved organic carbon from drinking water and showed similar or better performance to conventional coagulants. The study by Jiang and Graham (2003) motivated this work and thus, it was the objective of this study to;

1. produce a Fe(III) and Al(III) containing coagulant from AMD using precipitation/dissolution and SX

2. evaluate the performance of the AMD-derived coagulant against the conventional coagulants

7.2 Coagulation experimental methods

The two AMD-derived coagulants in this study are;

i) the precipitation derived coagulant which shall hence forth be termed as AMD-PAFS^{p} and

ii) the SX derived which shall be termed as AMD-PAFS^{sx}

7.2.1 Procedure used to obtain coagulant from the AMD precipitate

Initially, the AMD-PAFS^{p} coagulant was produced by dissolving the AMD precipitate containing Fe(III) and Al(III) in sulphuric acid. The equipment used was a magnetic hotplate and a beaker shown in **Figure 7.1**.

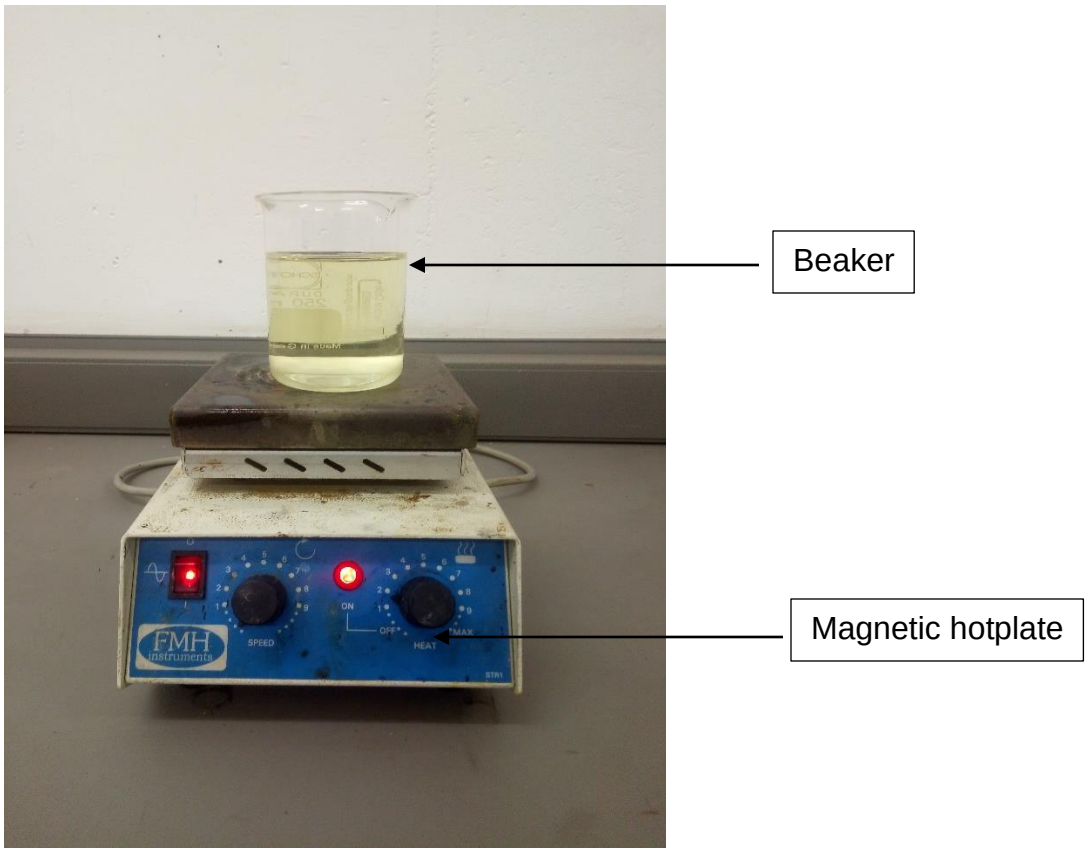

Figure 7.1: Experimental setup for precipitate dissolution to produce a coagulant

The solubility of the precipitate in sulphuric acid solutions of different acid strengths was measured by dosing increasing amounts of dried precipitate (25g) in 200 mL acid solution. Presented in **Table 7.1** are the experimental conditions. Acid solutions were prepared using analytical grade (98% v/v) sulphuric acid in deionized water. The different mixtures were left shaking for 24 hours times in a beaker, then vacuum filtered through Whatman filter papers. The solid residue left on the filter was dried for 24 h at 105°C, left to cool to room temperature in a silica gel desiccator and finally weighed.

Table 7.1: Experimental conditions

Parameter	Value
H_2SO_4 concentration, %	2, 5, 10, 20
Temperature, °C	25
Time, h	24

7.2.2 Procedure used to obtain coagulant from solvent extraction

The strip liquor from SX containing Fe(III) and Al(III) was generated according to the discussion in **Section 6.6** and used as a coagulant AMD-PAFS^{sx}.

7.2.3 Materials

The materials used in the coagulation test work are presented in **Table 7.2**. This included the generated coagulants, sulphuric acid and sodium hydroxide for pH control. All solutions were clearly labeled, with the date of preparation noted, and bottles kept clean and well stoppered.

Table 7.2: Materials used in coagulation tests

Name	Source	Physical form
AMD-PAFS^{p} and AMD-PAFS^{sx}	Generated	Liquid
Poly ferric sulphate (PFS)	Merck	Liquid
Sodium hydroxide	Sigman Aldrich	Pellets
Sulphuric acid	Sigman Aldrich	Liquid
Brewery wastewater	SA breweries	Liquid

7.2.4 Coagulation test equipment

The purpose of the jar test, or the laboratory coagulation test, is to test the coagulant, determine the optimum chemical conditions in terms of coagulant dose or determine the pH for treatment of the water. It is probably the most important routine test carried out in water treatment employing coagulation and flocculation as part of the treatment process. The principal piece of apparatus required for the test is a multiple stirrer unit with six reaction vessels and is shown in **Figure 7.2**. The equipment consists of a horizontal spindle, actuated from an electric motor by means of a belt and pulley system, driving vertical paddles in the reaction vessels. A speed selection system enabled the paddles to be driven at between 0-300 rev/min. Cleanliness of all glassware was essential as the basis of the test was to compare the appearance of the water in the jars. Reaction vessels, beakers and test tubes were washed in a solution of household detergent, using a test tube brush, and rinsed three times in clean water before being allowed to drain and then stored in a dust free place.

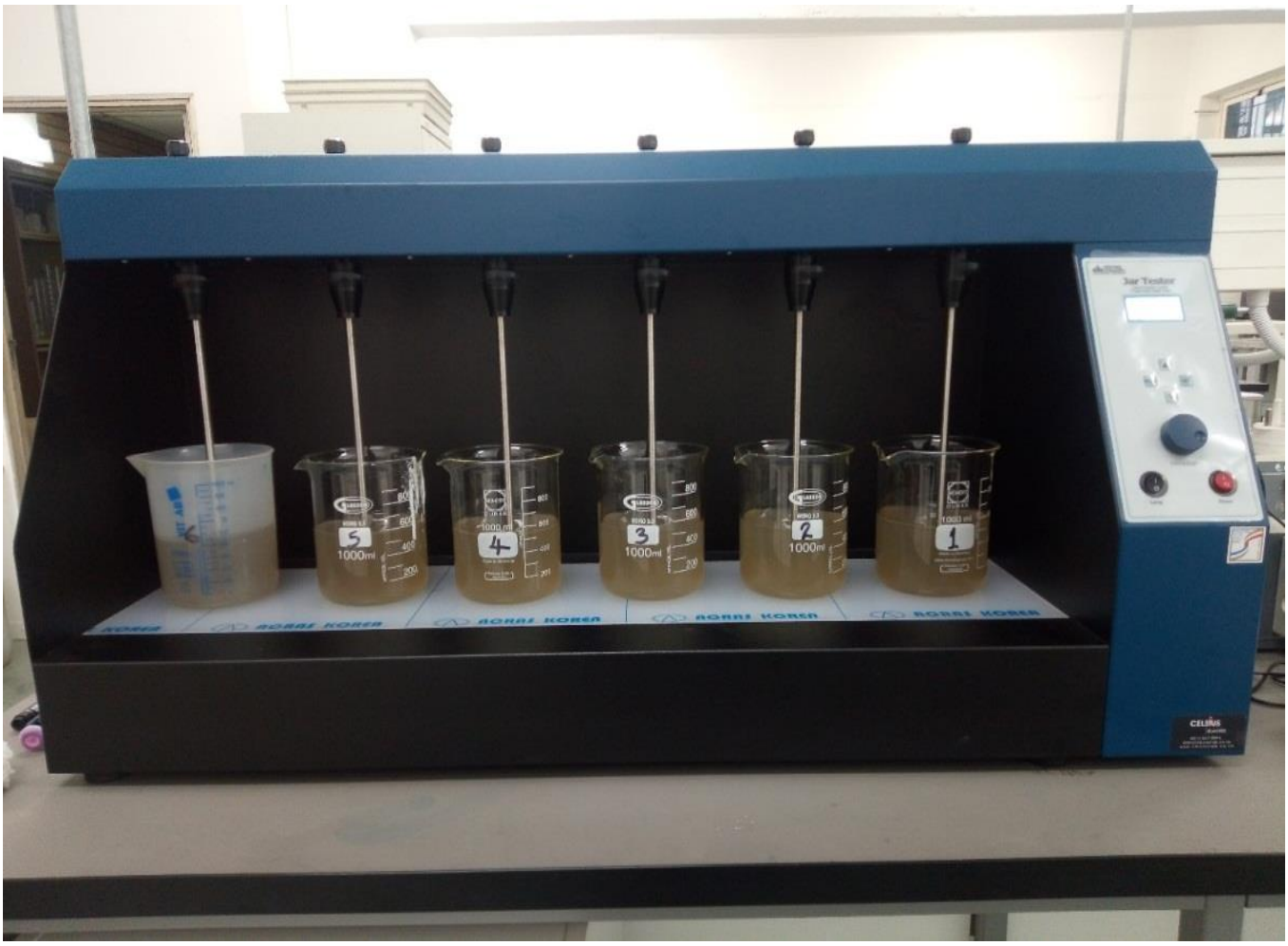

Figure 7.2: Jar tester for coagulation tests

7.2.5 Test procedure

Jar tests were conducted at temperatures ~25 °C for each of the coagulants (i.e., AMD-PAFS^{P}, AMD-PAFS^{SX} and PFS) with the temperature measured using a mercury thermometer. The experimental procedure involved filling each beaker with 500 mL of brewery wastewater. The coagulant, in varying dosages according to Table 7.3, was then added to each of the six (6) jars at the water surface. The dial on the jar tester was then rotated to 200 rev/min to induce rapid mixing for 3 minutes, followed by 10 minutes of slow mixing at 20 rev/min. The mixers were then shut off and the particles and/or aggregates were settled for 30 minutes. Qualitative observations of the water quality in

each jar were made. Two 20 mL grab samples of the supernatant were collected at 5 cm below the surface of the water using a pipette and placed into the viles. A drop of concentrated phosphoric acid, 85% reagent grade was added to one of the 40 mL samples from each jar for preservation for total organic carbon (TOC) analysis.

Table 7.3: Coagulation experimental conditions

Parameter	Value
Coagulant dose, mg/L	10, 50, 100, 150
pH	5, 6, 7
Temperature, °C	25
Agitation, rev/min	Fast = 200, slow = 20
Mixing time, min	Rapid = 3, slow = 10
Sedimentation time, min	30

7.2.6 Water Quality Analyzes

Five water quality parameters were measured as part of the jar testing procedure: turbidity [NTU], chemical oxygen demand (COD) (mg/L), total dissolved solids (TDS) (mg/L), electrical conductivity (EC) [µS/cm] and pH. All of the equipment was calibrated prior to analysis.

7.2.6.1 Turbidity

Turbidity was measured in the laboratory using a CyberScan TB 100 Portable Turbidity meter (ThermalFisher scientific, SA), which provided direct digital readings in NTU. According to the manufacturer, the resolution of the meter was 0.01 NTU on the lowest

range (i.e., readings from 0 and 9.99 NTU) and 0.1 when the range was adjusted to between 0 to 99.9 NTU. A 1 NTU turbidity standard was used to calibrate the equipment.

7.2.6.2 Chemical oxygen demand

Samples were analyzed for UV254 using a Merck Pharo 300 spectroquant (Merck, Johannesburg, South Africa).

7.2.6.3 Conductivity

Conductivity readings were obtained using a Hanna HI 9812-5 pH/EC/TDS/temperature portable meter (Hanna Instruments, Johannesburg, South Africa) which provided direct digital readings in µS/m. According to the manufacturer, the resolution of the meter was ± 0.5 % on the lowest range i.e., readings from 0 to 19990 µS/cm.

7.2.6.4 pH

The pH readings were obtained using a Hanna HI 9812-5 pH/EC/TDS/temperature portable meter (Hanna Instruments, Johannesburg, South Africa) which provided direct digital readings. The resolution of the meter was 0.001, as stated by the manufacturer.

7.3 Experimental results and discussion

7.3.1 Precipitate solubility and coagulant production

The solubility of the dried precipitate was determined in increasing sulphuric acid solutions and is presented **Figure 7.3**. As expected, the precipitate solubility generally increases with increasing acid strength. It therefore, took several experimental iterations to find the point at which the solution had lost its capacity to dissolve more precipitate. The experiments were done in triplets and the data points show results obtained for each experimental run. The lowest solubility obtained was at 2.0% (w/w) sulphuric acid with an average solubility of 43.3 mg/L. The difference in the precipitate solubility at 5.0% and 10.0% was 3.0% with solubilities of 84.0 mg/L and 87.8 mg/L at 5.0 and 10.0%. The precipitate solubility was higher in 10.0% sulphuric acid compared to 20% sulphuric acid with average solubilities of 87.7 mg/L and 62.9 mg/L, respectively. The fact that lower precipitate solubilities are seen at higher sulphuric acid concentration is probably due to the formation of insoluble sulphate salts (Sapsford et.al. 2015).

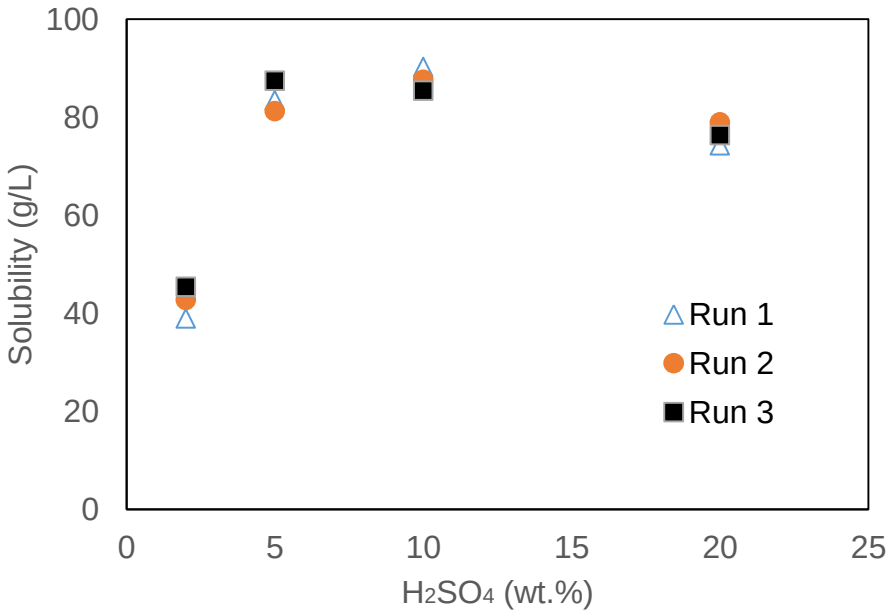

Figure 7.3: Solubility of ferrihydrite precipitate dissolved in sulphuric acid of varying strengths (w/w)

Since the solubility of the precipitate at 5.0% sulphuric acid was virtually the same as at 10.0%, 5.0% sulphuric acid was taken as the optimum acid concentration to dissolve the precipitate. The precipitate obtained at pH 5.0 and C_s = 1.0 was therefore dissolved in 5.0% sulphuric acid to produce a coagulant. On the other hand, the SX strip liquor was also used as a coagulant. **Table 7.4** summarizes the characteristics of the AMD-PAFS^{p}, AMD-PAFS^{sx} as well as the commercial PFS.

Table 7.4: Chemical composition of AMD-PAFS^{p} coagulant produced by precipitation at pH 5.0 and dissolution in 5.0% w/w sulphuric acid, AMD-PAFS^{sx} by SX using 0.47 M Cyanex 272 and stripping using 2 M sulphuric acid and conventional poly ferric sulphate coagulant

Parameter	AMD-PAFS^{p}	AMD-PAFS^{sx}	PFS
Fe (Total), mg/L	88,768.84	8141	115,000
Al, mg/L	9876.54	732	4419
Mg, mg/L	444.43	59.2	160.6
Ca, mg/L	6.1	8.9	56.8
Mn, mg/L	102.23	78.0	1585
Zn, mg/L	ND	ND	22.4
Ni, mg/L	ND	ND	ND
Co, mg/L	ND	ND	ND
Cu, mg/L	ND	ND	11.5
SO_4^{2-}, mg/L	122,000	88,000	130,800

(ND=not detected)

The AMD-PAFS^{p} coagulant was composed of 89.5% Fe and 10.0% Al with trace amounts of Mn, Mg and Ca. The total mass concentration of Fe(III) and Al(III) in the AMD-PAFS^{p} coagulant was 96,644 mg/L, which compares well with the commercial PFS with the Fe mass concentrations 115,000 mg/L. On the other hand, the concentration of AMD-PAFS^{sx} was 91.7% Fe(III) and 8.33% Al(III). However, despite the similar mass percentages of Fe(III) and Al(III) in AMD-PAFS^{p} and AMD-PAFS^{sx}, the Fe(III) concentration in AMD-PAFS^{sx} was only 8141 mg/L as compared to 88768.8 mg/L in AMD-PAFS^{p}. The Al(III) concentration was 9876.5 mg/L in AMD-PAFS^{p} as compared to 740 mg/L AMD-PAFS^{sx}. The difference in the concentration between the two coagulants is because SX is a solution based process and as such, there is a need to strike a balance between the volumes of the solution and the extraction (which translates into metal concentration).

Figure 7.4 is the picture of the AMD-PAFS^{P} generated using precipitation and dissolution.

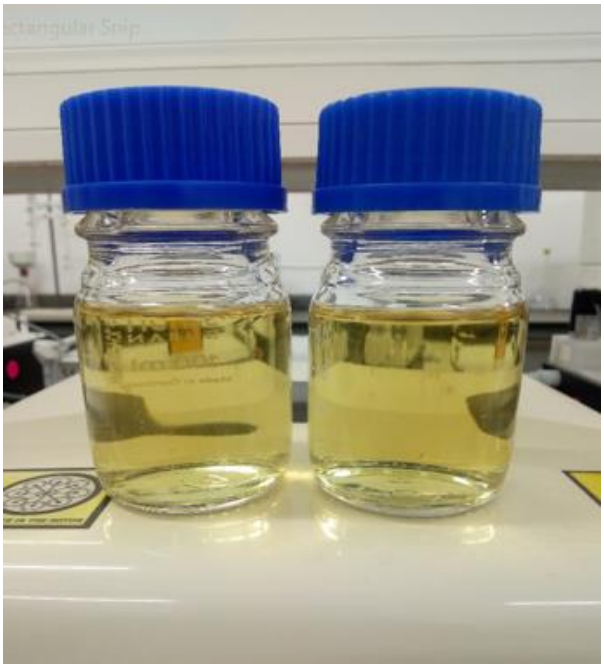

Figure 7.4: AMD-PAFS^{p} coagulant

7.3.2 Characteristics of the brewery wastewater

The AMD-PAFS^{p} and AMD-PAFS^{sx} were compared against the commercial FPS in the treatment of brewery wastewater. **Table 7.5** shows the characteristics of the brewery wastewater used in the study.

Table 7.5: Characteristics of the brewery wastewater that was treated with the AMD-PAFS and PFS coagulants

Parameter	Value
pH	7.1 ± 0.2
COD, mg/L	3160 ± 90
TDS, mg/L	1810 ± 30
Turbidity, NTU	99 ± 9
Electric conductivity, µS/cm	3510 ± 133

7.3.3 Effect of the coagulant on turbidity and chemical oxygen demand

Initially, the AMD-PAFS^{p} was compared against PFS coagulant because they had similar Fe(III) and Al(III) concentrations. The two coagulants were compared on their ability to reduce the turbidity of the brewery wastewater. The turbidity, which is the cloudiness of the water, has long been the targeted substance during the coagulation and flocculation processes and is largely used as an indicator for the efficiency of the coagulation process (Cheng et al., 2005). It is the principal physical characteristic of water and expresses the optical property that causes light to be scattered and absorbed by particles and molecules rather than transmitted in a straight line through the water sample. The turbidity removal efficiency was determined by adding different doses of the coagulants from 10 mg/L to 150 mg/L. As shown in **Figure 7.6**, the percentage removal of the turbidity of the brewery water samples increased from 18.1% at 10 mg/L to 91.92% at 150 mg/L AMD-PAFS^{p}. This compared favorably with results obtained from the use of PFS, where 22.3% and 87.8% turbidity removal at 10 and 150 mg/L PFS were obtained, respectively. The increment in the removal of turbidity was due to the increment in the active sites of the coagulants. The results obtained in this study

compare well with the results reported for other synthetic coagulants. For example, a poly-aluminium-silicate-chloride coagulant (PSiFAC) was synthesized and tested in the treatment of simulated surface water (Tolkou and Zouboulis, 2015). A 99% turbidity removal was obtained at a PSiFAC concentration of 100 mg/L. The relatively high performance of the PSiFAC can be attributed to the presence of the silicate species which act as a coagulant aid. The silicate species increases the bridge effect and thereby slows down the formation of $Fe(OH)_3$ precipitate, which results in enhanced coagulation (Wang and Tang, 2001).

The COD is the amount of oxygen required to break down an inorganic pollutant in water or wastewater. Contrary to turbidity removal, the COD removal at 150 mg/L PFS was 64%, which was higher than the COD removal of 56% obtained at the same concentration of AMD-PAFS^p. This result is not consistent with the previous studies such as the study by Xing and Sun (Xing and Sun, 2009), who obtained 72.4% COD removal from antibiotic fermentation wastewater albeit operating at a higher coagulant dosage of 200 mg/L PFS coagulant.

7.3.4 Effect of the Coagulants on Electric Conductivity

The EC is the measure of the dissolved ionic components in water and hence the electric characteristics. The EC gives an indication of the amount of total dissolved salts and inorganic material in water (Oyem et al., 2014). As shown in **Figure 7.6**, the electric conductivity of the brewery wastewater increased as the dose of the coagulants increased. The conductivity of the original water sample was 3510 µS/cm, but it was increased to 4010 and 4110 µS/cm for AMD-PAFS^p and PFS coagulants, respectively. The sporadic rise in EC observed in all the samples tested could be due to the presence of the dissolved ions of the wastewater coupled with the dissolved ions of the coagulants and the pH regulator (NaOH). Similar observations have been made by other researchers (Aniyikaiye et al., 2019; Miranda et al., 2015).

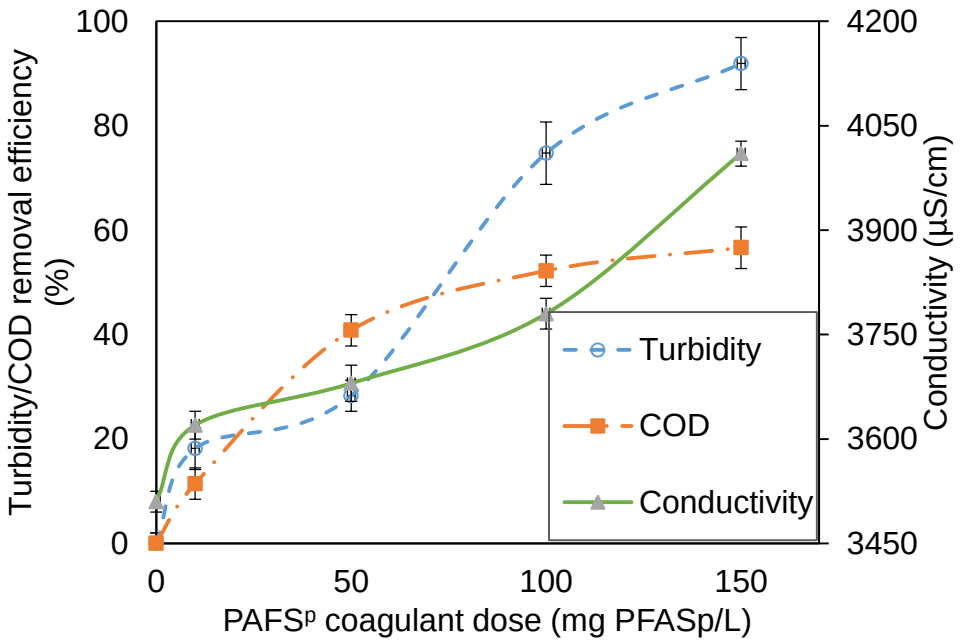

Figure 7.5: Performance evaluation of poly-alumino-ferric sulphate (Initial pH 7.0, temperature = 24.6 °C) during the treatment of brewery wastewater

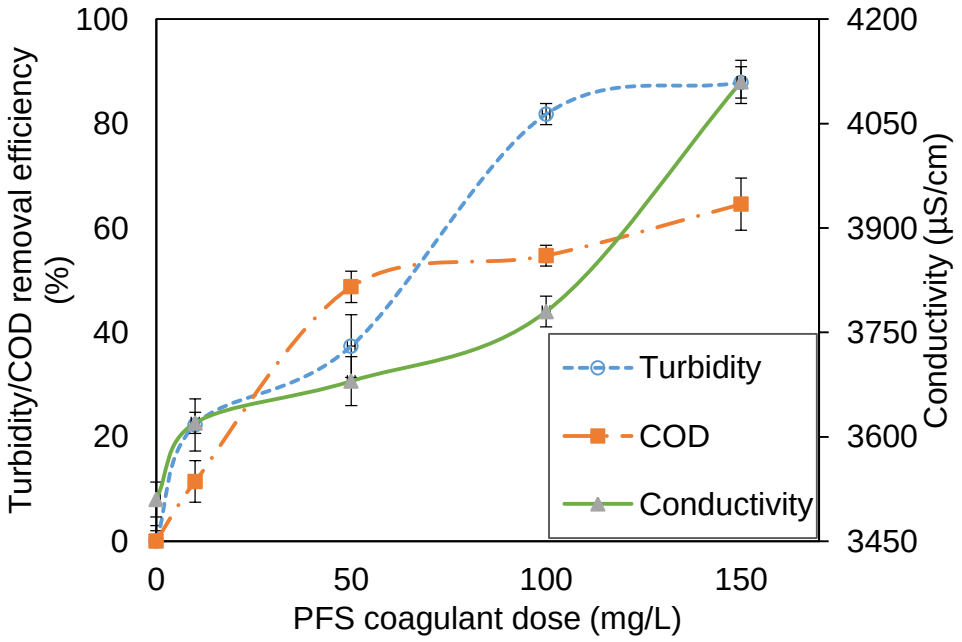

Figure 7.6: Performance evaluation of poly ferric sulphate coagulant (Initial pH 7.0, temperature = 24.6 °C) during the treatment of brewery wastewater

7.3.5 Effect of the Coagulant Dose on Total Dissolved Solids

TDS is one of the key parameters that can be used for water quality analysis. It is related to the quantity of material in water that can pass a filter size of 2 µm. The TDS increases the conductivities of water due to the presence of dissolved impurities (Kazi and Virupakshi, 2013). The TDS in water influence the quality of drinking water such as taste, alkalinity, hardness and corrosion properties. As shown in **Figure 7.7**, the TDS of the untreated brewery wastewater was 1810 mg/L. The TDS increases only slightly with an increase in coagulant dose for both the AMD-PAFS^{p} and PFS coagulants. In general, the increase in TDS is due to an increase in the number of solute particles or ions as a result of coagulant addition. The principal anions contributing to the TDS value include the carbonate, bicarbonate, chloride, sulphate and nitrates, and cations such as calcium, magnesium, potassium and sodium (Beyene et al., 2016). The sulphate components of the tested coagulants contributed to the increase in the TDS of the treated water when the coagulant dose was increased.

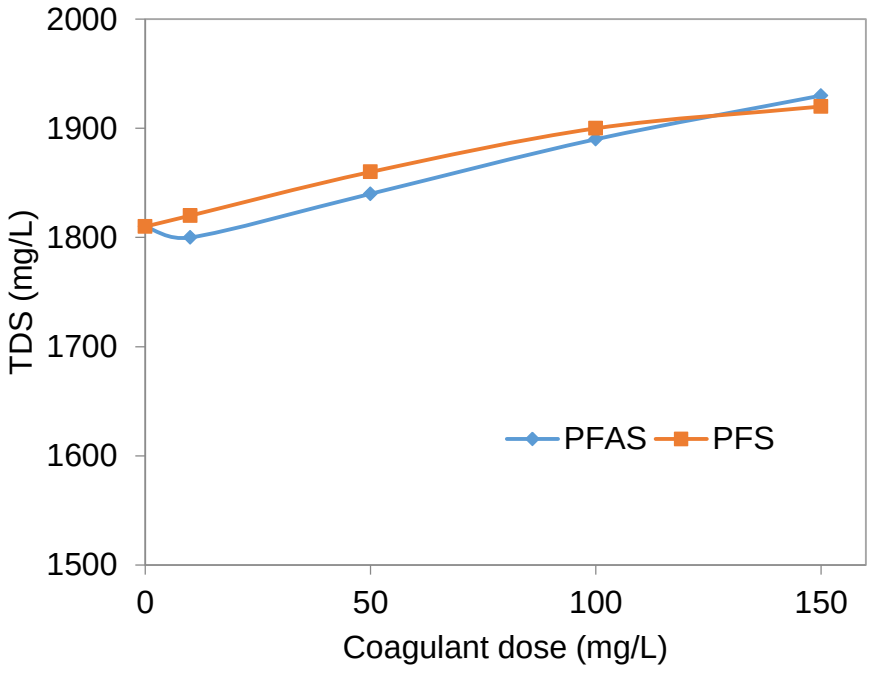

Figure 7.7: Total dissolved solids as a function of coagulant dose during treatment of brewery wastewater

7.3.6 Performance of precipitation derived against solvent extraction derived AMD-PAFS

Following the comparison of AMD-PAFS^{p} against PFS, the AMD-PAFS^{p} was tested against AMD-PAFS^{sx} in the turbidity removal efficiency. The low concentration of Fe(III) and Al(III) in the AMD-PAFS^{sx} was compensated by adding volume of AMD-PAFS^{sx} coagulant that gave equivalent concentration as that of AMD-PAFS^{p}. **Figure 7.8** shows the performance of the AMD-PAFS^{p} against AMD-PAFS^{sx}. From the graph, it can be seen that the AMD-PAFS^{sx} coagulant performed slightly better than AMD-PAFS^{p}. The turbidity removal of 18.2 and 24.3% were obtained at the 10 mg/L AMD-PAFS^{p} and AMD-PAFS^{sx}, respectively.

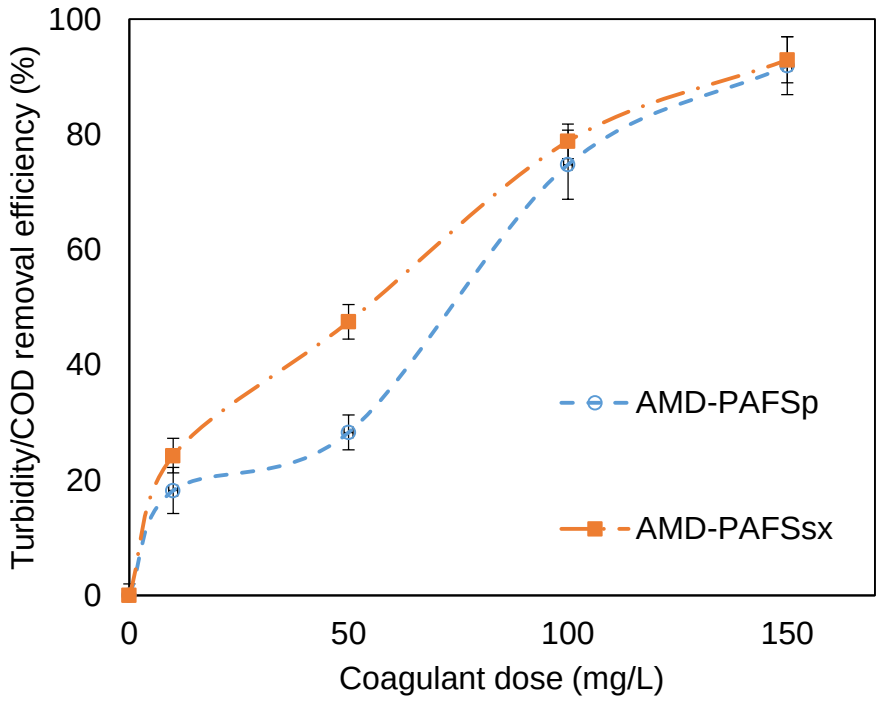

Figure 7.8: Performance of precipitation derived against solvent extraction derived AMD-PAFS coagulant

An increase in the coagulant dose to 100 mg/L increased the turbidity removal to 74.8 and 79.0% AMD-PAFS^{p} and AMD-PAFS^{sx}, respectively. The better performance of the AMD-PAFS^{sx} could have been due to the significantly higher concentration of Mn, which in itself has been used for water treatment (Liu et al., 2015; Wei et al., 2010; Zhao et al., 2015).

As already stated, TDS increases the conductivities of water due to the presence of dissolved impurities. The effect of AMD-PAFS^{sx} on the wastewater TDS was compared to the TDS of AMD-PAFS^{p} treated wastewater. As shown in **Figure 7.9**, there is a steady increase in the TDS of both the PAFS^{p} and AMD-PAFS^{sx} treated wastewater. The TDS values obtained at different coagulant dosages were marginally the same for both coagulants. Although PAFS^{sx} contained significantly higher mass percentage of Mn as compared to PAFS^{p} the principal anions contributing to the TDS such as the sulphate and cations such as calcium, magnesium, potassium and sodium were similar. This explains why the TDS values of the treated waters were the same.

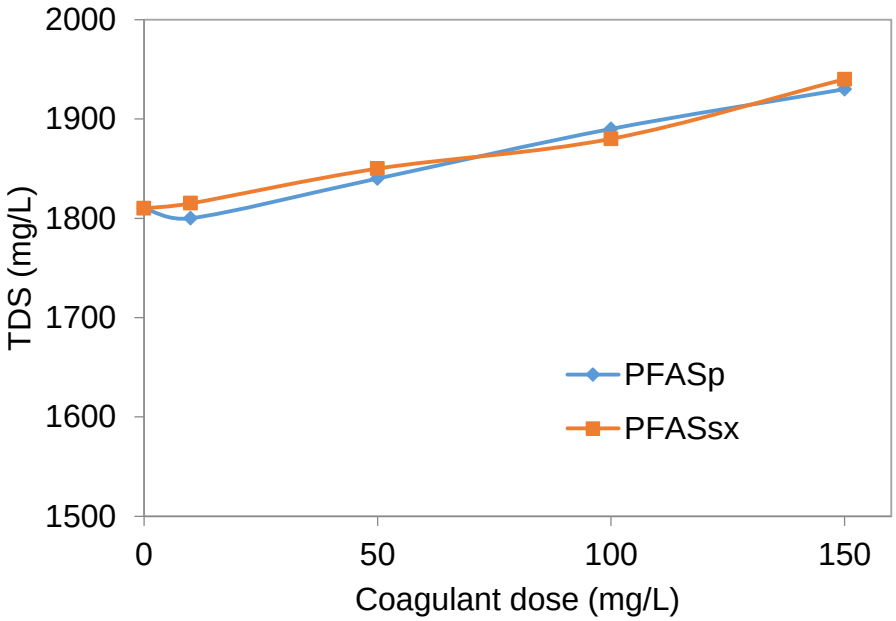

Figure 7.9: Total dissolved solids as a function of coagulant dose during treatment of brewery wastewater

7.4 Conclusion

This section of the research compared the performance of the AMD-generated coagulants against the conventional poly ferric sulphate coagulant. The following conclusions can be drawn from the results obtained.

- It was demonstrated that Fe(III) and Al(III) based coagulants can be obtained from AMD.

- The AMD-PAFS^{p} compared favorably with poly ferric sulphate coagulant in turbidity and COD removal in the treatment of brewery wastewater.

- When the AMD-PAFS^{p} was compared against AMD-PAFS^{sx}. It was established that the AMD-PAFS^{sx} slightly outperformed the AMD-PAFS^{p}. This was due to significantly higher mass concentration of Mn in the AMD-PAFS^{sx} as compared to AMD-PAFS^{p}.

8 Flowsheets and mass balances

Figure 8.1 and **Figure 8.2** show the proposed coagulant recovery flowsheets using either precipitation or SX, respectively. The stream balances are shown in **Table 8.1** and **Table 8.2**. The individual stream balances are calculated on the basis of either one liter AMD solution or one liter coagulant recovered. The masses are either calculated from ICP analysis results of AMD and coagulant or from the stoichiometric calculated reagent addition. The stream calculations are documented in **Appendix IV**.

8.1 Precipitation based flowsheet

Based on the oxidation and precipitation results, a single stage oxidation-precipitation unit at pH = 5.0 is recommended to avoid co-precipitation of other impurities. Seeding at concentration, C_s = 1.0 to improve the downstream dewatering processes is also recommended. Solid-liquid separation can be achieved by filtration. Below is the proposed flowsheet.

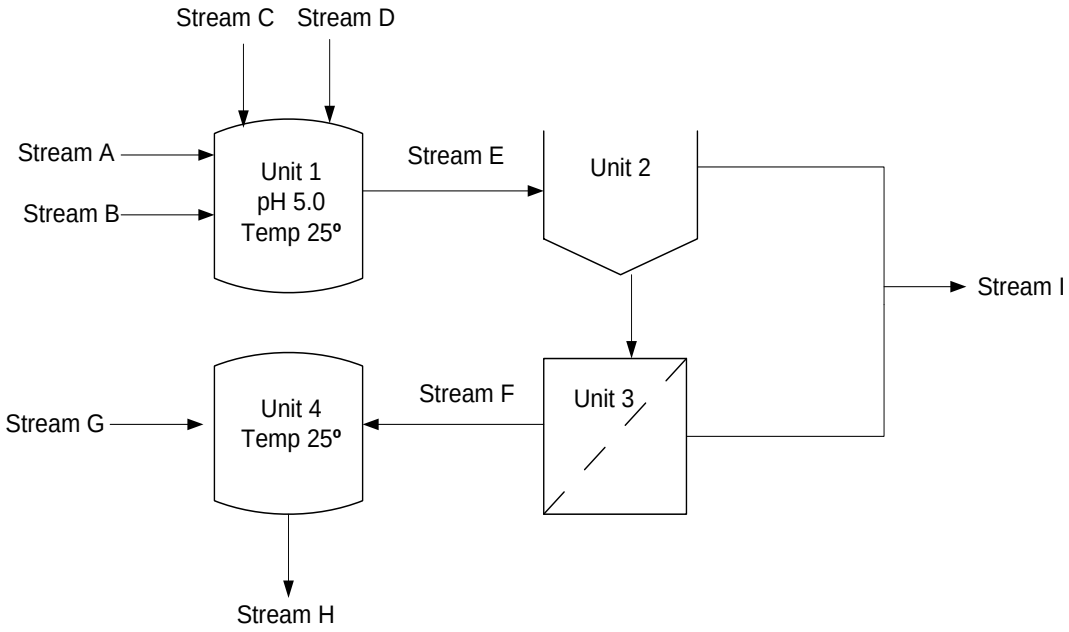

Figure 8.1: Coagulant recovery flowsheet through oxidation-precipitation-dissolution

Table 8.1: Precipitation based flowsheet mass balance for coagulant recovery

Unit	**Unit name**
Unit 1	Oxidation-precipitation reactor
Unit 2	Clarifier
Unit 3	Filter
Unit 4	Coagulant production reactor

		Species concentration, g/L AMD							
Stream	Stream name	Fe_T	Al	Mn	Mg	Ca	O_2	NaOH	H_2SO_4
A	AMD	4.3	0.4	0.09	0.5	0.5	-	-	0.8
B	Recycled sludge	4.25	0.4	-	-	-	-	-	-
C	Air	-	-	-	-	-	>>0.62	-	-
D	NaOH	-	-	-	-	-	-	14.4	-
E	Slurry	8.54	0.8	0.18	1.0	1.0	-	-	0.001
F	Precipitate	8.5	0.8	-	-	-	-	-	-
I	Fe/Al depleted water	0.1	0.02	~0.09	~0.5	~0.5	-	-	0.001
		Species concentration, g/L coagulant							
G	H_2SO_4	-	-	-	-	-	-	-	0.036
H	Coagulant	88.7	9.8	-	-	-	-	-	0.036

8.2 Solvent extraction based flowsheet

Based on batch equilibrium results, a unit of three mixer settlers (two for extraction and one for stripping) is recommended for the treatment of AMD to recover Fe(III) and Al(III), using an organic phase of 0.47 M Cyanex 272 in Shellsol D70. Below is the proposed flowsheet.

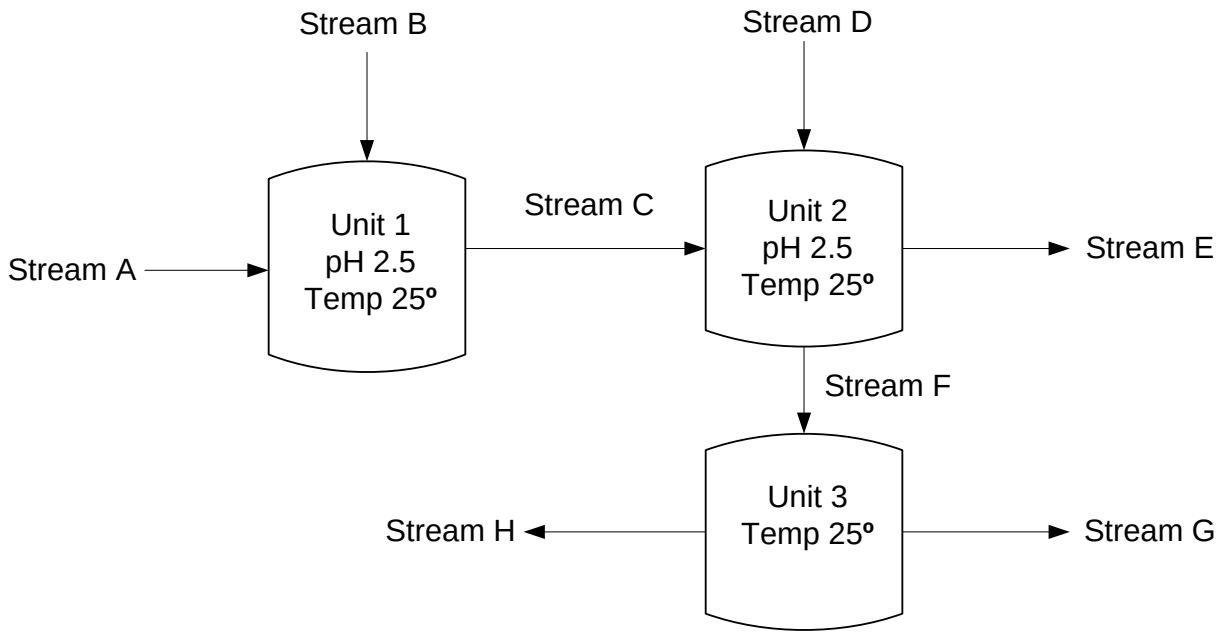

Figure 8.2: Coagulant recovery flowsheet through oxidation-solvent extraction

Table 8.2: Solvent extraction based flowsheet mass balance for coagulant recovery

Unit	**Unit name**
Unit 1	Fe Oxidation reactor
Unit 2	Extraction mixer-settler
Unit 3	Stripping mixer-settler

		Species concentration, g/L AMD								
Stream	Stream name	Fe_T	Al	Mn	Mg	Ca	O_2	NaOH	H_2SO_4	$C_{16}H_{35}O_2P$
A	AMD	4.3	0.4	0.09	0.5	0.5	-	-	0.8	-
B	Air	-	-	-	-	-	>>0.62	-	-	-
C	AMD with oxidized Fe	4.3	0.4	0.09	0.5	0.5	-	-	0.8	-
D	Cyanex 272	-	-	-	-	-	-	-	-	136.5
E	Fe/Al depleted Raffinate	0.1	0.02	~0.09	~0.5	~0.5	-	-	0.8	
F	Loaded organic	4.2	0.38	-	-	-	-	-	-	
		Species concentration, g/L coagulant								
G	Coagulant (Strip liquor)	8.1	0.73	0.08	0.06	0.009	-	-	0.001	
H	Stripped organic	-	-	-	-	-	-	-	-	136.5

8.3 Economic evaluation

To determine the chemical cost for the production of the AMD-derived coagulants, the costs of chemicals were obtained from online shopping websites such as Alibaba.com, Solvay.com and rightpricechemicals.com. Table 8.3 shows the costs of the chemicals used in the synthesis of the AMD-derived coagulants. Table 8.4 and Table 8.5 reveal the quantity of raw materials and their total cost for each assay. In this study, the organic solvent lost during the process was assumed as 0.05% and was thus, considered as the quantity of chemical used (Tanong et. al., 2017).

Using these raw materials, the cost to produce AMD-PAFS^{p} and AMD-PAFS^{sx} were 135 and \$303/m^3 coagulant, respectively. The chemical cost to produce AMD-PAFS^{sx} was more than two times the cost of producing AMD-PAFS^{p} due to the high cost of the extractant when compared to the cost of sodium hydroxide used to precipitate Fe(III) and Al(III). The total cost of producing AMD-derived coagulants in an AMD treatment plant should not exceed \$200/m^3 because the conventional coagulants are commonly sold at a price of \$300–500/m^3.

Table 8.3: Cost of chemicals

	Purity	\$/Ton	Reference
Sodium hydroxide	98%	300	Alibaba, 2020
Sulphuric acid	98%	210	Alibaba, 2020
Cyanex 272	85%	71 (\$/L)	Solvay SA, 2019
Shellsol D70	~	1 (\$/L)	Tanong et. al (2017)

Table 8.4: Chemical needed to produce AMD-PAFS[p]

Material	Quantity	Chemical cost, $/m^3 coagulant
AMD (m^3/m^3 coagulant)	27	
NaOH (kg/m^3 coagulant)	384	115
Water (precipitate washing) (m^3/m^3 coagulant)	5	
Vol H_2SO_4 (L/m^3 coagulant)	50	
Mass H_2SO_4 (kg/m^3 coagulant)	92	19
Total chemical cost, $/m^3 coagulant		135
Price of conventional coagulants, $		300-500

Table 8.5: Chemical needed to produce AMD-PAFS[sx]

Material	Quantity	Chemical cost, $/m^3 coagulant
AMD (m^3/m^3 coagulant)	2	
Cyanex (L/m^3 coagulant)	3,04	216
Shellsol D70 (L/m^3 coagulant)	16,96	25
H_2SO_4 (L/m^3 coagulant)	160	
Mass H2SO4 (kg/m^3 coagulant)	294	62
Total chemical cost, $/m^3 coagulant		303
Price of conventional coagulants, $/m^3		300-500

9 Conclusions and recommendations

9.1 Fe(III) oxidation

The oxidation mechanism of Fe(II) in the sulphate media medium at pH 5.0-7.0 has been illustrated. The objectives of this part of the study were achieved and the conclusions are summarized. From the results presented in this work, the following conclusions can be drawn on the oxidation of Fe(II) in unseeded and seeded systems

- The pH has a significant effect on ferrous iron oxidation and the rate increased with the use of seeding material in the precipitation experiments. The increase in the oxidation rate with pH is due to the change in the Fe speciation with the easily oxidizable species $FeOH^{+}$ and $Fe(OH)_2^{0}$ predominating over Fe^{2+} in the pH range 5.0-7.0. In the presence of oxide surfaces, the adsorption of Fe(II) onto the oxide particles is known to alter the co-ordination chemistry of Fe(II) and hydrolysis Fe(II) and thereby altering its speciation. The change in Fe(II) speciation was attributed to as the reason for the increase in Fe(II) oxidation with seeding. The Al(III)cations were found to have an insignificant effect on Fe(II) oxidation

- The rate equation was developed which agreed with what has been reported by several researchers with a first order dependency of Fe(II) while the 1.35 dependency of OH^{-} did not agree with most reported values

9.2 Fe(III) and Al(III) precipitation

It has been illustrated that supersaturation influences the precipitation mechanism. It has been demonstrated that the lower supersaturation promotes heterogeneous nucleation rather than homogeneous nucleation controlled precipitation. The heterogeneous precipitation mechanism resulted in bigger precipitate particles which translated into improved settling rates. The precipitates obtained were amorphous in nature with ferrihydrite as the major mineral phase. The precipitate purity was 99.0% and could subsequently be used in the production of an AMD-derived coagulant

9.3 Fe(III) and Al(III) solvent extraction and stripping

The SX was conducted to recover both Fe(III) and Al(III) while minimizing the co-extraction of other species. Both Fe(III) and Al(III) were extracted in percentages exceeding 98% for the pH values around 2.5 in a two-stage extraction system at 1:1 O/A ratio. Stripping of Fe(III) and Al(III) using with 2M sulphuric acid resulted in the stripping exceeding 95% for both species in a single stage stripping system. The strip liquor purity was > 98.8%.

9.4 Coagulation

The precipitate formed at pH 5.0 was used to produce a coagulant consisting of 89.5% and 10.0% Fe(III) and Al(III), respectively. The production of the coagulant was carried out by dissolving the precipitate in 5.0% (w/w) sulphuric acid. The strip liquor contained 91.7% Fe(III) and 8.33% Al(III). Subsequently, the treatment of the brewery wastewater showed that the AMD derived coagulants were as efficient as the conventional poly ferric sulphate coagulant. The developed process, which can easily be incorporated into existing AMD treatment plants, not only reduces the sludge disposal problems but also creates revenue from waste.

9.5 Recommendations

The following are the study recommendations:

- Since the coagulant generated in this study is generic in nature, it is recommended that the coagulants be tested on other wastewaters.
- It is also recommended that a study to determine the regeneration of the coagulants from the coagulant sludge be explored.

References

Alibaba, 2020. Available at: www.alibaba.com, Consulted on July 2020

Aniyikaiye, T.E., Oluseyi, T., Odiyo, J.O., Edokpayi, J.N., 2019. Physico-Chemical Analysis of Wastewater Discharge from Selected Paint Industries in Lagos, Nigeria. International journal of environmental research and public health 16, 1235.

Beyene, H.D., Hailegebrial, T.D., Direrssa, W.B., 2016. Investigation of coagulation activity of cactus powder in water treatment. Journal of Applied Chemistry 2016.

Cheng, W.P., Chi, F.H., Yu, R.F., Lee, Y.C., 2005. Using chitosan as a coagulant in recovery of organic matters from the mash and lauter wastewater of brewery. Journal of Polymers and the Environment 13, 383–388.

Jiang, J.-Q., Graham, N.J., 2003. Development of Optimal Poly-Alumino–Iron Sulphate Coagulant. Journal of Environmental Engineering 129, 699–708.

Kazi, T., Virupakshi, A., 2013. Treatment of tannery wastewater using natural coagulants. Development 2.

Liu, M., Lu, J., Wei, L., Wang, K., Zhao, J., 2015. Magnesium hydroxide coagulation performance and floc properties in treating high pH reactive orange wastewater. Water Science and Technology 71, 1310–1316.

Menezes, J., Silva, R., Arce, I., Schneider, I., 2010. Production of a poly-alumino-iron sulphate coagulant by chemical precipitation of a coal mining acid drainage. Minerals Engineering 23, 249–251.

Miranda, R., Latour, I., Hörsken, A., Jarabo, R., Blanco, A., 2015. Enhanced Silica Removal by Polyamine-and Polyacrylamide-Polyaluminum Hybrid Coagulants. Chemical Engineering & Technology 38, 2045–2053.

Oyem, H., Oyem, I., Ezeweali, D., 2014. Temperature, pH, electrical conductivity, total dissolved solids and chemical oxygen demand of groundwater in Boji-BojiAgbor/Owa area and immediate suburbs. Research Journal of Environmental Sciences 8, 444–450.

Solvay.com, 2020. Available at: www.solvay.com, Consulted on July 2020

Tanong, Kulchaya, Lan-Huong Tran, Guy Mercier, and Jean-Francois Blais. " Recovery of Zn (II), Mn (II), Cd (II) and Ni (II) from the unsorted spent batteries using solvent extraction, electrodeposition and precipitation methods. Journal of cleaner production, 148, pp.233-244

Tolkou, A., Zouboulis, A., 2015. Synthesis and coagulation performance of composite poly-aluminum-ferric-silicate-chloride coagulants in water and wastewater. Desalination and Water Treatment 53, 3309–3318.

Wang, D., Tang, H., 2001. Modified inorganic polymer flocculant-PFSi: its preparation, characterization and coagulation behavior. Water Research 35, 3418–3428.

Wei, Y., Bi, J., Hou, M., 2010. Preparation of a novel flocculant-polyferric magnesium sulfate and its application in wastewater treatment. Asian Journal of Chemistry 22, 4907–4912.

Xing, Z.-P., Sun, D.-Z., 2009. Treatment of antibiotic fermentation wastewater by combined polyferric sulfate coagulation, Fenton and sedimentation process. Journal of hazardous materials 168, 1264–1268.

Zhao, J., Liu, S., Chi, Y., Feng, N., 2015. Magnesium hydroxide coagulation performance and floc properties in treating kaolin suspension under high pH. Desalination and Water Treatment 53, 579–585.

Appendix I. Preparation of synthetic acid mine drainage

The following procedure was used during the preparation of synthetic AMD to study the Fe(II) oxidation kinetics:

- 500 mL of deionised water was added into a 1 L beaker and then a desired sulphuric acid was added to obtain a particular pH.
- A calculated amount of iron(II) sulphate and aluminium sulphate salts were added into the beaker containing deionised water with a specific acid molarity.
- Deionised water was toped up to a volume of 1000 mL.
- The mixture was agitated at 400 rev/min for about 1h at 25˚C. All the salts had dissolved completely after an hour.
- Fresh synthetic AMD solution was prepared in the manner outlined for each experimental run to avoid iron transformations or oxidation with time.

Appendix II. Analysis of Fe(II)

Wet chemistry was used to determine the amount of iron(II) in solution during oxidation investigations. ICIP analysis was used to determine the total iron. The following was the wet chemistry procedure;

- At least 10 mL of deionised water was added into a 250 mL Erlenmeyer flask.
- 5 mL of sample was added into the 250 mL Erlenmeyer flask using a 5 mL adjustable pipette.
- 5 mL of 98% phosphoric acid and 10 mL sulphuric acid was added into the 250 mL Erlenmeyer flask to mask the Fe(III)
- 3 to 5 drops of sodium diphenylamine indicator was then added into the flask

- The burette was set with 0.0017 M potassium dichromate ($K_2Cr_2O_7$)
- The potassium dichromate was then titrated against the contents of the Erlenmeyer flask to a purple end point.
- The concentration of Fe(II) was then calculated as per the balanced **Equation B1** using **Equation 5.1**.

$$Cr_2O_7^{2-} + 6Fe^{2+} + 14H^+ \rightarrow 2Cr^{3+} + 6Fe^{3+} + 7H_2O \qquad \text{B1}$$

Appendix III. SEM micrographs

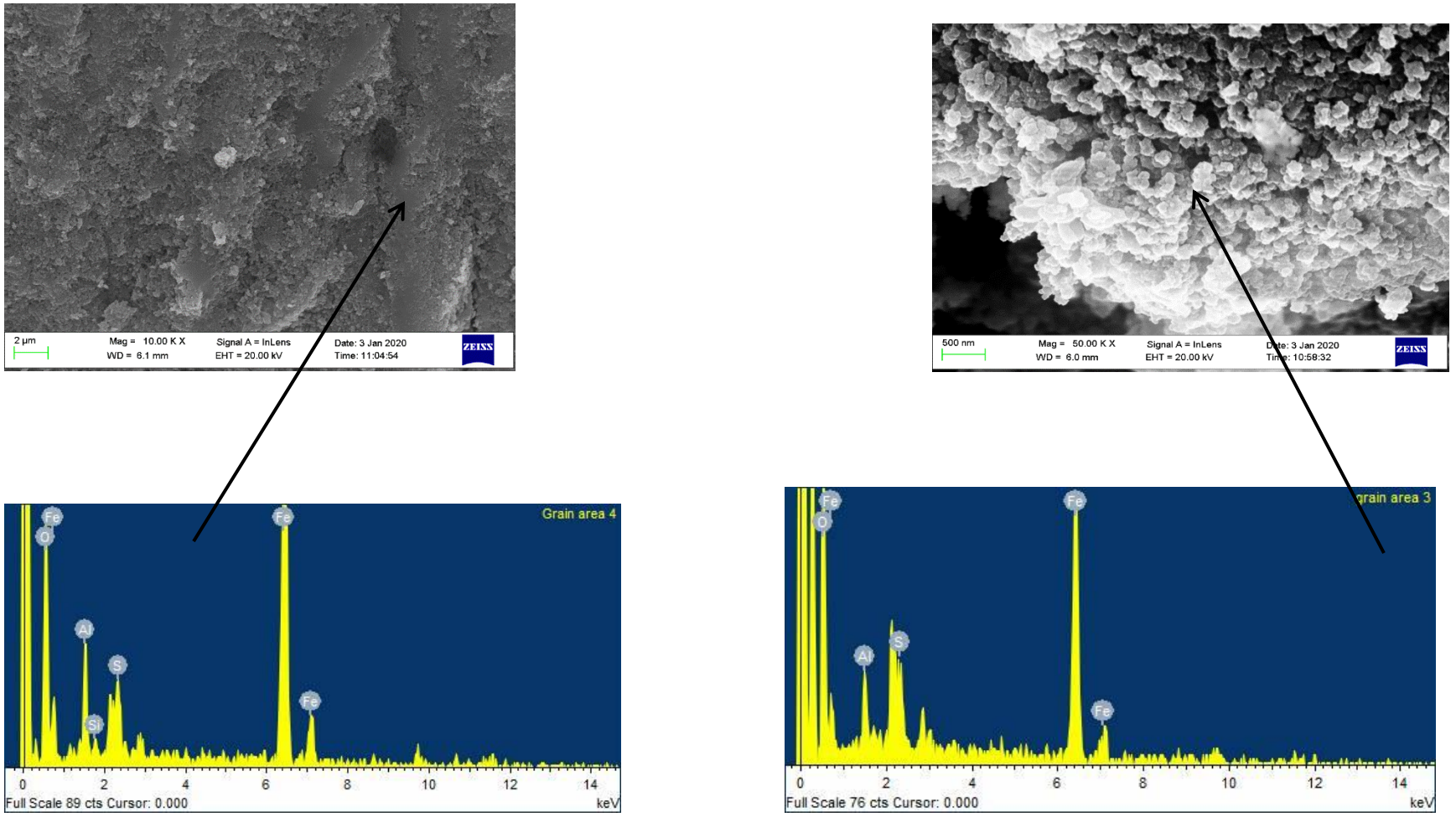

Figure A1: SEM-EDS micrographs for precipitate formed at pH 6.0 at C_s =1.0

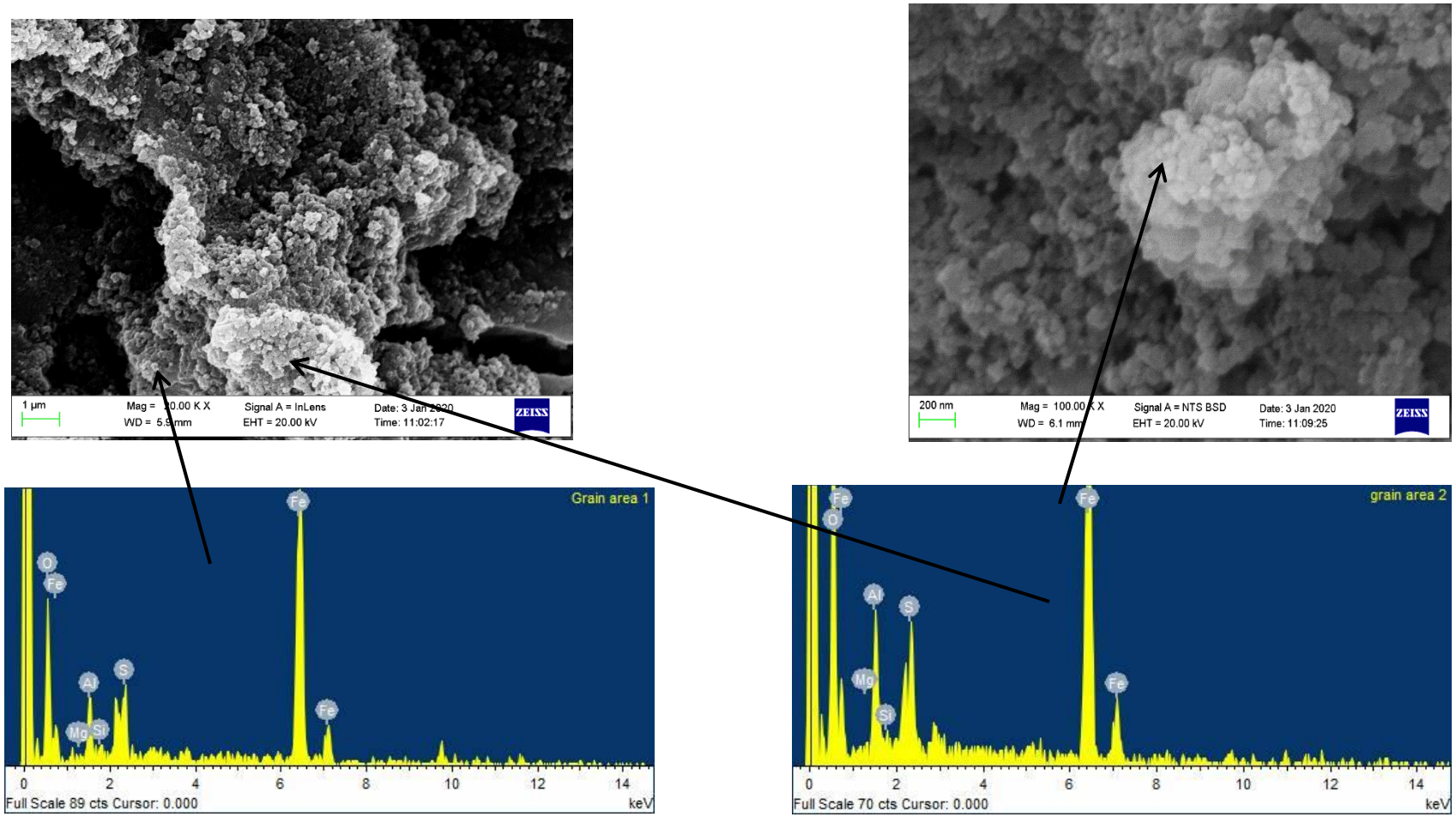

Figure A2: SEM-EDS micrographs for precipitate formed at pH 7.0 at C_s 1.0

Appendix IV. Mass balance streams

Flowsheet 1 : Precipitation based

Stream A = AMD solution

ICP analysis

Stream B = recycle sludge

Calculated based on 99.0% precipitation of Fe(III) and Al(III) and C_s = 1.0

(0.99x4.29)+(0.99x0.396) = 4.64 g

Stream C = Air

Oxygen requirement calculated based on the stoichiometry of Fe(II) oxidation according to **Equation 2.2**

4 moles of Fe(II) reacts with 1 mole of oxygen, therefore 0.077 moles (4.29 g) will require 0.0192 mol (0.614 g) oxygen

Stream D = NaOH

Calculated based on 90 mL of 4M NaOH required to raise the pH from 2.1 to 5.0

90 mL of 4 M NaOH = 0.36 mols = 14.4 g NaOH

Stream E: Slurry

Slurry containing the recycle sludge and Fe_T and Al(III) in the raw AMD

Fe_T= 4.29 + 4.25 g = 8.54g

Al(III) = 0.4 + 0.4 g = 0.8 g

Stream F = Precipitate

Calculated based on 99.0% precipitation of Fe(III) and Al(III)

Fe_T = 4.25 (recycle sludge) + 4.25 (from raw AMD) = 8.5 g

Al(III) = 0.4 (recycle sludge) + 0.4 (from raw AMD) = 0.8 g

Stream G = Sulphuric acid

Based on 200 mL of 0.5% (w/w) Sulphuric acid = 0.036 g

Stream H = Coagulant

Based on dissolution of 18.5 g of precipitate in 200 mL sulphuric acid

Stream I = Fe/Al(III) depleted water

Calculated based on mass balance from feed and precipitate, validated by ICP analysis

Flowsheet 2 : Solvent extraction based

Stream A = AMD solution

ICP analysis

Stream B = Air

Oxygen requirement calculated based on the stoichiometry of Fe(II) oxidation according to **Equation 2.2**

Stream C = Oxidized AMD

Same as stream A but with predominantly Fe(II)

Stream D = Cyanex 272

Calculated based on Cyanex 272 molar mass = 290.4 g/mol

Stream E = Rafinate

Calculated based on 99.0% extraction of both Fe(III) and Al(III), validated by ICP analysis results

Stream F: Loaded organic

Calculated based on mass balance from analytical concentration of the aqueous phase, validated by ICP analysis results

Stream G = Strip liquor

Calculated based on 99.0% precipitation of Fe(III) and Al(III)

Fe = 4.25 (recycle sludge) + 4.25 (from raw AMD) = 8.5 g

Al(III) = 0.4 (recycle sludge) + 0.4 (from raw AMD) = 0.8 g

Stream H = Stripped organic

Calculated based on mass balance